

Alma Mater Studiorum – Università di Bologna

**DOTTORATO DI RICERCA IN
BIODIVERSITÀ ED EVOLUZIONE**

Ciclo XXVI

Settore Concorsuale di afferenza: 05/B1 – ZOOLOGIA E ANTROPOLOGIA

Settore Scientifico disciplinare: BIO/05 - ZOOLOGIA

TITOLO TESI

**EFFECTS OF TEMPERATURE AND ACIDITY ON
MEDITERRANEAN BENTHIC CALCIFIERS, IN THE FACE
OF GLOBAL CLIMATE CHANGE**

Presentata da: Dott.ssa Fiorella Prada

Coordinatore Dottorato

Prof.ssa Barbara Mantovani

Relatore

Dott. Stefano Goffredo

Esame finale anno 2014

*“Escúchame mar:
ahora me voy. Me voy
pero no te dejo
porque es imposible dejar el corazon
y llevarse tan solo el cuerpo...”*

Luis E. Prieto

To my father

Index

Chapter 1. Introduction	1
Chapter 2. Environmental implications of skeletal micro-density and porosity variation in two scleractinian corals	15
Chapter 3. Time-Domain NMR study of Mediterranean scleractinian corals reveals skeletal-porosity sensitivity to environmental changes	28
Chapter 4. Different sensitivity among Mediterranean scleractinian corals to enhanced CO₂ along a natural pH gradient	38
Chapter 5. Biomineralization control related to population density under ocean acidification	74
Chapter 6. Skeletal porosity of a coral living in a natural model of ocean acidification increases with CO₂	112
Chapter 7. Conclusions	133
Acknowledgements	138

Chapter 1: General Introduction

Ocean warming and acidification

The oceans cover over two-thirds of the Earth's surface. They play a vital role in global biogeochemical cycles, contribute enormously to the planet's biodiversity and provide a livelihood for millions of people (Raven et al. 2005). In the marine realm, two of the main forces causing significant changes are ocean warming (OW) and ocean acidification (OA), both largely driven by the burning of fossil fuels, deforestation, industrialization, cement production, and other land-use changes (Wisshak et al. 2013). During the last 2-3 decades, an increase of at least 0.3-0.4°C has been recorded in mean annual sea surface temperatures (SST) across much of the global tropics and subtropics (Kleypas et al. 2008). Projections of future climatic change estimate a 0.3-4.8°C average increase in surface air temperature, and a 0.6-2.0°C average increase in surface ocean temperature by the end of 2100 (IPCC 2013). In temperate areas, the effect of temperature warming is expected to be even greater. For instance, the Mediterranean Sea, which can be regarded as a miniature ocean that is expected to react faster to global change compared to the open ocean (Bethoux et al. 1999), seems to be already showing warming rates three times higher than the global ocean (Solomon et al. 2007; Field et al. 2012). Over the last decades, there appears to have been a warming trend attributed to global warming in deep (Bethoux et al. 1990) and surface waters (Lelieveld et al. 2002; Nykjaer 2009). A warming of 0.02-0.03°C is reported for the period 1974-2005 in the NW Mediterranean shelf (Vargas-Yáñez et al. 2008).

Surface ocean CO₂ partial pressure (pCO₂) is also expected to rise in proportion with the atmospheric CO₂ increase due oceanic uptake of anthropogenic CO₂ (Sabine et al. 2004). When carbon dioxide is absorbed by seawater, chemical reactions occur that

lower seawater pH, carbonate ion (CO_3^{2-}) concentration, and saturation states of the biologically important calcium carbonate (CaCO_3) minerals calcite (Ω_{calc}) and aragonite (Ω_{arag}), in a process commonly referred to as “ocean acidification” (Orr et al. 2005). During preindustrial times the global mean pH of sea surface was 8.2. Since then, this value has decreased already by 0.1 units, and according to the Intergovernmental Panel on Climate Change (IPCC), at the current rate of CO_2 uptake, the average surface ocean pH will drop by further 0.06-0.32 units throughout this century (IPCC 2013). The current rate of CO_2 release is capable of driving a combination and magnitude of ocean geochemical changes potentially unparalleled in at least the last 300 million years of Earth history, raising the possibility that we are entering an unknown territory of marine ecosystem change (Hönisch et al. 2012).

Although OA acts at a global scale, its impact varies locally. In the case of the Mediterranean Sea, owing to its high alkalinity, more atmospheric CO_2 is absorbed than in the open ocean (CIESM 2008). The fast turnover time of its waters (50-100 years; Bethoux et al. 2005) and the very high concentration and fast penetration of anthropogenic CO_2 (Schneider et al. 2007; Schneider et al. 2010; Touratier and Goyet. 2009) makes it one of the world’s most sensitive regions to increasing atmospheric CO_2 (Ylmaz et al 2008; Calvo et al. 2011; Ziveri 2008). A recent study estimated a pH decrease of up to 0.14 units since the pre-industrial era (Touratier and Goyet 2011), larger than the global averaged surface ocean pH decrease of 0.1 pH units (Orr et al. 2005). It is consequently important to understand how anthropogenic pCO_2 has already affected and how it will affect Mediterranean Sea ecosystems and their key taxa.

Mediterranean corals and warming

My research included a study performed along a temperature gradient in the Italian western coast (Caroselli et al. 2011: Chapter 2), where we saw that porosity of the skeleton increases with temperature in the zooxanthellate (i.e. symbiotic with unicellular algae named zooxanthellae) solitary scleractinian *Balanophyllia europaea* (Risso, 1826) while it does not vary with temperature in the solitary non-zooxanthellate *Leptopsammia pruvoti* Lacaze-Duthiers, 1897. These results were confirmed by another study (Fantazzini et al. 2013: Chapter 3) I was involved in, that indicated that the increase in porosity with increasing temperature was accompanied by an increase of the fraction of the largest pores in the pore-space. The increase in porosity with temperature in the zooxanthellate species was ascribed to an inhibition of the photosynthetic process at elevated temperatures (Al-Horani 2005), causing an attenuation of calcification (Jokiel and Coles 1990). Furthermore, the calcification (Goffredo et al. 2009), abundance (Goffredo et al. 2007), and the stability of population structure (Goffredo et al. 2008) also decreased with increasing temperature. The negative correlations between temperature and various biological parameters generate concern for the future of *B. europaea*, endemic to the Mediterranean Sea, with respect to future climate change scenarios (Goffredo et al. 2008, 2009; Caroselli et al. 2011).

CO₂ vents as a model for ocean acidification studies

Knowledge on the potential effects of increased ocean acidity on marine ecosystems is very limited since almost all studies have been *in vitro*, short-term experiments on isolated organisms (Raven et al. 2005; Riebesell et al. 2007). Although laboratory

experiments are indispensable, most are too brief for full organism acclimatization to occur, and co-limiting factors (nutrients, currents and irradiance) are difficult to simulate *ex situ*. Experiments also provide little information about processes leading to ecosystem adaptation, such as altered reproduction, competition, food webs and disease susceptibility, or genetic adaptation. There is therefore great need for empirical data documenting the long-term effects of ocean acidification on marine ecosystems acclimatized to high pCO₂, as found around CO₂ vents. Areas with naturally high CO₂ may serve as useful sites to predict the impacts of ocean acidification on coastal environments (Barry et al. 2010). Vent systems are not perfect predictors of future ocean ecology, owing to pH variability, spatial proximity of unaffected populations, and co-varying environmental parameters (Hall-Spencer et al. 2008; Crook et al. 2013). However, vents acidify seawater on sufficiently large temporal and spatial scales to integrate ecosystem processes (Barry et al. 2010) and act as a “natural laboratory”. In Papua New Guinea, at three cool and shallow volcanic carbon dioxide seeps, reductions were found in coral diversity, recruitment and abundances of structurally complex framework builders, and shifts in competitive interactions between taxa (Fabricius et al. 2011). Recently, changes in shallow-water marine rocky shore ecosystems have been investigated at volcanic CO₂ seeps in the Mediterranean Sea. Studies at Ischia and Vulcano, in the south of Italy, have documented decreased diversity, biomass, and trophic complexity of benthic marine communities, major declines in many calcifying and non-calcifying organisms and increases in macroalgae and seagrasses at reduced seawater pH (Cigliano et al. 2010; Hall-Spencer et al. 2008; Porzio et al. 2011).

The Island of Panarea belongs to the Aeolian Archipelago (Italy), located in the southern Tyrrhenian Sea in the Mediterranean. At 10 m depth a crater 20 x 14 m wide generates a stable and sustained column of bubbles (mainly CO₂: Capaccioni et al. 2007), at ambient temperature, that naturally acidifies the surrounding seawater to levels matching different IPCC scenarios. In this unique site we performed a transplant experiment (*Manuscript in preparation*: Chapter 4) to study the effect of different pH conditions on the mortality rate and growth (extension rate and net calcification rate) of the solitary zooxanthellate *Balanophyllia europaea*, the solitary non-zooxanthellate *Leptopsammia pruvoti* and the colonial non-zooxanthellate *Astroides calycularis*. In all three species, high temperature exacerbated the negative effect of lowered pH on the mortality rate. The growth of the zooxanthellate species did not react to reduced pH, while the growth of the two non-zooxanthellate species was negatively affected, indicating that zooxanthellate species may be more resistant to ocean acidification than their non-zooxanthellate counterparts. These results indicate possible different levels of resilience/resistance to climate change among coral species, probably because of different modes of nutrition and/or biomineralization processes.

We also conducted a parallel study (*submitted to Nature Climate Change*: Chapter 5), where different species naturally occurring along the CO₂ gradient were collected to relate the control over the biomineralization process with the population density. The data indicate a decrease in the percentage cover of a scleractinian coral (*Balanophyllia europaea*), a mollusc (*Vermetus triqueter*), a calcifying (*Padina pavonica*) and a non-calcifying (*Lobophora variegata*) macroalgae while no variation in the abundance of a calcifying green alga (*Acetabularia acetabulum*) was observed. The mineralogy of the

calcified regions showed different responses to OA. With decreasing pH, *V. triqueter* and *B. europaea* did not change the mineralogy of their tubes and skeletons, while *P. pavonica* and *A. acetabulum* decreased the content of aragonite in favor of the less soluble calcium sulphates and whewellite (calcium oxalate), respectively, possibly as a mechanism of phenotypic plasticity.

In order to understand the effects of CO₂-driven acidity on the population density decrease of *B. europaea*, we analyzed the structure of the pore-space of the skeleton by means of TD-NMR analysis on specimens collected along the pH gradient (*Manuscript in preparation*: Chapter 6). Not only porosity (pore-volume to sample-volume ratio) but also pore-size distribution of mineralized tissues strongly influence the skeletal resistance to natural and anthropogenic breakage. The NMR results indicate that the decrease of pH determines an increase in porosity mainly driven by an increase in macroporosity (the fraction of the largest pores in the pore-space).

Natural CO₂-leaking marine sites like the one used in these studies can provide essential information on the combined effects of ocean acidification and global warming on benthic organisms, which may help understand how Mediterranean Sea ecosystems and their key taxa will be affected in the current century.

References

- Al-Horani FA (2005) Effects of changing seawater temperature on photosynthesis and calcification in the scleractinian coral *Galaxea fascicularis*, measured with O₂, Ca²⁺ and pH microsensors. *Sci Mar* 69:347-354
- Barry JP, Hall-Spencer JM, Tyrrell T (2010) In situ perturbation experiments: natural venting sites, spatial/temporal gradients in ocean pH, manipulative in situ p(CO₂) perturbations, in: Riebesell, U., Fabry, V.J., Hansson, L., Gattuso, J.P. (Eds), Guide to best practices for ocean acidification research and data reporting. Publications Office of the European Union, Luxembourg, pp. 123-136.
- Bethoux JP, Gentili B, Morin P, Nicolas E, Pierre C, Ruiz-Pino D (1999) The Mediterranean Sea: a miniature ocean for climatic and environmental studies and a key for the climatic functioning of the North Atlantic. *Prog Oceanogr* 44:131-146.
- Bethoux JP, Gentili B, Raunet J, Tailliez D (1990) Warming trend in the western Mediterranean deep water. *Nature* 347:660–662
- Bethoux JP, Boukhary MS, Ruiz-Pino D, Morin P, Copin Montegut C (2005) Nutrient, Oxygen and Carbon Ratios, CO₂ Sequestration and Anthropogenic Forcing in the Mediterranean Sea. *Hdb Environment Chemical* 5:67-86
- Calvo E, Simó R, Coma R, Ribes M, Pascual J, Sabatés A, Gili JM, Pelejero C (2011) Effects of climate change on Mediterranean marine ecosystems: the case of the Catalan Sea. *Climate Research* 50:1-29

- Capaccioni B, Tassi F, Vaselli D, Tedesco D, Poreda R (2007) Submarine gas burst at Panarea Island (Southern Italy) on 3 November 2002: a magmatic versus hydrothermal episode. *J Geophys Res* 112:B05201
- Caroselli E, Prada F, Pasquini L, Nonnis Marzano F, Zaccanti F, Falini G, Levy O, Dubinsky Z, Goffredo S (2011) Environmental implications of skeletal micro-density and porosity variation in two scleractinian corals. *Zoology* 114:255-264
- CIESM Impacts of ocean acidification on biological, chemical and physical systems in the Mediterranean and Black Seas. In *CIESM Workshop Monographs*, vol. 36 (ed. F. Briand), pp. 124. Monaco, 2008
- Cigliano M, Gambi MC, Rodolfo-Metalpa R, Patti FP, Hall-Spencer JM (2010) Effects of ocean acidification on invertebrate settlement at volcanic CO₂ vents. *Mar Biol* 157:2489-2502.
- Crook ED, Cohen AL, Rebolledo-Vieyrac M, Hernandez L, Paytan A (2013) Reduced calcification and lack of acclimatization by coral colonies growing in areas of persistent natural acidification. *Proc Natl Acad Sci USA*, doi: 10.1073/pnas.1301589110
- Dando PR, Stuben D, Varnavas SP (1999) Hydrothermalism in the Mediterranean Sea. *Prog Oceanogr* 44:333-367.
- Fabricius KE, Langdon C, Uthicke S, Humphrey C, Noonan S, De'ath G, Okazaki R, Muehllehner N, Glas MS, Lough JM (2011) Losers and winners in coral reefs acclimatized to elevated carbon dioxide concentrations. *Nat Clim Chang* 1:165-169.
- Fantazzini P, Mengoli S, Evangelisti S, Pasquini L, Mariani M, Brizi L, Goffredo S, Caroselli E, Prada F, Falini G, Levy O, Dubinsky Z (2013) Time-Domain NMR

- study of Mediterranean scleractinian corals reveals skeletal-porosity sensitivity to environmental changes. *Environ Sci Technol* 47:12679-12686.
- Field CB, Barros V, Stocker TF, Dahe Q (2012) Managing the Risks of Extreme Events and Disasters to Advance Climate Change Adaptation: Special Report of the Intergovernmental Panel on Climate Change. Cambridge University Press, Cambridge and New York.
- Goffredo S, Caroselli E, Mattioli G, Pignotti E, Dubinsky Z, Zaccanti F (2009) Inferred level of calcification decreases along an increasing temperature gradient in a Mediterranean endemic coral. *Limnol Oceanogr* 54:930-937.
- Goffredo S, Caroselli E, Mattioli G, Pignotti E, Zaccanti F (2007) Variation in biometry and demography of solitary corals with environmental factors in the Mediterranean Sea. *Mar Biol* 152:351-361.
- Goffredo S, Caroselli E, Mattioli G, Pignotti E, Zaccanti F (2008) Relationships between growth, population structure and sea surface temperature in the temperate solitary coral *Balanophyllia europaea* (Scleractinia, Dendrophylliidae). *Coral Reefs* 27:623-632.
- Hall-Spencer JM, Rodolfo-Metalpa R, Martin S, Ransome S, Fine M, Turner SM, Rowley SJ, Tedesco D, Buia MC (2008) Volcanic carbon dioxide vents show ecosystem effects of ocean acidification. *Nature* 454:96-99.
- Hönisch B, Ridgwell A, Schmidt DN, Thomas E, Gibbs SJ, Sluijs A, Zeebe R, Kump L, Martindale RC, Greene SE, Kiessling W, Ries J, Zachos JC, Royer DL, Barker S, Marchitto TM, Moyer R, Pelejero C, Ziveri P, Foster GL, Williams B (2012) The geological record of ocean acidification. *Science* 335:1058-1063.

- IPCC (2013) in *Climate Change 2013: The Physical Science Basis. Contribution of Working Group I to the Fifth Assessment Report of the Intergovernmental Panel on Climate Change*, eds Stocker TF, et al. (Cambridge University Press, Cambridge).
- Jokiel PL, Coles SL (1990) Response of Hawaiian and other Indo-Pacific reef corals to elevated temperature. *Coral Reefs* 4:155-162.
- Kleypas JA, Danabasoglu G, Lough JM(2008) Potential role of the ocean thermostat in determining regional differences in coral reef bleaching events. *Geophys. Res Lett* 35:L03613.
- Lelieveld J, Berresheim H, Borrmann S, Crutzen PJ (2002) Global air pollution crossroads over the Mediterranean. *Science* 298:794-799.
- Nykjaer L (2009) Mediterranean Sea surface warming 1985–2006. *Clim Res* 39:11-17.
- Orr JC, Fabry VJ, Aumont O, Bopp L, Doney SC, et al. (2005) Anthropogenic ocean acidification over the twenty-first century and its impact on calcifying organisms. *Nature* 437:681-686.
- Porzio L, Buia MC, Hall-Spencer JM (2011) Effects of ocean acidification on macroalgal communities. *J Exp Mar Biol Ecol* 400:278-287.
- Raven JA, Caldeira K, Elderfield H, Hoegh-Guldberg O, Liss P, Riebesell U, Shepherd J, Turley C, Watson A (2005) Ocean acidification due to increasing atmospheric carbon dioxide. Policy document 12/05, Royal Society, London.
- Riebesell U, Schulz K, Bellerby R, Botros M, Fritsche P, Meyerhofer M, Neill C, Nondal G, Oschlies A, Wohlers J, Zollner E (2007) Enhanced biological carbon consumption in a high CO₂ ocean. *Nature* 450:545-548.

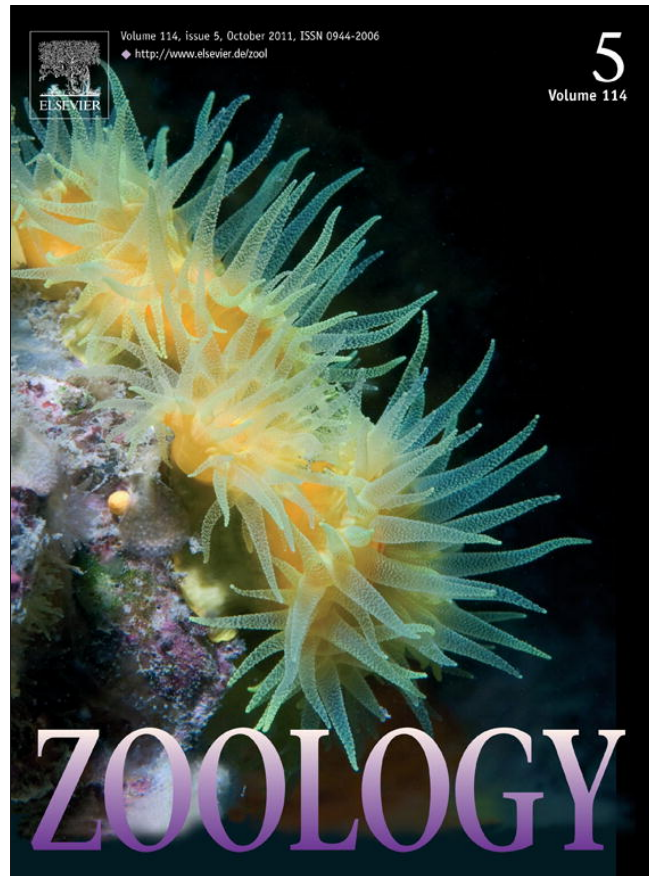
- Sabine CL, Feely RA, Gruber N, Key RM, Lee K, Bullister JL, Wanninkhof R, Wong CS, Wallace DWR, Tilbrook B, Millero FJ, Peng TH, Kozyr A, Ono T, Rios AF (2004) The oceanic sink for anthropogenic CO₂. *Science* 305: 367-371.
- Schneider A, Tanhua T, Körtzinger A and Wallace DWR (2010) High anthropogenic carbon content in the eastern Mediterranean. *J Geophys Res* 115:C12050.
- Schneider A, Wallace DWR, Körtzinger A. Alkalinity of the Mediterranean Sea (2007) *Geophys Res Lett* 34:1-5.
- Solomon S, Qin D, Manning M, Chen Z, Marquis M, Averyt K, Tignor MMB, Miller HR, Chin Z (2007) Climate change 2007: the physical science basis. Cambridge University Press, Cambridge.
- Touratier F, Goyet C (2009) Decadal evolution of anthropogenic CO₂ in the northwestern Mediterranean Sea from the mid-1990s to the mid-2000s. *Deep Sea Res Part 1 Oceanogr Res Pap* 56:1708-1716.
- Touratier F, Goyet C (2011) Impact of the Eastern Mediterranean Transient on the distribution of anthropogenic CO₂ and first estimate of acidification for the Mediterranean Sea. *Deep Sea Res Part 1 Oceanogr Res Pap* 58:1-15.
- Vargas-Yáñez M, Jesús García M, Salat J, García-Martínez MC, Pascual J, Moya F (2008) Warming trends and decadal variability in the Western Mediterranean shelf. *Glob Planetary Change* 63:177-184.
- Williams SN, Schaefer SJ, Calvache ML, Lopez D (1992) Global carbon dioxide emission to the atmosphere by volcanoes. *Geochim Cosmochim Acta* 56:1765-1770.

- Wisshak M, Schönberg CH, Form AU, Freiwald A (2013) Effects of ocean acidification and global warming on reef bioerosion-lessons from a clionaid sponge. *Aquatic Biology* 19:111-127.
- Ylmaz A, De Lange G, Dupont S, Fine M, Fowler SW, Gattuso JP, Gazeau F, Gehlen M, Goyet C, Jeffree R, Montagna P, Rees AP, Reynaud S, Rodolfo-Metalpa R, Ziveri P, Briand F (2008) Impact of Acidification on Biological, Chemical and Physical Systems in the Mediterranean & Black Sea Mediterranean, Mediterranean Science Committee (CIESM), Monograph Series, Vol. 36, 2009, pp. 124.
- Ziveri P (2012) Research turns to acidification and warming in the Mediterranean Sea, IMBER (Integrated Marine Biogeochemistry and Ecosystem Research), Newsletter, Issue n.#20.

**Chapter 2:
Environmental implications of skeletal
micro-density and porosity variation
in two scleractinian corals**

Published in *Zoology*

Provided for non-commercial research and education use.
Not for reproduction, distribution or commercial use.



This article appeared in a journal published by Elsevier. The attached copy is furnished to the author for internal non-commercial research and education use, including for instruction at the authors institution and sharing with colleagues.

Other uses, including reproduction and distribution, or selling or licensing copies, or posting to personal, institutional or third party websites are prohibited.

In most cases authors are permitted to post their version of the article (e.g. in Word or Tex form) to their personal website or institutional repository. Authors requiring further information regarding Elsevier's archiving and manuscript policies are encouraged to visit:

<http://www.elsevier.com/copyright>



Contents lists available at ScienceDirect

Zoology

journal homepage: www.elsevier.de/zool

ZOOLOGY

Environmental implications of skeletal micro-density and porosity variation in two scleractinian corals

Erik Caroselli^a, Fiorella Prada^a, Luca Pasquini^b, Francesco Nonnis Marzano^c, Francesco Zaccanti^a, Giuseppe Falini^d, Oren Levy^e, Zvy Dubinsky^e, Stefano Goffredo^{a,*}

^a Marine Science Group, Department of Evolutionary and Experimental Biology, University of Bologna, Via F. Selmi 3, I-40126 Bologna, Italy

^b Department of Physics, University of Bologna, Via Bertini-Pichat 6/2, I-40127 Bologna, Italy

^c Department of Evolutionary and Functional Biology, University of Parma, Via G.P. Usberti 11A, I-43100 Parma, Italy

^d Department of Chemistry, University of Bologna, Via Selmi 2, I-40126 Bologna, Italy

^e The Mina & Everard Goodman Faculty of Life Sciences, Bar-Ilan University, Ramat-Gan 52900, Israel

ARTICLE INFO

Article history:

Received 24 January 2011

Received in revised form 6 April 2011

Accepted 25 April 2011

Keywords:

Coral skeletons

Mediterranean Sea

Temperate corals

Sea surface temperature

Skeletal density

ABSTRACT

The correlations between skeletal parameters (bulk density, micro-density and porosity), coral age and sea surface temperature were assessed along a latitudinal gradient in the zooxanthellate coral *Balanophyllia europaea* and in the azooxanthellate coral *Leptopsammia pruvoti*. In both coral species, the variation of bulk density was more influenced by the variation of porosity than of micro-density. With increasing polyp age, *B. europaea* formed denser and less porous skeletons while *L. pruvoti* showed the opposite trend, becoming less dense and more porous. *B. europaea* skeletons were generally less porous (more dense) than those of *L. pruvoti*, probably as a consequence of the different habitats colonized by the two species. Increasing temperature had a negative impact on the zooxanthellate species, leading to an increase of porosity. In contrast, micro-density increased with temperature in the azooxanthellate species. It is hypothesized that the increase in porosity with increasing temperatures observed in *B. europaea* could depend on an attenuation of calcification due to an inhibition of the photosynthetic process at elevated temperatures, while the azooxanthellate species appears more resistant to variations of temperature, highlighting possible differences in the sensitivity/tolerance of these two coral species to temperature changes in face of global climate change.

© 2011 Elsevier GmbH. All rights reserved.

1. Introduction

Studying how terrestrial and marine ecosystems respond to present and future environmental shifts related to climate change is a fundamental challenge for ecologists (Karl and Trenberth, 2003; Harley et al., 2006). The rate of climate change is accelerating, and the average surface temperature of the Earth is likely to increase by 1.1–6.4 °C until the end of the 21st century, with a best estimate of 1.8–4.0 °C (Solomon et al., 2007). Growing evidence suggests that climate change is having more substantial and rapid effects on marine communities than on terrestrial ones (Richardson and Poloczanska, 2008). Increased seawater temperature, enhanced ultraviolet-B radiation, upper-ocean acidification, and anthropogenic stress will affect all levels of ecological hierarchies and a broad array of marine ecosystems (Walther et al., 2002).

The magnitude of temperature change is expected to be greater in temperate areas than in tropical ones (Solomon et al., 2007).

Climatic models further predict that the Mediterranean basin will be one of the regions most affected by the ongoing warming trend and by an increase in extreme events (Lejeune et al., 2010). This commends the Mediterranean Sea as a potential model of global scenarios to occur in the world's marine biota, and a natural focus of interest for research. The Mediterranean is already one of the most impacted seas in the world, since climate change interacts synergistically with many other disturbances such as eutrophication caused by increased use of agricultural phosphates and the damming of rivers (Tsimplis et al., 2006). In recent years, the coralligenous community of the Mediterranean Sea, one of the most diverse communities there (~1666 species; Ballesteros, 2006) where suspension feeders are dominant, has been strongly affected by several mass mortality events (Cerrano et al., 2000; Perez et al., 2000; Rodolfo-Metalpa et al., 2000; Romano et al., 2000; Coma et al., 2009; Garrabou et al., 2009). Ecosystem engineers, including gorgonians and sponges, have been the most affected taxa down to depths of 45 m (Cerrano et al., 2000; Perez et al., 2000; Garrabou et al., 2009).

The present study focuses on two scleractinian species commonly occurring in the Mediterranean Sea: *Balanophyllia europaea* and *Leptopsammia pruvoti*.

* Corresponding author. Tel.: +39 051 2094244; fax: +39 051 2094286.
E-mail address: stefano.goffredo@marinesciencegroup.org (S. Goffredo).

B. europaea is a solitary, ahermatypic, zooxanthellate, and scleractinian coral, which is endemic to the Mediterranean Sea and is distributed at 0–50 m depth due to its symbiosis with zooxanthellae (Zibrowius, 1980). Along the Italian coasts, its skeletal density and population abundance are negatively correlated with sea surface temperature (SST) (Goffredo et al., 2007). In addition, the population structures of this species become less stable and deviate from the steady state with increasing SST due to a progressive

deficiency of young individuals (Goffredo et al., 2008). Its calcification is negatively correlated with SST (Goffredo et al., 2009). It has been hypothesized that photosynthesis of the symbiotic algae of *B. europaea* is inhibited at high temperatures, consequently causing an inhibition of calcification (Goffredo et al., 2009). There is concern for the future of this species (Goffredo et al., 2008, 2009) with regard to the current predictions of global warming by the Intergovernmental Panel on Climate Change (IPCC).

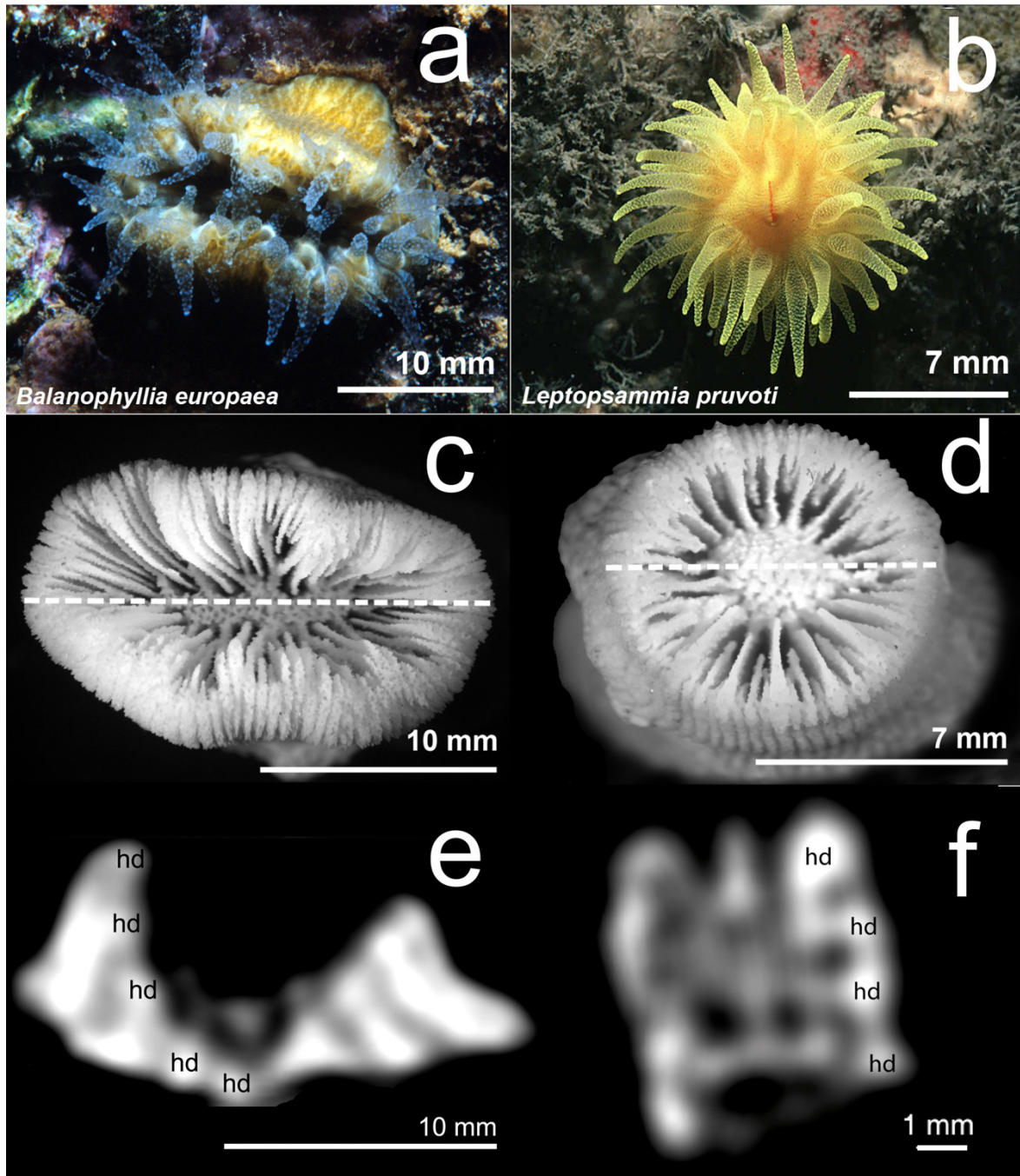


Fig. 1. Living specimens (top), skeletons (middle) and corallites (bottom) of (a, c and e) *Balanophyllia europaea* and (b, d and f) *Leptopsammia pruvoti*. Dotted lines in (b) and (d) indicate polyp lengths (L = maximum axis of the oral disc). (e and f) Computerized tomography scans of two corallites. Age was determined by counting the high density growth bands (hd). In these samples, the skeleton of *B. europaea* is 5 years old, while the skeleton of *L. pruvoti* is 4 years old.

L. pruvoti is an ahermatypic, non-zooxanthellate, and solitary scleractinian coral, which is distributed in the Mediterranean basin and along the European Atlantic coast from Portugal to Southern England and Ireland (Zibrowius, 1980). It is one of the most common organisms in semi-enclosed rocky habitats, under overhangs, in caverns, and small crevices at 0–70 m depth (Zibrowius, 1980). Sea surface temperature and solar radiation have been reported not to significantly influence its skeletal density, corallite length, width, height or population abundance along an 850-km latitudinal gradient on the west coast of Italy (Goffredo et al., 2007).

SST, whose variation is mainly influenced by latitude (Kain, 1989), is strongly linked to coral biometry, physiology, and demography (Kleypas et al., 1999; Lough and Barnes, 2000; Harriott and Banks, 2002; Al-Horani, 2005). Several studies have shown that coral growth is strongly related to temperature (Goreau and Goreau, 1959; Bak, 1974; Jokiel and Coles, 1978; Highsmith, 1979; Crossland, 1984; Kleypas et al., 1999; Lough and Barnes, 2000; Goffredo et al., 2007, 2008, 2009). Coral growth is defined by three related characteristics: calcification, skeletal density, and linear extension rate (calcification = skeletal density × linear extension; Lough and Barnes, 2000; Carricart-Ganivet, 2004). Most studies on coral skeletal density have focused on bulk density, which is the mass divided by the total enclosed volume, including the volume of the enclosed skeletal voids (porosity). Bulk density has been found to vary with exposure, latitude, depth, temperature, location within a colony, and also between different growth forms (see, e.g., Dustan, 1975; Schneider and Smith, 1982; Oliver et al., 1983; Hughes, 1987; Jiménez and Cortés, 1993; Harriott, 1997; Carricart-Ganivet, 2004; Goffredo et al., 2007, 2009; Dar and Mohammed, 2009; Tanzil et al., 2009). Another measure of skeletal density appearing in the literature is micro-density (mass per unit volume of the material which composes the skeleton; Barnes and Devereux, 1988). As porosity decreases, bulk density will approach micro-density, and neither can exceed the density of pure aragonite (2.94 mg mm^{-3} ; Marszalek, 1982; Bucher et al., 1998), due to the presence of an intra-crystalline organic matrix which is absent in abiotic carbonates (Cuif et al., 1999). Bulk density, porosity and micro-density have rarely been investigated together (Barnes and Devereux, 1988; Bucher et al., 1998), even though they are the factors influencing the ability of coral skeletons to resist natural and anthropogenic breakage (Wainwright et al., 1976; Chamberlain, 1978; Tunnicliffe, 1979; Schumacher and Plewka, 1981; Vosburgh, 1982; Liddle and Kay, 1987; Jiménez and Cortés, 1993; Rodgers et al., 2003). Variability in micro-density among colonies within and among species, localities, and environmental conditions remains largely unstudied (Bucher et al., 1998). This is the first study exploring all of these three skeletal parameters (bulk density, micro-density and porosity) in temperate corals, with the aim of defining their relationships with coral age and SST and highlighting possible differences in the sensitivity/tolerance of the two investigated coral species to temperature changes in face of global climate change.

2. Materials and methods

2.1. Collection and treatment of specimens

Specimens of *B. europaea* (Risso, 1826) and *L. pruvoti* Lacaze-Duthiers, 1897 (Fig. 1A and B) were collected between 9 November 2003 and 24 June 2008 from 6 sites along a latitudinal gradient, from 44°20'N to 36°45'N (Fig. 2). Corals of *B. europaea* were randomly collected along a reef with southerly exposure at a depth of 5–7 m. Corals of *L. pruvoti* were randomly collected on the vault of crevices at a depth of 15–17 m. The sampling was performed at depths known to have high population densities and where the reproductive biology of the two species had been

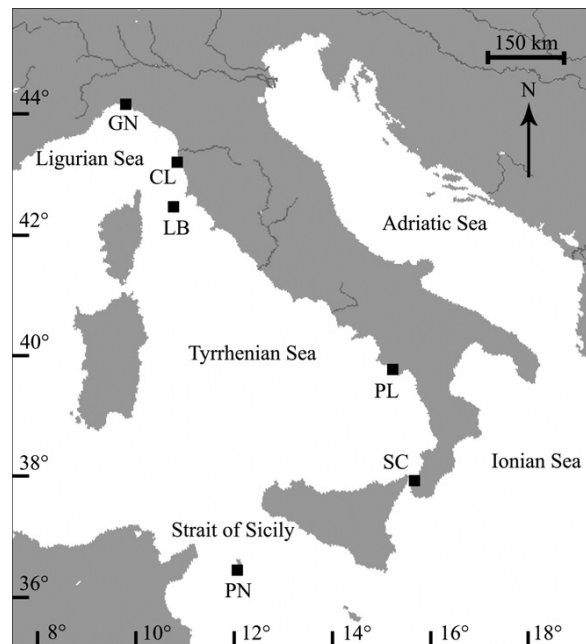


Fig. 2. Map of the Italian coastline indicating the sites where the corals were collected. Abbreviations and coordinates of the sites in decreasing order of latitude: GN, Genova, 44°20'N, 9°08'E; CL, Calafuria, 43°27'N, 10°21'E; LB, Elba Isle, 42°45'N, 10°24'E; PL, Palinuro, 40°02'N, 15°16'E; SC, Scilla, 38°01'N, 15°38'E; PN, Pantelleria Isle, 36°45'N, 11°57'E.

studied previously (Goffredo et al., 2002, 2004, 2006; Goffredo and Zaccanti, 2004).

Coral tissue was totally removed by immersing the samples in a solution of 10% commercial bleach for 3 days. Corals were dried for 4 days at a maximum temperature of 50°C to avoid phase transitions in the skeletal carbonate phases (Vongsavat et al., 2006). Each sample was inspected under a binocular microscope to remove fragments of substratum and calcareous deposits produced by other organisms. During this microscopic inspection, the few specimens that showed evident signs of bioerosion were separated and excluded from the analysis. Polyp length (L : longest axis of the oral disc), width (W : shortest axis of the oral disc), and height (h : oral–aboral axis) were measured using a pair of calipers (Fig. 1C and D; cf. Goffredo et al., 2007).

2.2. Age determination

Coral age was obtained by growth band analysis of about 40 skeletons randomly selected from the samples collected for each population, by means of computerized tomography (CT; von Bertalanffy, 1938; Goffredo et al., 2008; Fig. 1E and F). This technique is commonly applied to scleractinian corals (Bosscher, 1993; Helmle et al., 2000) and has also been successfully used in solitary corals (Goffredo et al., 2004, 2008, 2010). The age of each skeleton was determined by counting the growth bands, which are distinguished by a high-density band in winter and a low-density band in summer (Peirano et al., 1999; Goffredo et al., 2004, 2008). For *L. pruvoti*, a power function model was used to correlate the age/length data obtained by the CT scans of each population, since it produced the best fit. Using this model, the age of each coral sample was determined from its length. For *B. europaea*, the age of each sample was estimated using the von Bertalanffy's growth function for analyzing the data obtained by CT growth band analysis (cf. Goffredo et al., 2008).

2.3. Determination of skeletal parameters

To obtain the skeletal parameters, the buoyant weight of 250 specimens of *B. europaea* and 248 specimens of *L. pruvoti* was measured using the density determination kit of the Ohaus Explorer Pro balance (± 0.0001 g; Ohaus Corp., Pine Brook, NJ, USA). For buoyant weight measurements, the standard pan was replaced by a suspended weighing cradle attached to an underwater weighing pan submerged in a glass beaker filled with distilled water. A cover isolated the device from air flow within the laboratory. Measurements required for calculating the skeletal parameters were:

ρ	density of the fluid medium (in this case, distilled water: 1 g cm^{-3} at 20°C and 1 atm)
DW	dry weight of the skeleton
BW	buoyant weight of the skeleton = weight of the skeleton minus weight of the water displaced by it. To obtain this measurement, corals were placed in a desiccator connected to a mechanical vacuum pump for about 4 h in order to suck out all of the water and air from the pores (Barnes and Devereux, 1988). Still under vacuum conditions, the dry corals were soaked by gradually pouring distilled water inside the desiccator. The coral was then slowly lowered onto the underwater weighing pan, ensuring that no air bubbles adhered to its surface. The buoyant weight measurement was taken when the reading was stable, to avoid errors caused by measurement instability in the first few seconds due to water movement. This simple and nondestructive method has been widely used on various corals (Franzisket, 1964; Bak, 1973, 1976; Jokiel et al., 1978; Graus and Macintyre, 1982; Hughes, 1987; Barnes and Devereux, 1988; Davies, 1989; Mann, 1994; Marubini et al., 2003; Ammar et al., 2005; Spiske et al., 2008; Shi et al., 2009).
SW	saturated weight of the coral = weight of the skeleton plus weight of the water enclosed in its pores. The coral was taken out of the water, quickly blotted with a humid paper towel to remove surface water, and weighed in air, making sure that no water droplets were left on the weighing platform, which would lead to an overestimation.
$V_{\text{MATRIX}} = \frac{DW - BW}{\rho}$	matrix volume = volume of the skeleton, excluding the volume of its pores.
$V_{\text{PORES}} = \frac{SW - DW}{\rho}$	pore volume = volume of the pores in the skeleton.
$V_{\text{TOT}} = (V_{\text{MATRIX}} + V_{\text{PORES}})$	total volume = volume of the skeleton including its pores.

Additionally, the following skeletal parameters were calculated:

Micro-density (matrix density) = DW/V_{MATRIX}
 Porosity = $(V_{\text{PORES}}/V_{\text{TOT}}) \times 100$
 Bulk density = DW/V_{TOT} .

Table 1

Balanophyllia europaea and *Leptosammia pruvoti*. Values of sea surface temperature (SST), date of sample collection, number of collected samples and age of the samples at each site. The Genova site is characterized by particular local conditions (xerotherm site due to local currents and rock composition; see www.apat.gov.it) and typically has higher SST than expected for this latitude (annual SST of Ligurian Sea: 18°C ; Genova: 19.6°C). In both coral species, the ages of sampled individuals differed significantly among the sites (Kruskal–Wallis test, $df=5$; *B. europaea*: $p < 0.050$; *L. pruvoti*: $p < 0.001$). The sites are arranged in order of increasing seawater temperature.

Population	Code	SST ($^\circ\text{C}$)		Date of collection	Species	n	Age (years)	
		Annual mean (SE)	Range				Mean (SE)	Range (years)
Calafuria	CL	18.02 (0.04)	12.6–29.4	31 January 2004/24 June 2008	<i>B. europaea</i>	38	7.05 (0.80)	1.5–17.1
					<i>L. pruvoti</i>	44	4.52 (0.19)	2.0–6.6
Elba	LB	18.74 (0.04)	12.5–26.7	10–11 November 2003	<i>B. europaea</i>	17	6.16 (0.21)	4.0–7.5
					<i>L. pruvoti</i>	42	8.05 (0.40)	3.2–13.7
Palinuro	PL	19.14 (0.03)	12.9–27.1	2–3 April 2004	<i>B. europaea</i>	49	7.77 (0.36)	1.6–16.2
					<i>L. pruvoti</i>	45	5.07 (0.31)	1.6–9.5
Scilla	SC	19.54 (0.02)	15.3–25.3	6–7 January 2005	<i>B. europaea</i>	8	7.59 (0.49)	5.7–9.7
					<i>L. pruvoti</i>	29	8.69 (0.10)	1.4–19.7
Genova	GN	19.56 (0.04)	13.1–34.7	24 October 2004	<i>B. europaea</i>	23	8.42 (0.63)	1.3–13.8
					<i>L. pruvoti</i>	43	8.29 (0.52)	1.6–13.8
Pantelleria	PN	19.88 (0.04)	13.1–26.8	29–30 September 2005/1 August 2006	<i>B. europaea</i>	115	7.92 (0.23)	1.7–13.5
					<i>L. pruvoti</i>	45	7.74 (0.60)	1.7–14.8

n, number of individuals; SE, standard error.

The above method was slightly different from the one proposed by Bucher et al. (1998), since we decided not to use acetone or wax in order to preserve the samples for further analyses. However, the results of this buoyant weighing technique were confirmed by the strong relationship between bulk density and porosity obtained for both species and all locations (see Section 3).

As in other studies on the influence of environmental parameters on coral growth (i.e., Harriott, 1999; Lough and Barnes, 2000; Carricart-Ganivet, 2004; Peirano et al., 2005a,b), SST data were obtained from data banks. During 2003–2005, SST data for each site were obtained from the National Mareographic Network of the Agency for the Protection of the Environment and Technical Services (APAT, available at <http://www.apat.gov.it>). These data were measured by mareographic stations (SM3810; SIAP, Bologna, Italy), which were located close to the sampling sites (<1 km). Mean annual SST was obtained from hourly values measured from January 2001 to January 2005 (number of hourly values = 35,064 for each site; Table 1).

2.4. Statistical analyses

Spearman's rank correlation coefficient was used to calculate the significance of the correlations between skeletal parameters and sea surface temperature. Spearman's rank correlation coefficient is an alternative to Pearson's correlation coefficient (Altman, 1991). It is useful for data that are non-normally distributed and do not meet the assumptions of Pearson's correlation coefficient. The Kruskal–Wallis test was used to compare SST, age, and skeletal parameter characteristics among study sites. The Kruskal–Wallis test is a non-parametric alternative to the analysis of variance (ANOVA) and is used to compare groups of means. The advantage of this test is that it does not require normality of the data, as the test is based on the ranks of data. This distribution-free test proved to be more robust than its parametric counterpart in the case of a non-normal distribution of sample data, and it is a viable alternative to parametric statistics (Potvin and Roff, 1993). All analyses were computed using SPSS. 12.0.

3. Results

SST varied among the sites, with mean values spanning from 18.0°C to 19.9°C (Kruskal–Wallis test, $df=5$, $p < 0.001$; Table 1). In both coral species, the ages of the sampled individuals differed significantly among the sites (Kruskal–Wallis test, $df=5$; *B. europaea*: $p < 0.050$; *L. pruvoti*: $p < 0.001$; Table 1).

Table 2

Balanophyllia europaea. Correlation analysis between polyp age (independent variable) and skeletal parameters (dependent variable) at 6 sites along the west coast of Italy. Relationships were fitted to a power function model $y = ax^b$. The exponent (b) and factor (a) values are indicated only where the relationship was significant. The sites are arranged in order of increasing seawater temperature.

Population	Code	n	Dependent variable	Factor	Exponent	r^2	r
Calafuria	CL	38	Micro-density	–	–	0.051	0.226
			Porosity	35.293	–0.117	0.109	–0.330 [*]
			Bulk density	1.740	0.052	0.123	0.350 [*]
Elba	LB	17	Micro-density	–	–	0.012	0.110
			Porosity	–	–	0.013	0.116
			Bulk density	–	–	0.005	–0.068
Palinuro	PL	49	Micro-density	–	–	0.026	–0.162
			Porosity	–	–	0.058	–0.241
			Bulk density	–	–	0.030	0.173
Scilla	SC	8	Micro-density	2.485	0.043	0.591	0.768 [*]
			Porosity	–	–	0.377	0.614
			Bulk density	–	–	0.194	–0.440
Genova	GN	23	Micro-density	2.559	0.030	0.531	0.729 [*]
			Porosity	–	–	0.026	–0.162
			Bulk density	–	–	0.084	0.290
Pantelleria	PN	115	Micro-density	2.528	0.032	0.494	0.703 ^{***}
			Porosity	41.548	–0.084	0.056	–0.237 [*]
			Bulk density	1.461	0.086	0.156	0.394 ^{***}

n , number of individuals; r^2 , Pearson's coefficient of determination; r , Pearson's correlation coefficient.

^{*} $p < 0.050$.

^{***} $p < 0.001$.

In *B. europaea*, when bulk density correlated positively with age (Calafuria and Pantelleria), porosity correlated negatively, regardless of the response of micro-density. When bulk density did not vary with age (Genova, Elba, Palinuro and Scilla), neither did porosity vary, regardless of micro-density patterns (Table 2). In two cases (Scilla and Genova), micro-density was positively correlated with age (Table 2).

In *L. pruvoti*, when bulk density correlated negatively with age (Genova, Calafuria, Elba and Scilla), porosity correlated positively, regardless of the response of micro-density. When bulk density remained constant (Palinuro and Pantelleria), porosity was also

unchanged, irrespective of micro-density (Table 3). In three cases (Calafuria, Genova and Pantelleria), micro-density was positively correlated with age (Table 3).

Thus, in both species, the variation of bulk density with age was determined by the variation of porosity rather than by the variation of micro-density. Whenever the relationship between bulk density and micro-density or age was significant, it showed a positive trend.

The mean porosity of *B. europaea* was significantly lower than that of *L. pruvoti* in 4 out of 6 populations (Genova, Calafuria, Elba and Pantelleria; Student's t -test, $p < 0.001$). In the Palinuro population, porosity was significantly lower in *L. pruvoti* (Student's t -test,

Table 3

Leptopsammia pruvoti. Correlation analysis between polyp age (independent variable) and skeletal parameters (dependent variable) at 6 sites along the west coast of Italy. Relationships were fitted to a power function model $y = ax^b$. The exponent (b) and factor (a) values are indicated only where the relationship was significant. The sites are arranged in order of increasing seawater temperature.

Population	Code	n	Dependent variable	Factor	Exponent	r^2	r
Calafuria	CL	44	Micro-density	2.525	0.031	0.14	0.374 [*]
			Porosity	27.600	0.285	0.19	0.431 ^{**}
			Bulk density	1.943	–0.178	0.13	–0.361 [*]
Elba	LB	42	Micro-density	–	–	0.07	–0.273
			Porosity	23.156	0.250	0.12	0.349 [*]
			Bulk density	2.331	–0.188	0.13	–0.365 [*]
Palinuro	PL	45	Micro-density	–	–	0.01	0.071
			Porosity	–	–	0.00	–0.049
			Bulk density	–	–	0.01	0.069
Scilla	SC	29	Micro-density	–	–	0.09	–0.298
			Porosity	26.852	0.128	0.17	0.417 [*]
			Bulk density	2.029	–0.074	0.19	–0.437 [*]
Genova	GN	43	Micro-density	2.634	0.012	0.20	0.445 ^{**}
			Porosity	27.799	0.205	0.24	0.491 ^{***}
			Bulk density	1.917	–0.112	0.15	–0.382 [*]
Pantelleria	PN	45	Micro-density	2.532	0.036	0.39	0.621 ^{***}
			Porosity	–	–	0.04	0.194
			Bulk density	–	–	0.03	0.157

n , number of individuals; r^2 , Pearson's coefficient of determination; r , Pearson's correlation coefficient.

^{*} $p < 0.050$.

^{**} $p < 0.010$.

^{***} $p < 0.001$.

Table 4

Balanophyllia europaea and *Leptosammia pruvoti*. Mean porosity of the samples at each site and significance of Student's *t*-test used to compare the values between the two species. The sites are arranged in order of increasing seawater temperature.

Population	Code	Species	<i>n</i>	Mean porosity (%)	SE	Significance
Calafuria	CL	<i>B. europaea</i>	1814	29.58	0.04	<i>p</i> < 0.001
		<i>L. pruvoti</i>	210	37.35	0.48	
Elba	LB	<i>B. europaea</i>	38	30.00	0.25	<i>p</i> < 0.001
		<i>L. pruvoti</i>	76	36.05	0.78	
Palinuro	PL	<i>B. europaea</i>	80	38.20	0.20	<i>p</i> < 0.001
		<i>L. pruvoti</i>	152	31.02	0.05	
Scilla	SC	<i>B. europaea</i>	48	30.78	0.94	ns
		<i>L. pruvoti</i>	115	30.99	0.44	
Genova	GN	<i>B. europaea</i>	55	31.44	0.16	<i>p</i> < 0.001
		<i>L. pruvoti</i>	123	36.26	0.80	
Pantelleria	PN	<i>B. europaea</i>	171	35.11	0.09	<i>p</i> < 0.001
		<i>L. pruvoti</i>	144	41.84	0.10	

n, number of individuals; SE, standard error.

p < 0.001), while in the Scilla population both species exhibited the same porosity (Table 4).

In both species and in all locations, a strong correlation was observed between bulk density and porosity. In *B. europaea*, the relationship between bulk density and porosity was 1.8–45.0 times stronger than that with micro-density, as indicated by the ratio of the *r*² values of the regressions (Table 5). In *L. pruvoti*, this relationship was even more emphasized, the correlation with porosity being 1.7–185.0 times stronger than that with micro-density (Table 6).

Since the average age of the samples differed among the sites (Table 1), analyses of correlations between SST and skeletal parameters were performed after applying to the data the method of the adjusted values in relation to age (Steel, 1980; see Goffredo et al., 2007 for an example of application on corals). In *B. europaea*, SST did not correlate with micro-density, while it was positively correlated with porosity, explaining 4.5% of its variation, and negatively correlated with bulk density, explaining 4.2% of its variation (Fig. 3). In *L. pruvoti*, SST was positively correlated with micro-density, explaining 15.4% of its variation, but showed no correlation with porosity and bulk density (Fig. 3).

4. Discussion

4.1. Relationships among skeletal parameters

In both species and in all locations, the strong relationship between bulk density and porosity was expected and indicates that the buoyant weighing technique we used gave reasonable results (Tables 5 and 6; Bucher et al., 1998). Bulk density trends were always diametrically opposed to porosity trends (Tables 2, 3, 5 and 6; Fig. 3), regardless of the trend of micro-density, thus indicating that the variations in micro-density, even when significant, were not strong enough to cause significant variations in bulk density.

4.2. Relationships between micro-density and age

Bulk density is determined by the pattern in which the material is laid down (micro-density) and by the volume of skeletal voids it encloses (porosity) (Bucher et al., 1998). Micro-density is the specific gravity of the material of which the skeleton is made. The scleractinian coral skeleton is a two-phase composite material

Table 5

Balanophyllia europaea. Correlation analysis between bulk density, micro-density and porosity at the 6 sites. The exponent and factor values are indicated only where the relationship was significant. The sites are arranged in order of increasing seawater temperature.

Population	Code	<i>n</i>	Dependent variable	Independent variable	Factor	Exponent	<i>r</i> ²	<i>r</i>
Calafuria	CL	38	Bulk density	Porosity	7.532	−0.409	0.963	0.981***
			Bulk density	Micro-density	0.160	2.462	0.241	0.491**
			Micro-density	Porosity	3.035	−0.032	0.143	0.378*
Elba	LB	17	Bulk density	Porosity	9.701	−0.490	0.956	0.978***
			Bulk density	Micro-density	0.003	6.515	0.532	0.729***
			Micro-density	Porosity	2.992	−0.036	0.417	0.646**
Palinuro	PL	49	Bulk density	Porosity	13.728	−0.581	0.931	0.965***
			Bulk density	Micro-density	0.377	1.510	0.125	0.353*
			Micro-density	Porosity	–	–	0.015	0.122
Scilla	SC	8	Bulk density	Porosity	8.436	−0.440	0.950	0.975***
			Bulk density	Micro-density	–	–	0.021	0.145
			Micro-density	Porosity	–	–	0.003	0.055
Genova	GN	23	Bulk density	Porosity	8.273	−0.435	0.920	0.959***
			Bulk density	Micro-density	–	–	0.037	0.192
			Micro-density	Porosity	–	–	0.0001	0.01
Pantelleria	PN	115	Bulk density	Porosity	14.315	−0.593	0.936	0.967***
			Bulk density	Micro-density	0.157	2.427	0.253	0.503***
			Micro-density	Porosity	3.093	−0.039	0.093	0.305**

n, number of individuals; *r*², Pearson's coefficient of determination; *r*, Pearson's correlation coefficient.

* *p* < 0.050.

** *p* < 0.010.

*** *p* < 0.001.

Table 6

Leptopsammia pruvoti. Correlation analysis between bulk density, micro-density and porosity at the 6 sites. The exponent and factor values are indicated only where the relationship was significant. The sites are arranged in order of increasing seawater temperature.

Population	Code	n	Dependent variable	Independent variable	Factor	Exponent	r ²	r
Calafuria	CL	44	Bulk density	Porosity	21.824	-0.717	0.925	0.961 ^{***}
			Bulk density	Micro-density	0.091	2.881	0.230	0.480 ^{**}
			Micro-density	Porosity	-	-	0.092	0.303
Elba	LB	42	Bulk density	Porosity	19.874	-0.692	0.924	0.961 ^{***}
			Bulk density	Micro-density	0.003	6.398	0.547	0.740 ^{***}
			Micro-density	Porosity	3.250	-0.054	0.417	0.646 ^{***}
Palinuro	PL	45	Bulk density	Porosity	8.798	-0.458	0.900	0.949 ^{***}
			Bulk density	Micro-density	-	-	0.011	0.105
			Micro-density	Porosity	-	-	0.016	0.126
Scilla	SC	29	Bulk density	Porosity	11.711	-0.536	0.950	0.975 ^{***}
			Bulk density	Micro-density	-	-	0.015	0.122
			Micro-density	Porosity	-	-	1.00E-06	0.001
Genova	GN	43	Bulk density	Porosity	19.743	-0.685	0.943	0.971 ^{***}
			Bulk density	Micro-density	-	-	0.019	0.138
			Micro-density	Porosity	-	-	0.0001	0.01
Pantelleria	PN	45	Bulk density	Porosity	13.069	-0.569	0.742	0.861 ^{***}
			Bulk density	Micro-density	-	-	0.004	0.063
			Micro-density	Porosity	1.581	0.144	0.195	0.442 ^{**}

n, number of individuals; r², Pearson's coefficient of determination; r, Pearson's correlation coefficient.

* p < 0.050.

** p < 0.010.

*** p < 0.001.

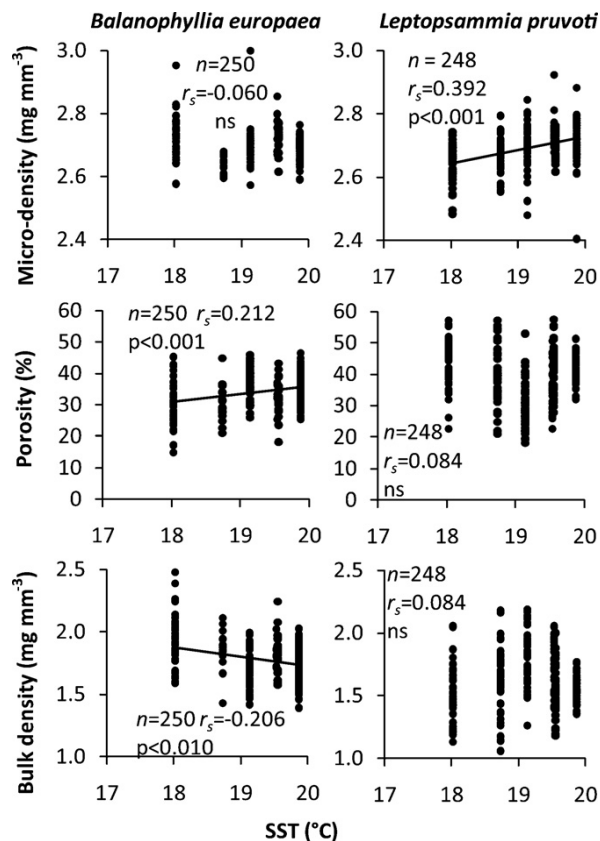


Fig. 3. Variation in the skeletal parameters of two corals, *Balanophyllia europaea* and *Leptopsammia pruvoti*, with sea surface temperature (SST). r², Spearman's determination coefficient, r_s Spearman's correlation coefficient, n number of individuals.

consisting of fiber-like crystals of aragonitic calcium carbonate phases (crystal fibers and micro-spherulites) intimately associated with an intra-crystalline organic matrix (OM) (Cuif et al., 1999). OM generally constitutes <0.1% of the total skeleton weight (Constantz and Weiner, 1988) and is believed to initiate nucleation of calcium carbonate and provide a framework for crystallographic orientation and species-specific architecture (Towe, 1972; Addadi and Weiner, 1985; Lowenstam and Weiner, 1989).

For both species, in the populations where the relationship between micro-density and age was significant (Scilla, Genova and Pantelleria for *B. europaea* and Calafuria, Genova and Pantelleria for *L. pruvoti*; Tables 2 and 3), micro-density increased from 2.6 mg mm⁻³ at minimum age (1.3–5.7 years) to 2.8 mg mm⁻³ at maximum age (9.7–17.1 years). This variation is quite relevant with respect to the density of inorganic CaCO₃ (2.94 mg mm⁻³ for aragonite and 2.71 mg mm⁻³ for calcite; Marszalek, 1982) and might be determined by the influence of OM. A decrease of intracrystalline OM content with increasing age could explain the increase of micro-density with age found in this study. As an alternative hypothesis, which is currently being tested, the production of different kinds of OM along the life cycle of the polyp could lead to the precipitation of crystal phases with different densities, thus causing the observed increase of micro-density with age. The different densities of crystal phases could result from different processes, e.g., an increased isomorphous substitution of strontium to calcium in the aragonite structure, a different polymorphic selection between calcium carbonate polymorphs (aragonite is denser than calcite) or a decrease of the relative number of low-density centers of calcification (possibly amorphous calcium carbonate; Cohen and McConnaughey, 2003) with respect to the aragonitic fibrous structure. Indeed, preliminary data on *B. europaea* skeletons show a decreasing calcite content (and increasing aragonite content) with age (S. Goffredo, personal observation), thus supporting the latter hypothesis.

4.3. Relationships between porosity and age

In *L. pruvoti*, porosity increased with age in 4 out of 6 populations (Genova, Calafuria, Elba and Scilla). Thus, younger individuals were less porous and, as they got older, the skeleton's porosity increased.

In most populations of *B. europaea*, porosity did not vary with age, while in 2 out of 6 populations (Calafuria and Pantelleria) porosity decreased with age.

To compare the average porosity between the two species, the relationships between porosity and age obtained in the present study (when significant) were used to estimate the porosity values of samples collected for previous analyses (Goffredo et al., 2007). For this earlier study, a higher number of samples of the two species had been collected within quadrats in the same sites as used for the present study. The inverse of the age–porosity relationship obtained in the present work was applied to their age, thus obtaining their porosity. For those populations with a non-significant age–porosity relationship, the average porosity value calculated in the present study was assigned to all the samples of Goffredo et al. (2007). The mean porosity of *B. europaea* was significantly lower than that of *L. pruvoti* in 4 out of 6 populations (Genova, Calafuria, Elba and Pantelleria; Student's *t*-test, $p < 0.001$). In the Palinuro population, porosity was significantly lower in *L. pruvoti* (Student's *t*-test, $p < 0.001$), while in the Scilla population both species showed no differences in porosity (Table 4). A possible explanation for the generally lower porosity of *B. europaea* compared to *L. pruvoti* might be the adaptation to two very different habitats. Several studies show that in protected habitats extension is faster, but branches are more lightly calcified, so skeletal porosity is higher than in non-protected habitats. Where water movement is high, branches are thicker, shorter and more heavily calcified, making them more resistant to wave action (Chamberlain, 1978; Oliver et al., 1983; Harriott, 1997, 1998). Indeed, *B. europaea* is found in open and light habitats often subject to currents and water motion and may need stronger skeletons, while *L. pruvoti* lives in much more sheltered environments such as crevices and caves.

4.4. Relationships between skeletal parameters and sea surface temperature

While in *B. europaea* there was an increase of porosity with increasing temperature and no correlation with micro-density, in *L. pruvoti* there was an increase of micro-density with increasing temperature and no correlation with porosity.

The relationship between temperature and porosity in *B. europaea*, which is a zooxanthellate coral, suggests a possible effect of temperature on photosynthesis in the algal symbionts. The same hypothesis was proposed in earlier studies (Goffredo et al., 2007, 2008, 2009) investigating the relationship between SST and biological parameters (population density, population stability, percentage of immature individuals, calcification) in this species. In zooxanthellate corals, photosynthesis enhances calcification (Gattuso et al., 1999; Al-Horani et al., 2005), and both processes have temperature optima (Howe and Marshall, 2002; Al-Horani, 2005). Thus, the increase of porosity with increasing SST in *B. europaea* could result from an attenuation of calcification due to an inhibition of the photosynthetic process at higher temperatures (Goffredo et al., 2009).

Alternatively, suspension feeding could also explain the increase of porosity with increasing SST observed in *B. europaea*. In the Mediterranean Sea, nutrient levels and zooplankton availability are typically lower in summer (i.e., at higher SST) than in winter (i.e., at lower SST; Coma et al., 2000; Coma and Ribes, 2003). Low nutrient and zooplankton availability causes stress and starvation in *Cladocora caespitosa* (Peirano et al., 2005a) and a summer dormancy in the metabolism of several benthic suspension feeders (Coma et al., 2000; Coma and Ribes, 2003). In colonies of the tropical corals *Stylophora pistillata* and *Galaxea fascicularis*, calcification and photosynthesis are significantly lower in starved corals than in fed ones (Houlbrèque et al., 2004; Borell and Bischof, 2008; Borell et al., 2008). The high skeletal porosity observed in *B. europaea* at high SST

might thus be explained as being a consequence of low energetic resources. However, if this were the case, the inhibition would have to be stronger in *L. pruvoti*, which is fully heterotrophic, than in *B. europaea*, which can also rely on the symbiont. In the present study, however, skeletal porosity of *L. pruvoti* did not vary with increasing temperature. Thus, the hypothesis of photosynthetic inhibition at high SST seems to be more appropriate for explaining the results regarding porosity in *B. europaea*. Yet, the role of feeding in determining the increase of porosity cannot be completely excluded, since the proportion of energy obtained by autotrophy versus heterotrophy has never been quantified for this species in the currently available literature.

In *L. pruvoti*, the fact that temperature did not correlate with porosity could be due to the absence of zooxanthellae, and thus the lack of a physiological dependence of calcification on photosynthesis. However, the increase of micro-density with increasing temperature observed in *L. pruvoti* is intriguing. A possible explanation could be that aragonite, whose density is greater than that of calcite (2.94 mg mm^{-3} for aragonite vs. 2.71 mg mm^{-3} for calcite; Marszalek, 1982), is more stable at high temperatures than is calcite. In many carbonate-producing taxa, the precipitation of biominerals depends on several aspects of the environment they live in, such as temperature and chemistry, which strongly influence aragonite and magnesium calcite deposition (Morse et al., 1997; Stanley and Hardie, 1998; Montañez, 2002; Skinner and Jahren, 2003; Feely et al., 2004; Smith and Key, 2004). In particular, the abundance of various polymorphs of calcium carbonate strongly depends on SST (Wray and Daniels, 1957; Ogino et al., 1987). Calcite is the dominant polymorph at low temperatures. With increasing temperature, calcite abundance decreases in favor of aragonite (Sawada, 1997). High-Mg calcites and aragonite are predominantly associated with warm tropical to subtropical waters and low-Mg calcite levels are generally found at higher latitudes or in cold, deep waters (Lopez et al., 2009). An increase of aragonite with increasing temperature could cause the increase of micro-density with temperature in *L. pruvoti* found in the present study (Fig. 3).

5. Conclusion

In conclusion, it is hypothesized that high SST has a negative impact on the zooxanthellate *B. europaea*, since it compromises the photosynthetic efficiency of its symbionts, lowering its skeletal resistance due to increasing porosity. In contrast, the porosity of the azooxanthellate *L. pruvoti* is unaffected by temperature, and the skeletal resistance of this species may even benefit from the increased micro-density achieved in warmer waters. These results have to be considered in the context of global climate change, since they highlight possible differences of these two coral species in their sensitivity/tolerance to temperature change. Interestingly, *B. europaea*, which can count on both heterotrophy and symbiotic algae for its nourishment, seems to be negatively affected by increasing temperatures, while *L. pruvoti*, which is fully heterotrophic, seems to be tolerant to higher temperatures. It seems likely that photosynthesis plays a role in determining the different sensibilities of these two species, and experimental measurements of photosynthesis at different temperatures may clarify its role in determining the observed patterns of skeletal parameters.

Acknowledgments

The research leading to these results has received funding from the European Research Council under the European Union's Seventh Framework Program (FP7/2007–2013)/ERC grant agreement no. 249930 (CoralWarm: Corals and global warming: the

Mediterranean versus the Red Sea). We wish to thank L. Bortolazzi, M. Ghelia, G. Neto, and L. Tomesani for their underwater assistance in collecting the samples. The diving centers Centro Immersioni Pantelleria, Il Pesciolino, Polo Sub, and Sub Maldive supplied logistic assistance in the field. The Bologna Scuba Team collaborated in the underwater activities. The Marine Science Group (<http://www.marinesciencegroup.org>) and the Department of Physics of the University of Bologna supplied scientific, technical, and logistical support. This research was financed by the Associazione dei Tour Operator Italiani (ASTOI), the Marine and Freshwater Science Group Association (<http://www.msgassociation.net>), and the Ministry of Education, University and Research (MIUR). Two anonymous reviewers supplied comments which significantly improved the manuscript quality. The experiments complied with current Italian law.

References

- Addadi, L., Weiner, S., 1985. Interactions between acidic proteins and crystals: stereochemical requirements in biomineralization. *Proc. Natl. Acad. Sci. U.S.A.* 82, 4110–4114.
- Al-Horani, F.A., 2005. Effects of changing seawater temperature on photosynthesis and calcification in the scleractinian coral *Galaxea fascicularis*, measured with O₂, Ca²⁺ and pH microsensors. *Sci. Mar.* 69, 347–354.
- Al-Horani, F.A., Ferdelman, T., Al-Moghrabi, S.M., de Beer, D., 2005. Spatial distribution of calcification and photosynthesis in the scleractinian coral *Galaxea fascicularis*. *Coral Reefs* 24, 173–180.
- Altman, D.G., 1991. *Practical Statistics for Medical Research*. Chapman & Hall, London.
- Ammar, M.S., Mohammed, T.A., Mahmoud, M.A., 2005. Skeletal density (strength) of some corals in an actively flooding and a non flooding site, south Marsa Alam, Red Sea, Egypt. *J. Egypt. Germ. Soc. Zool.* 46, 125–139.
- Bak, R.P.M., 1973. Coral weight increment in situ. A new method to determine coral growth. *Mar. Biol.* 20, 40–49.
- Bak, R.P.M., 1974. Available light and other factors influencing growth of stony corals through the year in Curacao. In: *Proceedings of the 2nd International Coral Reef Symposium*, vol. 2, pp. 229–233.
- Bak, R.P.M., 1976. The growth of coral colonies and the importance of crustose coralline algae and burrowing sponges in relation with carbonate accumulation. *Neth. J. Sea Res.* 10, 285–337.
- Ballesteros, E., 2006. Mediterranean coralligenous assemblages: a synthesis of the present knowledge. *Oceanogr. Mar. Biol. Annu. Rev.* 44, 123–195.
- Barnes, D.J., Devereux, M.J., 1988. Variations in skeletal architecture associated with density banding in the hard corals *Porites*. *J. Exp. Mar. Biol. Ecol.* 121, 37–54.
- Borell, E.M., Bischof, K., 2008. Feeding sustains photosynthetic quantum yield of a scleractinian coral during thermal stress. *Oecologia* 157, 593–601.
- Borell, E.M., Yuliantri, A.R., Bischof, K., Richter, C., 2008. The effect of heterotrophy on photosynthesis and tissue composition of two scleractinian corals under elevated temperature. *J. Exp. Mar. Biol. Ecol.* 364, 116–123.
- Bosscher, H., 1993. Computerized tomography and skeletal density of coral skeletons. *Coral Reefs* 12, 97–103.
- Bucher, D.J., Harriott, V.J., Roberts, L.G., 1998. Skeletal micro-density, porosity and bulk density of acroporid corals. *J. Exp. Mar. Biol. Ecol.* 228, 117–136.
- Carricart-Ganivet, J.P., 2004. Sea surface temperature and the growth of the West Atlantic reef-building coral *Montastrea annularis*. *J. Exp. Mar. Biol. Ecol.* 302, 249–260.
- Cerrano, C., Bavestrello, G., Bianchi, C.N., Cattaneo-Vietti, R., Bava, S., Morganti, C., Morri, C., Picco, P., Sara, G., Schiaparelli, S., Siccardi, A., Spongia, F., 2000. A catastrophic mass-mortality episode of gorgonians and other organisms in the Ligurian Sea (NW Mediterranean), summer 1999. *Ecol. Lett.* 3, 284–293.
- Chamberlain, J.A., 1978. Mechanical properties of coral skeleton: compressive strength and its adaptive significance. *Paleobiology* 4, 419–435.
- Cohen, A.L., McConnaughey, T.A., 2003. Geochemical perspectives on coral mineralization. *Rev. Miner. Geochem.* 54, 151–187.
- Coma, R., Ribes, M., 2003. Seasonal energetic constraints in Mediterranean benthic suspension feeders: effects at different levels of ecological organization. *Oikos* 101, 205–215.
- Coma, R., Ribes, M., Gili, J.M., Zabala, M., 2000. Seasonality in coastal ecosystems. *Trends Ecol. Evol.* 12, 448–453.
- Coma, R., Ribes, M., Serrano, E., Jimenez, E., Salat, J., Pascual, J., 2009. Global warming-enhanced stratification and mass mortality events in the Mediterranean. *Proc. Natl. Acad. Sci. U.S.A.* 106, 6176–6181.
- Constantz, B., Weiner, S., 1988. Acidic macromolecules associated with the mineral phase of scleractinian coral skeletons. *J. Exp. Zool.* 248, 253–258.
- Crossland, C.J., 1984. Seasonal variations in the rates of calcification and productivity in the coral *Acropora formosa* on a high latitude reef. *Mar. Ecol. Prog. Ser.* 15, 135–140.
- Cuif, J.P., Dauphin, Y., Gautret, P., 1999. Compositional diversity of soluble mineralizing matrices in some recent coral skeletons compared to fine-scale growth structures of fibres: discussion of consequences for biomineralization and diagenesis. *Int. J. Earth Sci.* 88, 582–592.
- Dar, M.A., Mohammed, T.A., 2009. Seasonal variations in the skeletogenesis process in some branching corals of the Red Sea. *Thalassas* 25, 31–44.
- Davies, P.S., 1989. Short-term growth measurements of corals using an accurate buoyant weighing technique. *Mar. Biol.* 101, 389–395.
- Dustan, P., 1975. Growth and form in the reef-building coral *Montastrea annularis*. *Mar. Biol.* 33, 101–107.
- Franzisket, L., 1964. The metabolic intensity of the reef corals and their ecological, phylogenetic and sociological significance. *Z. Vergl. Physiol.* 49, 91–113 (in German).
- Feeley, R.A., Sabine, C.L., Lee, K., Berelson, W., Kleypas, J., Fabry, V.J., Millero, F.J., 2004. Impact of anthropogenic CO₂ on the CaCO₃ system in the ocean. *Science* 305, 362–366.
- Garrabou, J., Coma, R., Bensoussan, N., Bally, M., Chevaldonne, P., Cigliano, M., Diaz, D., Harmelin, J.G., Gambi, M.C., Kersting, D.K., Ledoux, J.B., Lejeune, C., Linares, C., Marschal, C., Perez, T., Ribes, M., Romano, J.C., Serrano, E., Teixido, N., Torrens, O., Zabala, M., Zuberer, F., Cerrano, C., 2009. Mass mortality in the NW Mediterranean rocky benthic communities: effects of the 2003 heat wave. *Glob. Change Biol.* 15, 1090–1103.
- Gattuso, J.P., Allemand, D., Frankignoulle, M., 1999. Photosynthesis and calcification at cellular, organismal and community levels in coral reefs: a review on interactions and control by carbonate chemistry. *Am. Zool.* 39, 160–183.
- Goffredo, S., Zaccanti, F., 2004. Laboratory observations of larval behavior and metamorphosis in the Mediterranean solitary coral *Balanophyllia europaea* (Scleractinia, Dendrophylliidae). *Bull. Mar. Sci.* 74, 449–458.
- Goffredo, S., Arnone, S., Zaccanti, F., 2002. Sexual reproduction in the Mediterranean solitary coral *Balanophyllia europaea* (Scleractinia, Dendrophylliidae). *Mar. Ecol. Prog. Ser.* 229, 83–94.
- Goffredo, S., Mattioli, G., Zaccanti, F., 2004. Growth and population dynamics model of the Mediterranean solitary coral *Balanophyllia europaea* (Scleractinia, Dendrophylliidae). *Coral Reefs* 23, 433–443.
- Goffredo, S., Airo, V., Radetić, J., Zaccanti, F., 2006. Sexual reproduction of the solitary sunset cup coral *Leptopsammia pruvoti* (Scleractinia, Dendrophylliidae) in the Mediterranean. 2. Quantitative aspects of the annual reproductive cycle. *Mar. Biol.* 148, 923–932.
- Goffredo, S., Caroselli, E., Mattioli, G., Pignotti, E., Zaccanti, F., 2007. Variation in biometry and demography of solitary corals with environmental factors in the Mediterranean Sea. *Mar. Biol.* 152, 351–361.
- Goffredo, S., Caroselli, E., Mattioli, G., Pignotti, E., Zaccanti, F., 2008. Relationships between growth, population structure and sea surface temperature in the temperate solitary coral *Balanophyllia europaea* (Scleractinia, Dendrophylliidae). *Coral Reefs* 27, 623–632.
- Goffredo, S., Caroselli, E., Mattioli, G., Pignotti, E., Dubinsky, Z., Zaccanti, F., 2009. Inferred level of calcification decreases along an increasing temperature gradient in a Mediterranean endemic coral. *Limnol. Oceanogr.* 54, 930–937.
- Goffredo, S., Caroselli, E., Mattioli, G., Zaccanti, F., 2010. Growth and population dynamic model for the non-zooxanthellate temperate solitary coral *Leptopsammia pruvoti* (Scleractinia, Dendrophylliidae). *Mar. Biol.* 157, 2603–2612.
- Goreau, T.F., Goreau, N.I., 1959. The physiology of skeleton formation in corals. II. Calcium deposition by hermatypic corals under different conditions. *Biol. Bull.* 117, 239–250.
- Graus, R.R., Macintyre, I.G., 1982. Variation in growth forms of the reef coral *Montastrea annularis* (Ellis and Solander): a quantitative evaluation of growth response to light distribution using computer simulation. In: Rützler, K., Macintyre, I.G. (Eds.), *The Atlantic Barrier Reef Ecosystem at Carrie Bow Cay, Belize*. Smithsonian Inst. Press, Washington, DC, pp. 441–465.
- Harley, C.D.G., Hughes, A.R., Hultgren, K.M., Miner, B.G., Sorte, C.J.B., Thornber, C.S., Rodriguez, L.F., Tomanek, L., Williams, S.L., 2006. The impacts of climate change in coastal marine systems. *Ecol. Lett.* 9, 228–241.
- Harriott, V.J., 1997. Skeletal bulk density of the scleractinian coral *Acropora formosa* (Dana 1846) in tropical and subtropical Western Australia. In: Wells, F.E. (Ed.), *The Flora and Fauna of the Houtman Abrolhos Islands, Western Australia*. Western Australian Museum Publications, Perth, pp. 75–82.
- Harriott, V.J., 1998. Growth of the staghorn coral *Acropora formosa* at Houtman Abrolhos, Western Australia. *Mar. Biol.* 132, 319–325.
- Harriott, V.J., 1999. Coral growth in subtropical eastern Australia. *Coral Reefs* 15, 281–291.
- Harriott, V.J., Banks, S.A., 2002. Latitudinal variation in coral communities in eastern Australia: a qualitative biophysical model of factors regulating coral reefs. *Coral Reefs* 21, 83–94.
- Helmle, K.P., Dodge, R.E., Ketcham, R.A., 2000. Skeletal architecture and density banding in *Diploria strigosa* by X-ray computed tomography. *Proceedings of the 9th International Coral Reef Symposium* 1, 365–371.
- Highsmith, R.C., 1979. Coral growth rates and environmental control of density banding. *J. Exp. Mar. Biol. Ecol.* 37, 105–125.
- Houlibrèque, F., Tambutté, E., Allemand, D., Ferrier-Pagès, C., 2004. Interactions between zooplankton feeding, photosynthesis and skeletal growth in the scleractinian coral *Stylophora pistillata*. *J. Exp. Mar. Biol. Ecol.* 207, 1461–1469.
- Howe, S.A., Marshall, A.T., 2002. Temperature effects on calcification rate and skeletal deposition in the temperate coral *Plesiastrea versipora* (Lamarck). *J. Exp. Mar. Biol. Ecol.* 275, 63–81.
- Hughes, T.P., 1987. Skeletal density and growth form of corals. *Mar. Ecol. Prog. Ser.* 35, 259–266.
- Jiménez, C., Cortés, J., 1993. Density and compressive strength of the coral *Siderastrea sidera* (Scleractinia: Siderastreidae): intraspecific variability. *Rev. Biol. Trop.* 41, 39–43.

- Jokiel, P.L., Coles, S.L., 1978. Effects of temperature on the mortality and growth of Hawaiian reef corals. *Mar. Biol.* 43, 201–208.
- Jokiel, P.L., Maragos, J.E., Franzisket, L., 1978. Coral growth: buoyant weight technique. In: Stoddart, D.R., Johannes, R.E. (Eds.), *Coral Reef: Research Methods*. UNESCO Publishing, Paris, pp. 379–396.
- Kain, J.M., 1989. The seasons in the subtidal. *Br. Phycol. J.* 24, 203–215.
- Karl, T.R., Trenberth, K.E., 2003. Modern global climate change. *Science* 302, 1175–1177.
- Kleypas, J.A., McManus, J.W., Menez, L.A.B., 1999. Environmental limits to coral reef development: where do we draw the line? *Am. Zool.* 39, 146–159.
- Lejeune, C., Chevaldonné, P., Pergent-Martini, C., Boudouresque, C.F., Pérez, T., 2010. Climate change effects on a miniature ocean: the highly diverse, highly impacted Mediterranean Sea. *Trends Ecol. Evol.* 25, 250–260.
- Liddle, M.J., Kay, A.M., 1987. Resistance, survival and recovery of trampled corals on the Great Barrier Reef. *Biol. Conserv.* 42, 1–18.
- Lopez, O., Zuddas, P., Faivre, O., 2009. The influence of temperature and seawater composition on calcite crystal growth mechanisms and kinetics: implications for Mg incorporation in calcite lattice. *Geochim. Cosmochim. Acta* 73, 337–347.
- Lough, J.M., Barnes, D.J., 2000. Environmental controls on growth of the massive coral *Porites*. *J. Exp. Mar. Biol. Ecol.* 245, 225–243.
- Lowenstam, H.A., Weiner, S., 1989. *On Biomineralization*. Oxford University Press, New York.
- Mann, G.S., 1994. Distribution, abundance and life history of the reef coral *Favia fragum* (Esper) in Barbados: effects of eutrophication and of the black sea urchin *Diadema antillarum* (Philippi). M. Sc. Thesis, McGill University, Montreal.
- Marszalek, D.S., 1982. The role of heavy skeletons in vertical movements of non-motile zooplankton. *Mar. Freshw. Behav. Physiol.* 8, 295–303.
- Marubini, F., Ferrier-Pages, C., Cuif, J.P., 2003. Suppression of skeletal growth in scleractinian corals by decreasing ambient carbonate-ion concentration: a cross-family comparison. *Proc. R. Soc. Lond. B* 270, 179–184.
- Montañez, I.P., 2002. Biological skeletal carbonate records changes in major ion chemistry of paleo-oceans. *Proc. Natl. Acad. Sci. U.S.A.* 99, 5852–5854.
- Morse, J.W., Wang, Q., Tsio, M.Y., 1997. Influence of temperature and Mg:Ca ratio on CaCO₃ precipitates from seawater. *Geology* 25, 85–87.
- Ogino, T., Suzuki, T., Sawada, K., 1987. The formation and transformation mechanism of calcium carbonate in water. *Geochim. Cosmochim. Acta* 51, 2757–2767.
- Oliver, J.K., Chalker, B.E., Dunlap, W.C., 1983. Bathymetric adaptations of reef-building corals at Davies Reef, Great Barrier Reef, Australia. I. Long-term growth responses of *Acropora formosa* (Dana 1846). *J. Exp. Mar. Biol. Ecol.* 73, 11–35.
- Peirano, A., Morri, C., Bianchi, C.N., 1999. Skeleton growth and density pattern of the temperate, zooxanthellate scleractinian *Cladocora caespitosa* from the Ligurian Sea (NW Mediterranean). *Mar. Ecol. Prog. Ser.* 185, 195–201.
- Peirano, A., Abbate, M., Cerrati, G., Difesa, V., Peroni, C., Rodolfo-Metalpa, R., 2005a. Monthly variations in calyx growth, polyp tissue, and density banding of the Mediterranean scleractinian *Cladocora caespitosa* (L.). *Coral Reefs* 24, 404–409.
- Peirano, A., Damasso, V., Montefalcone, M., Morri, C., Bianchi, C.N., 2005b. Effects of climate, invasive species and anthropogenic impacts on the growth of the seagrass *Posidonia oceanica* (L.) Delile in Liguria (NW Mediterranean Sea). *Mar. Pollut. Bull.* 50, 817–822.
- Perez, T., Garrabou, J., Sartoretto, S., Harmelin, J.G., Francour, P., Vacelet, J., 2000. Mass mortality of marine invertebrates: an unprecedented event in the Northwestern Mediterranean. *C. R. Acad. Sci. Paris, Ser. III* 323, 853–865.
- Potvin, C., Roff, D.A., 1993. Distribution-free and robust statistical methods: viable alternatives to parametric statistics? *Ecology* 74, 1617–1628.
- Richardson, A.J., Poloczanska, E.S., 2008. Under-resourced, under threat. *Science* 320, 1294–1295.
- Rodgers, K., Cox, E., Newston, C., 2003. Effects of mechanical fracturing and experimental trampling on Hawaiian corals. *Environ. Manage.* 31, 377–384.
- Rodolfo-Metalpa, R., Bianchi, C.N., Peirano, A., Morri, C., 2000. Coral mortality in NW Mediterranean. *Coral Reefs* 19, 24.
- Romano, J.C., Bensoussan, N., Younes, W.A.N., Arhac, D., 2000. Thermal anomaly in the waters of the Gulf of Marseilles during summer 1999. A partial explanation of the mortality of certain fixed invertebrates? *C. R. Acad. Sci. Paris Ser. III* 323, 415–427.
- Sawada, K., 1997. The mechanisms of crystallization and transformation of calcium carbonates. *Pure Appl. Chem.* 69, 921–928.
- Schneider, R.C., Smith, S.V., 1982. Skeletal Sr content and density in *Porites* spp. in relation to environmental factors. *Mar. Biol.* 66, 121–131.
- Schumacher, H., Plewka, M., 1981. The adaptive significance of mechanical properties versus morphological adjustments in skeletons of *Acropora palmata* and *Acropora cervicornis* (Cnidaria, Scleractinia). In: *Proceedings of the 4th International Coral Reef Symposium*, vol. 2, pp. 121–128.
- Shi, Q., Zhao, M.X., Zhang, Q.M., Yu, K.F., Chen, T.R., Li, S., Wang, H.K., 2009. Estimate of carbonate production by scleractinian corals at Luhuitou fringing reef, Sanya, China. *Chin. Sci. Bull.* 54, 696–705.
- Skinner, H.C.W., Jahren, A.H., 2003. Biomineralization. In: Schlesinger, W.H. (Ed.), *Treatise on Geochemistry*. Elsevier, Amsterdam, pp. 117–184.
- Smith, A.M., Key Jr., M.M., 2004. Controls, variation, and a record of climate change in detailed stable isotope record in a single bryozoan skeleton. *Quat. Res.* 61, 123–133.
- Solomon, S., Qin, D., Manning, M., Marquis, M., Averyt, K., Tignor, M.M.B., Le Roy Miller Jr., H., Chen, Z., 2007. *Climate Change 2007: The Physical Science Basis*. Contribution of Working Group I to the Fourth Assessment Report of the Intergovernmental Panel on Climate Change. Cambridge University Press, Cambridge, UK.
- Spisic, M., Böröcz, Z., Bahlburg, H., 2008. The role of porosity in discriminating between tsunami and hurricane emplacement of boulders—a case study from the Lesser Antilles, southern Caribbean. *Earth Planet. Sci. Lett.* 268, 384–396.
- Stanley, S.M., Hardie, L.A., 1998. Secular oscillations in carbonate mineralogy of reef-building and sediment producing organisms driven by tectonically forced shifts in seawater chemistry. *Palaeogeogr. Palaeoclimat. Palaeoecol.* 144, 3–19.
- Steel, R.G.D., 1980. *Principles and Procedures of Statistics: A Biometrical Approach*, 2nd ed. McGraw-Hill College, New York.
- Tanzil, J.T.I., Brown, B.E., Tudhope, A.W., Dunne, R.P., 2009. Decline in skeletal growth of the coral *Porites lutea* from the Andaman Sea. South Thailand between 1984 and 2005. *Coral Reefs* 28, 519–528.
- Towe, K.M., 1972. Invertebrate shell structure and the organic matrix concept. *Biominer. Res. Rep.* 4, 2–14.
- Tsimplis, M.N., Zervakis, V., Josey, S., Peeneva, E., Struglia, M.V., Stanev, E., Lionello, P., Malanotte-Rizzoli, P., Artale, V., Theocharis, A., Tragou, E., Oguz, T., 2006. Changes in the oceanography of the Mediterranean Sea and their link to climate variability. In: Lionello, P., Malanotte-Rizzoli, P., Boscolo, R. (Eds.), *Mediterranean Climate Variability*. Elsevier, Amsterdam, pp. 227–282.
- Tunncliffe, V., 1979. The role of boring sponges in coral fracture. In: Levi, C., Bowry-Esnau, N. (Eds.), *Biologie des Spongiaires*, vol. 291. *Colloq. Int. C.N.R.S.*, pp. 309–315.
- von Bertalanffy, L., 1938. A quantitative theory of organic growth (inquiries on growth laws II). *Hum. Biol.* 10, 181–213.
- Vongsavat, V., Winotai, P., Meejoo, S., 2006. Phase transitions of natural corals monitored by ESR spectroscopy. *Nucl. Instr. Meth. Phys. Res. B* 243, 167–173.
- Vosburgh, F., 1982. *Acropora reticulata*: structure, mechanics and ecology of a reef coral. *Proc. R. Soc. Lond. B* 214, 481–499.
- Wainwright, S.A., Biggs, W.D., Curry, J.D., Gosline, J.M., 1976. *Mechanical Design in Organisms*. Edward Arnold, London.
- Walther, G.R., Post, E., Convey, P., Menzel, A., Parmesan, C., Beebee, T.J.C., Fromentin, J.M., Hoegh-Guldberg, O., Bairlein, F., 2002. Ecological responses to recent climate change. *Nature* 416, 389–395.
- Wray, J.L., Daniels, F., 1957. Precipitation of calcite and aragonite. *J. Am. Chem. Soc.* 79, 2031–2034.
- Zibrowius, H., 1980. The scleractinians of the Mediterranean and of the North-Eastern Atlantic. *Mem. Inst. Oceanogr.* 11, 1–284 (in French).

**Chapter 3:
A Time-Domain Nuclear Magnetic
Resonance Study of Mediterranean
Scleractinian Corals Reveals Skeletal-
Porosity Sensitivity to Environmental
Changes**

Published in Environmental Science & Technology

A Time-Domain Nuclear Magnetic Resonance Study of Mediterranean Scleractinian Corals Reveals Skeletal-Porosity Sensitivity to Environmental Changes

Paola Fantazzini,^{*,†,‡} Stefano Mengoli,[§] Stefania Evangelisti,[†] Luca Pasquini,[†] Manuel Mariani,^{†,‡} Leonardo Brizi,^{†,‡} Stefano Goffredo,^{||} Erik Caroselli,^{||} Fiorella Prada,^{||} Giuseppe Falini,[⊥] Oren Levy,[@] and Zvy Dubinsky[@]

[†]Department of Physics and Astronomy, University of Bologna, Viale Berti Pichat 6/2, 40127 Bologna, Italy

[‡]Centro Enrico Fermi, 00184 Roma, Italy

[§]Management Department, University of Bologna, Via Capo di Lucca 34, 40126 Bologna, Italy

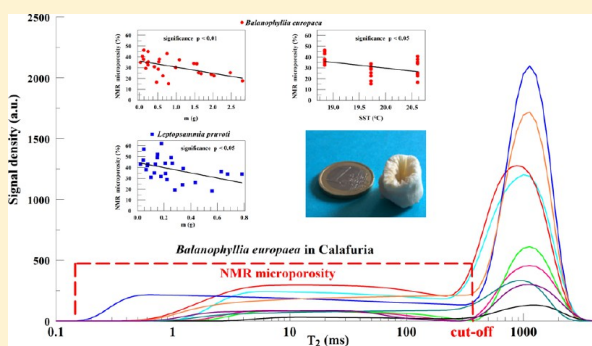
^{||}Marine Science Group, Department of Biological, Geological and Environmental Sciences, Section of Biology, University of Bologna, Via F. Selmi 3, 40126 Bologna, Italy

[⊥]Department of Chemistry, "G. Ciamician", University of Bologna, Via F. Selmi 2, 40126 Bologna, Italy

[@]The Mina and Everard Goodman Faculty of Life Sciences, Bar-Ilan University, Ramat-Gan 52900, Israel

Supporting Information

ABSTRACT: Mediterranean corals are a natural model for studying global warming, as the Mediterranean basin is expected to be one of the most affected regions and the increase in temperature is one of the greatest threats for coral survival. We have analyzed for the first time with time-domain nuclear magnetic resonance (TD-NMR) the porosity and pore-space structure, important aspects of coral skeletons, of two scleractinian corals, *Balanophyllia europaea* (zooxanthellate) and *Leptopsammia pruvoti* (nonzooxanthellate), taken from three different sites on the western Italian coast along a temperature gradient. Comparisons have been made with mercury intrusion porosimetry and scanning electron microscopy images. TD-NMR parameters are sensitive to changes in the pore structure of the two coral species. A parameter, related to the porosity, is larger for *L. pruvoti* than for *B. europaea*, confirming previous non-NMR results. Another parameter representing the fraction of the pore volume with pore sizes of less than 10–20 μm is inversely related, with a high degree of statistical significance, to the mass of the specimen and, for *B. europaea*, to the temperature of the growing site. This effect in the zooxanthellate species, which could reduce its resistance to mechanical stresses, may depend on an inhibition of the photosynthetic process at elevated temperatures and could have particular consequences in determining the effects of global warming on these species.



INTRODUCTION

Corals and Global Warming. Global climate change is the defining environmental issue of our times and is expected to profoundly affect all levels of ecological hierarchies and a broad array of terrestrial and marine ecosystems.^{1–5} Marine communities are expected to be affected more than terrestrial ones by the effects of climate change,⁶ especially in temperate areas.⁷ Thus, the Mediterranean basin⁸ represents a natural focus of interest for researchers and at the same time a natural laboratory for modeling and predicting climate change and its ecological effects. In particular, the increase in temperature is one of the greatest threats for corals, which can be considered as a probe of global warming effects, as it triggers bleaching events and widespread mortality.^{9–11} Several recent mass

mortality events of Mediterranean corals have been reported as being related to high temperatures.^{12–16}

This study focuses on two scleractinian species of the Mediterranean Sea, already studied as a model for climate change: *Balanophyllia europaea* (Risso, 1826) and *Leptopsammia pruvoti* (Lacaze-Duthiers, 1897)¹⁷ (Figure 1). *B. europaea* is a solitary, zooxanthellate (i.e., symbiotic with unicellular algae named zooxanthellae) coral, endemic to the Mediterranean Sea. Its distribution is limited to depths of 0–50 m because of its symbiosis with zooxanthellae, which require light.^{17–19} *L.*

Received: November 12, 2012

Revised: September 13, 2013

Accepted: October 21, 2013

Published: October 21, 2013

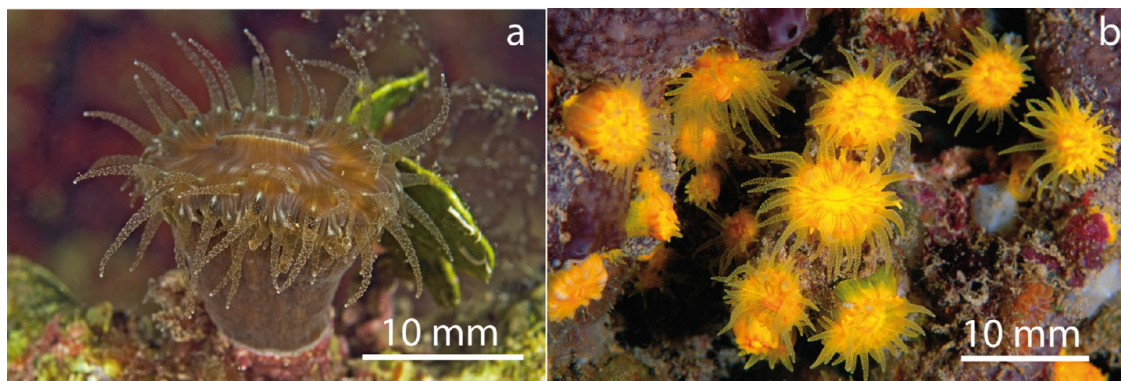


Figure 1. (a) Living polyp of *B. europaea* and (b) several living polyps of *L. pruvoti*.

pruvoti is a nonzooxanthellate and solitary scleractinian coral, distributed in the Mediterranean basin and along the European Atlantic coast from Portugal to Southern England and Ireland. Its distribution is limited to semienclosed rocky habitats, under overhangs, in caverns, and in small crevices, at depths of 0–70 m.^{17,18} Corals were collected at three different Italian sites (see Figure 2), where the porosity of the two species has been

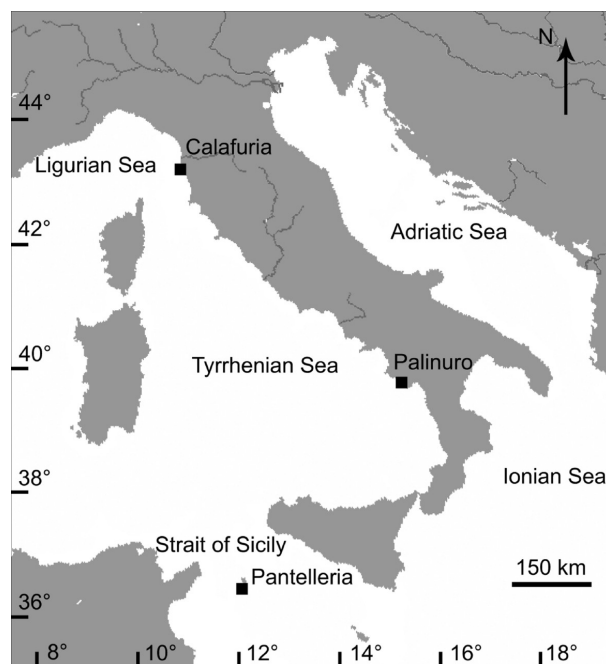


Figure 2. Map of the sites in Italy where corals were collected.

studied previously,¹⁷ along a latitude and sea surface temperature (SST) gradient. Temperature, the variation of which is mainly influenced by latitude,²⁰ is linked to coral biometry, physiology, and demography.^{21–23}

Coral Porosity and Pore-Size Distribution. The porosity (ratio of pore volume to sample volume) and pore-space structure of mineralized tissues are crucially important in determining overall properties and biological functions, such as the coral skeleton resistance to natural and anthropogenic breakage. They are important parameters for studying the growth of scleractinian corals and the effects of abiotic and

anthropogenic influences on coral reefs.²⁴ Of additional interest is a good knowledge of the role of porosity in diagenesis.

The measured values of these parameters depend on the measurement methods^{24,25} and can present spatial variations.²⁶ This could be the reason why their dependence on environmental conditions remains largely unstudied, notwithstanding their importance and their variation with factors such as exposure, temperature, latitude, depth, and species.

Recent investigations^{17,19,27} have shown that along the Italian coast the porosity of *B. europaea* is positively correlated with SST. There is concern for the future of this species^{17,27,28} in relation to the current predictions of global warming by the Intergovernmental Panel on Climate Change.⁷ On the other hand, for *L. pruvoti*, both SST and solar radiation do not seem to influence significantly the porosity or space colonization potential.^{17,19,29} An important aspect is the possible hierarchical structure of the porosity. Recently,³⁰ the flaw tolerance in nacre has been ascribed to the nanoparticle architecture of the aragonite platelet, which makes a crack propagate in an intergranular manner. The structure of porous media at different length scales is of great importance also in the use of corals as potential bone graft substitute material.³¹

Porosity and pore-size distributions can be investigated by many methods.^{32–36} The results strongly depend on the physical principles adopted and on the assumptions of pore shape and connectivity (see the Supporting Information). Porosity and pore-size distributions determined by mercury intrusion porosimetry (MIP) for eight different coral species³⁶ showed large differences, with diameters ranging from 0.2 to 100 μm . However, it has been emphasized that particle compression and rupture can result from the high Hg pressure used. Time-domain nuclear magnetic resonance (TD-NMR)³⁷ has the advantage of being nondestructive and noninvasive. TD-NMR and in particular magnetic resonance relaxometry of ^1H nuclei of water saturating the pore space are efficient tools for investigating pore-space structure. Known since the 1950s,^{38,39} and validated over time by comparison with MIP and, for specific surface, the Brunauer, Emmett, Teller (BET) method, it is now widely applied.^{40–52} It is particularly useful for porous media with wide pore-sizes distributions, like those of corals. In this paper, the distributions of the local transverse relaxation time (T_2) of ^1H of water saturating the pore space of the cleaned coral skeletons, corresponding to distributions of “NMR pore sizes”, are used (more details on NMR and surface effects in the Supporting Information). To the best of our

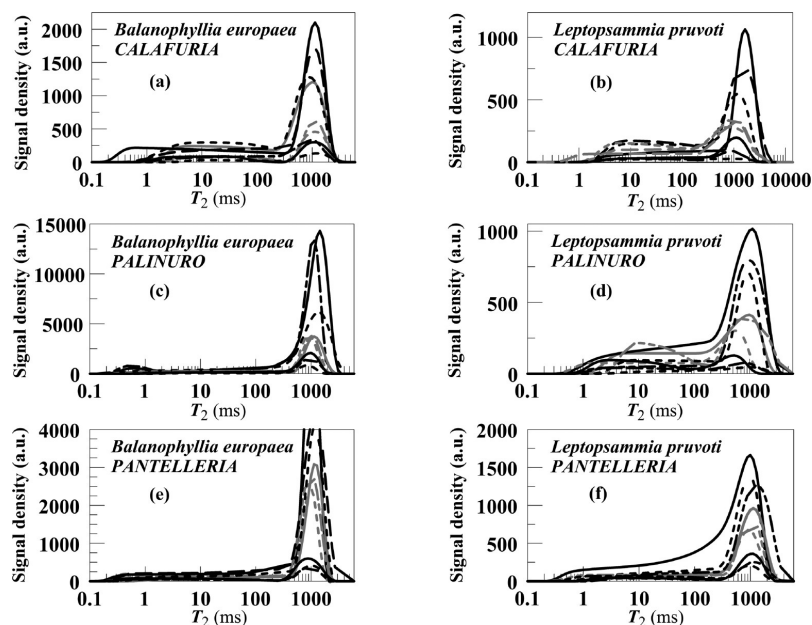


Figure 3. T_2 relaxation time distributions of the ^1H NMR signal from samples of cleaned skeletons of *B. europaea* (left) and *L. pruvoti* (right), after water saturation of the connected pore space. The samples were from three different sites. Distributions from all corals are represented (nine corals for each site). The sites were Calafuria (a and b), Palinuro (c and d), and Pantelleria (e and f). The total NMR signal (S_{NMR}) is represented by the area below each T_2 distribution and is proportional to the amount of water saturating the pore space and, therefore, to the volume of the connected pore space itself.

knowledge, this is the first time that this technique has been applied in this kind of investigation of corals.

MATERIALS AND METHODS

Corals. Specimens of *B. europaea* and *L. pruvoti* (54 specimens in all) were randomly collected from three sites: Calafuria (CL), Palinuro (PL), and Pantelleria Isle (PN) (see Figure 2). Coral tissue was totally removed, and corals were cleaned as described in ref 17. The skeletons were weighed to determine the mass (m). The total volume (V_T) was determined,¹⁹ including the volume of the oral cavity. Then the specimens were saturated with water for NMR measurements. Further details are reported in the Supporting Information.

Total NMR Signal, Microporosity, and Cutoff Definitions. The total NMR signal (S_{NMR}), represented by the area below each T_2 distribution, is proportional to the volume of water saturating the pore-space volume (V_p). This signal divided by the total sample volume gives a value proportional to the total porosity of the specimen (see the Supporting Information). The fraction of water with relaxation times over a given interval of the distribution corresponds to the pore volume fraction over a corresponding pore-size range. “NMR microporosity”, “microporosity” for short, will indicate the fraction of V_p where the smaller pores are weakly coupled by water diffusion to the large ones on the local relaxation time scale. This can be accomplished if the slope of the distribution shows a strong increase at a certain T_2 value, to be chosen as the point of separation between “smaller” and “larger” pores. This relaxation time will be called the “cutoff”. The microporosity is then defined as the fraction of ^1H signal with a T_2 smaller than the cutoff, divided by the total ^1H signal. Operatively, it is the ratio of the area under the distribution

for T_2 smaller than the cutoff to the total area under the distribution.

Statistical Analysis. Statistical analysis was performed using Statistical Package STATA 9.0 (StataCorp LP). To test the significance of the differences among species and growth sites, parametric and nonparametric tests were performed. Multivariate analyses were conducted using both ordinary least squares (OLS) robust to outliers and a nonparametric bootstrapping regression procedure following Efron,⁵³ applied to check the robustness of the results, that could be affected by small sample bias. The models are described by the function

$$y_i = a + b_1 m_i + b_2 \text{SST}_i + \varepsilon_i \quad (1)$$

where index i refers to the n observations, y_i is the value of the dependent variable, and ε_i is the corresponding error. Parameters a and b_j ($j = 1$ or 2) are the best fit parameters, to be determined by OLS referring to the independent variables m and SST. More details can be found in the Supporting Information.

RESULTS AND DISCUSSION

Figure 3 shows the T_2 distributions of all *B. europaea* and *L. pruvoti* specimens. All the distributions show a main peak at long relaxation times and a long tail, with a smaller amplitude, ~ 3 orders of magnitudes wide. The major shape difference between the two species is the length of the tail. For *B. europaea* (panels a, c, and e), the tails go down to T_2 values of 0.1–0.2 ms, values shorter than those for *L. pruvoti* (panels b, d, and f). The principal differences among each group are given by the total areas and are due to the wide range of masses and volumes of the specimens. In principle, the ^1H signal can be produced by sources other than water, namely, the intraskeletal organic matrix, consisting of proteins, polysaccharides, and lipids. To check this possibility, T_2 distributions for a dry coral and the

same after complete water saturation were obtained and are shown in Figure 4. The discussion reported in the Supporting

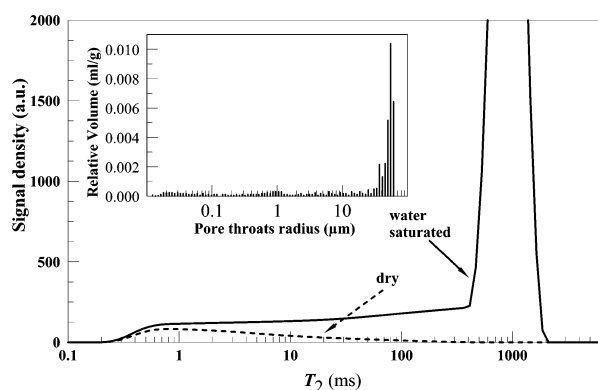


Figure 4. T_2 distribution of a dry coral (---) after 1 month in a desiccator and that of the same coral after full water saturation (—). In the inset, the MIP results for the same coral are shown. On the x -axis of the inset is given the pore throat radius distribution.

Information (referring to refs 54–61) leads us to conclude that in the distribution for the fully water saturated sample there is no contribution to the signal from macromolecular nuclei and only a maximum on the order of 2% could be attributed to lipids.

To discuss the distributions in Figure 3 in terms of pore sizes, one should get an approximate value for the radius of the pores inside the coral. The inset in Figure 4 reports the MIP distribution for the same specimen. The major fraction of the pore volume is given by pores whose entrance radii are on the

order of tens of micrometers, while a minor fraction corresponds to a 3 order of magnitude long tail of very small pores, down to tens of nanometers. NMR and MIP results are exceptionally similar and consistent. The two classes of pores are easily distinguished also in the distributions in Figure 3, so that the two parameters microporosity and cutoff were determined for each distribution. The sharp boundary between the two classes, with a cutoff in the T_2 range of 200–400 ms, suggests that the two classes of pores are not well connected by water diffusion during a local relaxation time. Also, the long tail indicates that these pores are poorly connected both to the other small pores and to the large ones in the major class. On the basis of the comparison with MIP, microporosity should correspond to pore sizes in the range from ~ 10 nm to ~ 10 – 20 μm . The existence of a wide class of pores with sizes of less than 10 – 20 μm is described well in the SEM images of both species reported in Figure 5.

Table 1 lists means, standard errors, and statistical significances of the differences between the two species by both parametric and nonparametric tests for all the variables considered: microporosity, cutoff, mass, total volume, S_{NMR} , and $S_{\text{NMR}}/V_{\text{T}}$. The two species behave differently with a high degree of statistical significance ($p < 0.01$ for all variables, including NMR parameters). In particular, the mass and total volume for *B. europaea* are much larger than for *L. pruvoti*, and vice versa, the total porosity estimated by the ratio $S_{\text{NMR}}/V_{\text{T}}$ is larger for *L. pruvoti* than for *B. europaea*. This result is consistent with the higher porosity obtained for *L. pruvoti* by previous non-NMR analysis,¹⁷ where the difference was considered to be likely a consequence of the different habitats of the two species.

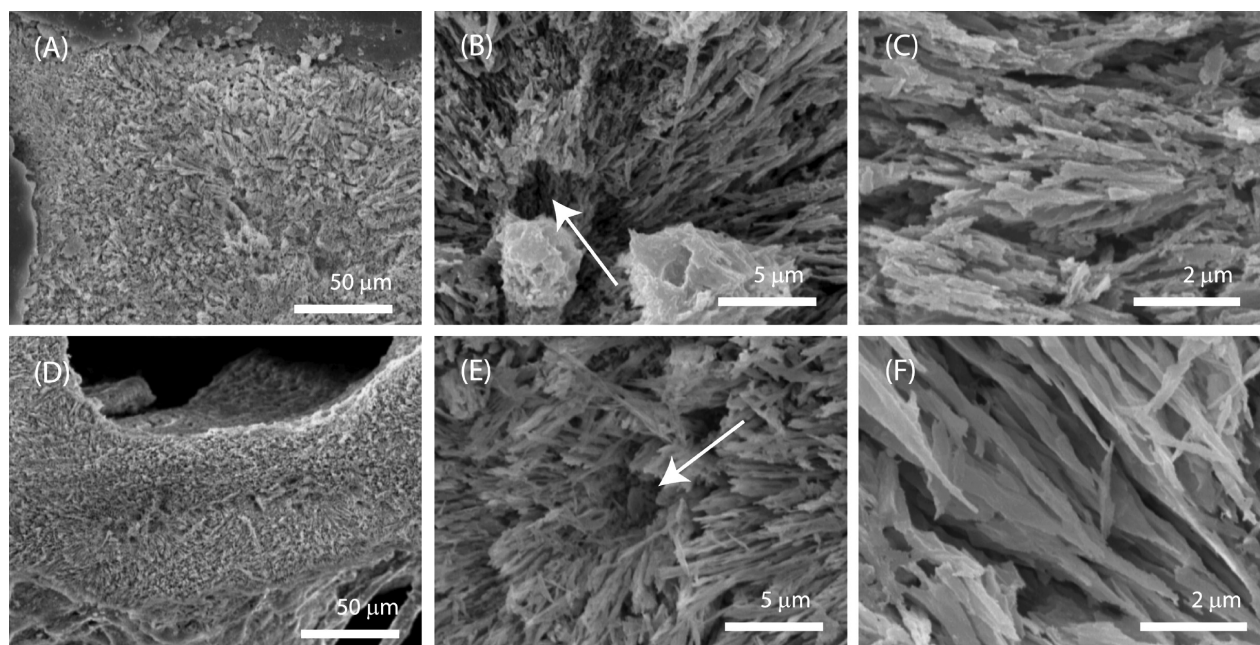


Figure 5. Scanning electron microscope pictures of a cross section of the tip region of a septum, the primary macroscopic structure of the coral skeleton, from *B. europaea* (A–C) and *L. pruvoti* (D–F). The building blocks of the skeleton are formed of thin aragonite crystals or fibers (0.04 – 0.05 μm in diameter), which form a three-dimensional structure. Their growth occurs in periodic layers and starts from the centers of calcification (see the arrows). The texture of the fibers of aragonite and the distribution of centers of calcification depend on the species of coral and are genetically controlled.

Table 1. Descriptive and Test Statistics Split by Species^a

	<i>B. europaea</i>			<i>L. pruvoti</i>			<i>t</i>	<i>Z</i>
	<i>n</i>	mean	standard error	<i>n</i>	mean	standard error		
microporosity (%)	27	31.3	1.6	26	38.6	2.1	2.79	6.66
cutoff (ms)	27	337	15	26	249	20	3.59	12.92
<i>m</i> (g)	27	0.88	0.15	26	0.25	0.04	3.92	11.19
<i>V_T</i> (cm ³)	27	0.92	0.17	27	0.20	0.03	4.13	17.46
<i>S_{NMR}</i> (arbitrary units)	27	4060	820	27	1233	165	3.38	11.21
<i>S_{NMR}/V_T</i> (arbitrary units)	27	4800	275	27	6993	349	4.94	17.60

^aNumber of observations (*n*), means, standard errors, and statistical significances of differences in microporosity, cutoff, mass (*m*), total volume (*V_T*, including the oral cavity), NMR signal (*S_{NMR}*), and *S_{NMR}/V_T* for *B. europaea* and *L. pruvoti*. The values of the *t* test and *Z* test suggest a high degree of statistical significance (*p* < 0.01) between the two species for all the variables considered.

Table 2. Descriptive and Test Statistics of the Same Data in Table 1 Split by Site^a

	CL			PL			PN			<i>F</i>	χ^2
	<i>n</i>	mean	standard error	<i>n</i>	mean	standard error	<i>n</i>	mean	standard error		
(A) <i>B. europaea</i>											
microporosity	9	38.6	1.6	9	26.1	2.1	9	29.0	2.7	8.89 ^b	11.83 ^b
cutoff	9	283	18	9	361	23	9	367	28	3.98 ^c	6.10 ^c
<i>m</i>	9	0.42	0.11	9	1.3	0.3	9	0.9	0.3	3.35 ^d	4.72 ^d
<i>V_T</i>	9	0.4	0.1	9	1.5	0.4	9	0.9	0.2	3.39 ^d	4.70 ^d
<i>S_{NMR}</i>	9	1806	426	9	6990	1996	9	3382	792	4.42 ^c	7.01 ^c
<i>S_{NMR}/V_T</i>	9	4447	436	9	4860	301	9	5092	655	0.45	1.95
(B) <i>L. pruvoti</i>											
microporosity	8	40.5	2.3	9	42.8	4.3	9	32.8	3.3	2.26	4.71 ^d
cutoff	8	294	49	9	186	21	9	272	19	3.40 ^d	6.88 ^c
<i>m</i>	8	0.17	0.04	9	0.25	0.07	9	0.33	0.08	1.34	2.03
<i>V_T</i>	9	0.15	0.03	9	0.17	0.05	9	0.28	0.06	2.19	3.27
<i>S_{NMR}</i>	9	989	202	9	1090	246	9	1621	369	1.45	1.95
<i>S_{NMR}/V_T</i>	9	7700	729	9	7311	582	9	5967	334	2.53	4.17

^aThe sites are Calafuria (CL), Palinuro (PL), and Pantelleria (PN). The variables and units are the same as in Table 1. The values of the *F* test and χ^2 test suggest statistical significance of differences among the three sites for *B. europaea*. For *L. pruvoti*, only NMR parameters microporosity and cutoff show statistical significance, even if at a lower level. ^b*p* < 0.01. ^c*p* < 0.05. ^d*p* < 0.1.

Table 2 lists the differences in the means of the same species among growing sites. For *B. europaea*, the differences have a high degree of statistical significance for almost all variables. Microporosity has the highest degree of significance (microporosity, *p* < 0.01; cutoff, *p* < 0.05; mass and total volume, *p* < 0.1; *S_{NMR}*, *p* < 0.05). For *L. pruvoti*, only NMR parameters cutoff and microporosity show significant differences among sites (*p* < 0.05–0.1).

Table S1 of the Supporting Information lists the results of the correlation among variables performed separately for *B. europaea* (part A) and *L. pruvoti* (part B). For both species, pairs of variables, mass and total volume, mass and *S_{NMR}*, and total volume and *S_{NMR}* are significantly correlated (*p* < 0.01). The correlations between microporosity and cutoff and between microporosity and mass are statistically significant for both species (*p* < 0.01 for *B. europaea*, and *p* < 0.05 for *L. pruvoti*).

Figure 6 reveals a counterintuitive behavior: the longer the cutoffs, the smaller the microporosities; at the first glance, one would expect the contrary. The pore-space architecture differs between samples with higher or lower cutoffs (between lower or higher microporosities). The scatter plots in Figure S2 of the Supporting Information and in Figure 7, showing cutoff versus mass and microporosity versus mass, respectively, suggest that the observed correlations between the cutoff and mass are governed by the mass: the smaller the mass, the higher the microporosity and the shorter the cutoff. As the mass of the

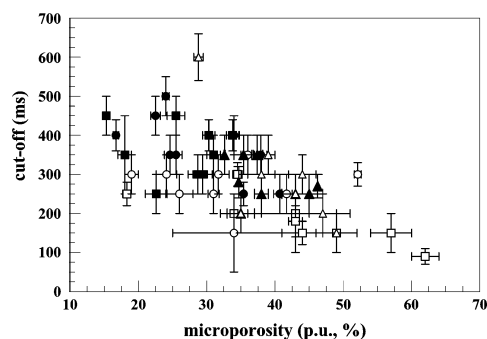


Figure 6. Scatter plot of the cutoff vs microporosity for all the samples. Filled symbols depict data for *B. europaea*, and empty symbols depict data for *L. pruvoti*. The symbols for the three sites are triangles (Calafuria), squares (Palinuro), and circles (Pantelleria).

corals increases, both the cutoff (which separates the two main pore classes) and the ratio between the fraction of the two pore classes change, with larger pores becoming more abundant. This effect is shown also by *L. pruvoti*, but it is not as marked as in *B. europaea* because of the smaller range of masses of corals. This is consistent with the gradual “filling up” of the smaller pores with the growth of the coral. A secondary infilling of skeletal pores in the older portion of the skeleton is a consistent characteristic of the skeletal density of branches of tall

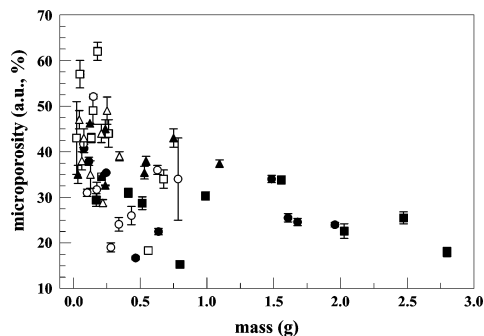


Figure 7. Scatter plot of microporosity vs mass for all the samples. Filled symbols depict data for *B. europaea*, and empty symbols depict data for *L. pruvoti*. The symbols of the three sites are triangles (Calafuria), squares (Palinuro), and circles (Pantelleria).

branching corals, in which growing tips are very porous while basal regions are extremely dense.⁸²

To study how microporosity, considered a dependent variable, is affected by mass and SST, multiple-regression analysis was performed (eq 1) both for all the specimens and for the two species separately. Part A of Table 3 summarizes the results. First, it is important to observe that from a statistical point of view a potential correlation between m and SST does not invalidate the results, as all the values of the variance inflation factor (VIF) are $\ll 10$. By considering all the specimens, the variable mass ($p < 0.01$) and SST ($p < 0.05$) significantly and negatively affect microporosity. In other words, the larger the mass and the higher the temperature, the smaller the microporosity. These relationships are mainly in place in the *B. europaea* species. For *L. pruvoti*, only the mass appears to be significantly related to the microporosity with a high degree of significance ($p < 0.05$). That means that SST appears to be a significant parameter in determining microporosity for *B. europaea* even if it is not as important as mass. The bootstrapping procedure (Table 3, part B) gives robustness to the evidence showing that those are not driven by small sample bias.

To better visualize and further discuss these relationships, the linear dependencies among microporosity, mass, and SST, for *L. pruvoti* and *B. europaea* separately, have been studied. Figure S3 of the Supporting Information lists the scatter plots and

statistical significances. The results confirm the multivariate analysis. For both *L. pruvoti* and *B. europaea*, SST does not significantly affect mass, as the probability values of the slope of the linear best fit are not statistically significant ($p > 0.1$). Overall, the fact that the mass significantly affects microporosity at least at the 5% level emerges ($p < 0.05$ for *L. pruvoti*, and $p < 0.01$ for *B. europaea*). Results for microporosity versus SST show that a significant relationship exists for *B. europaea* ($p < 0.05$) but not for *L. pruvoti* ($p > 0.1$).

In a previous study,¹⁷ it has been shown that porosity depends on temperature for *B. europaea*, but not for *L. pruvoti*. It has been hypothesized that the increase in porosity with temperature in the zooxanthellate species could depend on an inhibition of the photosynthetic process at elevated temperatures,^{23,63} causing an attenuation of calcification⁶⁴ with possible negative consequences also for space colonization and population density.^{19,27} The NMR results point in the same direction and seem to indicate also that this effect could be accompanied by a decrease in microporosity, meaning an increase in the fraction of the largest pores in the pore space.

TD-NMR is a quick, noninvasive, nondestructive method that does not use ionizing radiation, which can be applied to gain insight into the pore-space architecture of scleractinian corals, showing differences between species and growing sites, and sensitivity to environmental changes. Of course, this method, as well as MIP, BET, and the hydrostatic balance method, provides information about the connected porosity only and, as such, can be applied to systems with low fractions of isolated pores. This method can provide information that cannot be attained in other ways, like changes in the internal architecture of corals described by microporosity and cutoff with increasing mass and growing temperature. Even if this method cannot spatially locate the heterogeneity of the pore space, the existence of a clear cutoff in almost all the distributions (a very high slope at a certain point of the distribution) means that the smallest pores are not well connected by diffusion on the NMR time scale (corresponding to the local value of T_2) to the largest ones. Moreover, the NMR-defined microporosity can quantify the ratio between the volume of the smallest pores (sizes of less than 10–20 μm) and the total pore volume.

The increased fraction of larger pores in the zooxanthellate corals with increasing SST values, which could reduce their

Table 3. Regression Analysis for Microporosity^a

	(A) OLS			(B) bootstrap (5000 replications)		
	1	2	3	1	2	3
	all	<i>B. europaea</i>	<i>L. pruvoti</i>	all	<i>B. europaea</i>	<i>L. pruvoti</i>
m (g)	-7.19^b (−5.86)	-4.69^b (−3.28)	-21.04^c (−2.32)	-6.88^b (−4.69)	-5.57^b (−3.72)	-22.47^{d1} (−1.79)
SST (°C)	-3.53^c (−2.41)	-4.06^c (−2.11)	-2.53 (−0.96)	-3.53^c (−2.38)	-3.34^{d1} (−1.76)	-2.76 (−0.99)
constant	108.6 ^b (3.85)	115.5 ^b (3.12)	94.0 ^{d1} (1.85)	107.2 ^b (3.70)	108.3 ^b (2.95)	101.4 ^{d1} (1.77)
mean VIF (maximum)	1.22 (1.33)	1.20 (1.24)	1.34 (1.43)			
no. of observations	53	27	26	53	27	26
R^2 adjusted	0.32	0.41	0.24	0.32	0.38	0.24
F test	30.7 ^b	15.8 ^b	4.7 ^c			
Wald χ^2				43.2 ^b	37.0 ^b	6.2

^aOLS robust to outliers (robust t statistics in parentheses) and bootstrap (values of bootstrapped Z test in parentheses). (1) All specimens, (2) *B. europaea*, and (3) *L. pruvoti*. The coefficients in the columns are the parameters b_j ($j = 1$ or 2) and the parameter a (constant) of eq 1, where y_i is the value of the microporosity for each observation considered. Values of VIF of $\ll 10$ indicate that a possible correlation between m and SST does not invalidate the results. ^b $p < 0.01$. ^c $p < 0.05$. ^{d1} $p < 0.1$.

resistance to mechanical stresses, could have particular consequences in determining the effects of global warming on these species.⁶⁵ The described method will be applied in future work to the effects of ocean acidification on the skeletal properties of corals⁶⁶ and other calcifying organisms.

■ ASSOCIATED CONTENT

📄 Supporting Information

Additional observations and data (all reference numbers refer to the reference list in the main text). This material is available free of charge via the Internet at <http://pubs.acs.org>.

■ AUTHOR INFORMATION

Corresponding Author

*Telephone: +390512095119. Fax: +390512095047. E-mail: paola.fantazzini@unibo.it.

Notes

The authors declare no competing financial interest.

■ ACKNOWLEDGMENTS

This research has received funding from the European Research Council under the European Union's Seventh Framework Programme (FP7/2007-2013)/ERC Grant 249930 (Coral-Warm: Corals and global warming: the Mediterranean versus the Red Sea). We thank F. Gizzi, C. Marchini, and S. Prantoni for help in collecting the samples, the diving centers Centro Immersioni Pantelleria and Il Pesciolino for logistic assistance in the field, the Scientific Diving School for collaboration in the underwater activities, Fausto Peddis for MIP measurements, Gianni Neto for pictures of living specimens, and Robert James Sidford Brown for carefully reading the manuscript.

■ REFERENCES

- (1) Stenseth, N. H. Ecological effects of climate fluctuations. *Science* **2002**, *297*, 1292–1296.
- (2) Karl, T. R.; Trenberth, K. E. Modern global climate change. *Science* **2003**, *302*, 1175–1177.
- (3) Parmesan, C. Ecological and evolutionary responses to recent climate change. *Annual Review of Ecology and Systematics* **2006**, *37*, 637–669.
- (4) Helmuth, B.; Mieszkowska, N.; Moore, P.; Hawkins, S. J. Living on the edge of two changing worlds: Forecasting the responses of rocky intertidal ecosystems to climate change. *Annual Review of Ecology and Systematics* **2006**, *37*, 373–404.
- (5) Harley, C. D. G.; Hughes, A. R.; Hultgren, K. M.; Miner, B. G.; Sorte, C. J. B.; Thornber, C. S.; Rodriguez, L. F.; Tomaneck, L.; Williams, S. L. The impacts of climate change in a coastal marine systems. *Ecology Letters* **2006**, *9*, 228–241.
- (6) Richardson, A. J.; Poloczanska, S. Under-resourced, under threat. *Science* **2008**, *320*, 1294–1295.
- (7) Solomon, S.; Qin, D.; Manning, M.; Marquis, M.; Averyt, K.; Tignor, M. M. B.; Le Roy Miller, H., Jr.; Chen, Z. Climate Change 2007: The Physical Science Basis. Contribution of Working Group I to the Fourth Assessment Report of the Intergovernmental Panel on Climate Change. Cambridge University Press: Cambridge, U.K., 2007.
- (8) Lejeune, C.; Chevaldonné, P.; Pergent-Martini, C.; Boudouresque, C. F.; Pérez, T. Climate change effects on a miniature ocean: The highly diverse, highly impacted Mediterranean Sea. *Trends in Ecology & Evolution* **2010**, *25*, 250–260.
- (9) Hughes, T. P.; Baird, A. H.; Bellwood, D. R.; Card, M.; Connolly, S. R.; Folke, C.; Grosberg, R.; Hoegh-Guldberg, O.; Jackson, J. B. C.; Kleypas, J.; Lough, J. M.; Marshall, P.; Nyström, M.; Palumbi, S. R.; Pandolfi, J. M.; Rosen, B.; Roughgarden, J. Climate change, human impacts, and the resilience of coral reefs. *Nature* **2003**, *301*, 929–933.
- (10) Hoegh-Guldberg, O. The impact of Climate Change on Coral Reef Ecosystems. In *Coral Reefs: An Ecosystem in Transition*; Dubinsky, Z., and Stambler, N., Eds.; Springer: Dordrecht, The Netherlands, 2011; pp 391–404.
- (11) Lesser, M. Coral Bleaching: Causes and Mechanisms. In *Coral Reefs: An Ecosystem in Transition*; Dubinsky, Z., and Stambler, N., Eds.; Springer: Dordrecht, The Netherlands, 2011; pp 405–420.
- (12) Cerrano, C.; Bavestrello, G.; Bianchi, C. N.; Cattaneo-Vietti, R.; Bava, S.; Morganti, C.; Morri, C.; Picco, P.; Sara, G.; Schiaparelli, S.; Siccardi, A.; Sponga, F. A catastrophic mass-mortality episode of gorgonians and other organisms in the Ligurian Sea (North-Western Mediterranean), summer 1999. *Ecology Letters* **2000**, *3*, 284–293.
- (13) Perez, T.; Garrabou, J.; Sartoretto, S.; Harmelin, J. G.; Francour, P.; et al. Mass mortality of marine invertebrates: An unprecedented event in the Northwestern Mediterranean. *C. R. Acad. Sci., Ser. III* **2000**, *323*, 853–865.
- (14) Rodolfo-Metalpa, R.; Bianchi, C. N.; Peirano, A.; Morri, C. Coral mortality in NW Mediterranean. *Coral Reefs* **2000**, *19*, 24.
- (15) Coma, R.; Ribes, M.; Serrano, E.; Jimenez, E.; Salat, J.; Pasqual, J. Global warming-enhanced stratification and mass mortality events in the Mediterranean. *Proc. Natl. Acad. Sci. U.S.A.* **2009**, *106*, 6176–6181.
- (16) Garrabou, J.; Coma, R.; Bensoussan, N.; Bally, M.; Chevaldonne, P.; Cigliano, M.; Diaz, D.; Harmelin, J. G.; Gambi, M. C.; Kersting, D. K.; Ledoux, J. B.; Lejeune, C.; Linares, C.; Marschal, C.; Perez, T.; Ribes, M.; Romano, J. C.; Serrano, E.; Teixido, N.; Torrents, O.; Zabala, M.; Zuberer, F.; Cerrano, C. Mass mortality in the NW Mediterranean rocky benthic communities: Effects of the 2003 heat wave. *Global Change Biology* **2009**, *15*, 1090–1103.
- (17) Caroselli, E.; Prada, F.; Pasquini, L.; Nonnis Marzano, F.; Zaccanti, F.; Falini, G.; Levy, O.; Dubinsky, Z.; Goffredo, S. Environmental implications of skeletal micro-density and porosity variation in two scleractinian corals. *Zoology* **2011**, *114*, 255–264.
- (18) Zibrowius, H. *The scleractinians of the Mediterranean and of the North-Eastern Atlantic*; Memorial Institute of Oceanography, 1980; Vol. 11, pp 1–284.
- (19) Goffredo, S.; Caroselli, E.; Mattioli, G.; Pignotti, E.; Zaccanti, F. Variation in biometry and demography of solitary corals with environmental factors in the Mediterranean Sea. *Mar. Biol.* **2007**, *152*, 351–361.
- (20) Kain, J. M. The seasons in the subtidal. *British Phycological Journal* **1989**, *24*, 203–215.
- (21) Kleypas, J. A.; McManus, J. W.; Menez, L. A. B. Environmental limits to coral reef development: Where do we draw the line? *Am. Zool.* **1999**, *39*, 146–159.
- (22) Lough, J. M.; Barnes, D. J. Environmental controls on growth of the massive coral *Porites*. *J. Exp. Mar. Biol. Ecol.* **2000**, *245*, 225–243.
- (23) Al-Horani, F. A. Effects of changing seawater temperature on photosynthesis and calcification in the scleractinian coral *Galaxea fascicularis*, measured with O₂, Ca²⁺ and pH microsensors. *Sci. Mar.* **2005**, *69*, 347–354.
- (24) Roche, R. C.; Abel, R. A.; Johnson, K. G.; Perry, C. T. Quantification of porosity in *Acropora pulchra* (Brook 1891) using X-ray micro-computed tomography techniques. *J. Exp. Mar. Biol. Ecol.* **2010**, *396*, 1–9.
- (25) Bucher, D. J.; Harriott, V. J.; Roberts, L. G. Skeletal micro-density, porosity and bulk density of acroporid corals. *J. Exp. Mar. Biol. Ecol.* **1998**, *228*, 117–136.
- (26) Roche, R. C.; Abel, R. L.; Johnson, K. G. Spatial variation in porosity and skeletal element characteristics in apical tips of the branching coral *Acropora pulchra* (Book 1891). *Coral Reefs* **2011**, *30*, 195–201.
- (27) Goffredo, S.; Caroselli, E.; Mattioli, G.; Pignotti, E.; Dubinsky, Z.; Zaccanti, F. Inferred level of calcification decreases along an increasing temperature gradient in a Mediterranean endemic coral. *Limnol. Oceanogr.* **2009**, *54*, 930–937.
- (28) Goffredo, S.; Caroselli, E.; Mattioli, G.; Pignotti, E.; Zaccanti, F. Relationships between growth, population structure and sea surface temperature in the temperate solitary coral *Balanophyllia europaea* (Scleractinia, Dendrophylliidae). *Coral Reefs* **2008**, *27*, 623–632.

- (29) Caroselli, E.; Zaccanti, F.; Mattioli, G.; Falini, G.; Levy, O.; Dubinsky, Z.; Goffredo, S. Growth and demography of the solitary scleractinian coral *Leptopsammia pruvoti* along a sea surface temperature gradient in the Mediterranean Sea. *PLoS One* **2012**, *7*, e37848.
- (30) Huang, Z.; Li, X. Origin of flaw-tolerance in nacre. *Sci. Rep.* **2013**, *3*, 1693.
- (31) Nomura, T.; Katz, J. L.; Powers, M. P.; Saito, C. Evaluation of the micromechanical elastic properties of potential bone-grafting materials. *J. Biomed. Mater. Res., Part B* **2005**, *73*, 29–34.
- (32) Espinal, L. Porosity and its measurement. In *Characterization of Materials*; John Wiley and Sons: New York, 2012 (Wiley online library, published online June 25, 2012).
- (33) Klobes, P.; Meyer, K.; Munro, R. G. Porosity and specific surface area measurements for solid materials. In *Recommended Practice Guide*; Special Publication 960-17; National Institute of Standards and Technology: Gaithersburg, MD, 2006.
- (34) Sing, K. The use of nitrogen adsorption for the characterization of porous materials. *Colloids Surf., A* **2001**, *187–188*, 3–9.
- (35) Stapf, S.; Han, S.-I., Eds. *NMR imaging in chemical engineering*; Wiley-VCH Verlag GmbH & Co. KGa: Weinheim, Germany, 2006.
- (36) Laine, J.; Labady, M.; Alborno, A.; Yunes, S. Porosities and pore sizes in coralline calcium carbonate. *Mater. Charact.* **2008**, *59*, 1522–1525.
- (37) Cowan, B. *Nuclear Magnetic Resonance and Relaxation*; Cambridge University Press: Cambridge, U.K., 1997.
- (38) Brown, R. J. S. Measurements of nuclear spin relaxation of fluids in bulk for large surface-to-volume ratios. *Bulletin of the American Physics Society, Series II* **1956**, *1*, 216.
- (39) Brown, R. J. S. Nuclear magnetism logging at the Coyote institute. *Magn. Reson. Imaging* **1996**, *14*, 811–817.
- (40) Brownstein, K. R.; Tarr, C. E. Importance of classical diffusion in NMR studies of water in biological cells. *Phys. Rev. A* **1979**, *19*, 2446–2453.
- (41) D’Orazio, F.; Tarczon, J. C.; Halperin, W. P. Application of nuclear magnetic resonance pore structure analysis to porous silica glass. *J. Appl. Phys.* **1989**, *65*, 742–751.
- (42) Fantazzini, P.; Bortolotti, V.; Kärger, J.; Galvosas, P., Eds. *Conference Proceedings Series 1330*; American Institute of Physics: College Park, MD, 2011.
- (43) Borgia, G. C.; Brancolini, A.; Brown, R. J. S.; Fantazzini, P.; Ragazzini, G. Water-air saturation changes in restricted geometries studied by proton relaxation. *Magn. Reson. Imaging* **1994**, *12*, 191–195.
- (44) Borgia, G. C.; Brown, R. J. S.; Fantazzini, P.; Mesini, E.; Valdré, G. Diffusion weighted spatial information from ^1H relaxation in restricted geometries. *Il Nuovo Cimento* **1992**, *14D*, 745–759.
- (45) Dunn, K.-J.; Bergman, D. J.; Latorraca, G. A. *Nuclear magnetic resonance petrophysical and logging applications*; Pergamon: New York, 2002.
- (46) Hirasaki, G. J. NMR applications in Petroleum Reservoir Studies. In *NMR Imaging in Chemical Engineering*; Stapf, S., and Han, S.-I., Eds.; Wiley-VCH Verlag GmbH & Co. KGaA: Weinheim, Germany, 2006; pp 321–340.
- (47) Kleinberg, R. L. Utility of NMR T_2 distributions, connection with capillary pressure, clay effect, and determination of the surface relaxivity parameter ρ_2 . *Magn. Reson. Imaging* **1996**, *14*, 761–767.
- (48) Borgia, G. C.; Brown, R. J. S.; Fantazzini, P. Nuclear magnetic resonance relaxivity and surface-to-volume ratio in porous media with a wide distribution of pore sizes. *J. Appl. Phys.* **1996**, *79*, 3656–3664.
- (49) Brai, M.; Casieri, C.; De Luca, F.; Fantazzini, P.; Gombia, M.; Terenzi, C. Validity of NMR pore-size analysis of cultural heritage ancient building materials containing magnetic impurities. *Solid State Nucl. Magn. Reson.* **2007**, *32*, 129–135.
- (50) Borgia, G. C.; Brown, R. J. S.; Fantazzini, P. Examples of marginal resolution of NMR relaxation peaks using UPEN and diagnostics. *Magn. Reson. Imaging* **2001**, *19*, 473–475.
- (51) Fantazzini, P.; Brown, R. J. S. Units in distributions of relaxation times. *Concepts Magn. Reson.* **2005**, *27A*, 122–123.
- (52) Bortolotti, V.; Brown, R. J. S.; Fantazzini, P. *UpWin: A software to invert multi-exponential decay data* (www.unibo.it/Portale/Ricerca/Servizi+Imprese/UpWin.htm).
- (53) Efron, B. Bootstrap methods: Another look to the Jackknife. *Annals of Statistics* **1979**, *7*, 1–26.
- (54) Goffredo, S.; Vergni, P.; Reggi, M.; Caroselli, E.; Sparla, F.; Levy, O.; Dubinsky, Z.; Falini, G. The skeletal organic matrix from Mediterranean coral *Balanophyllia europaea* influences calcium carbonate precipitation. *PLoS One* **2011**, *6*, e22338.
- (55) Fantazzini, P.; Galassi, F.; Bortolotti, V.; Brown, R. J. S.; Vittur, F. The search for negative amplitude components in quasi-continuous distributions of relaxation times: The example of ^1H magnetization exchange in articular cartilage and hydrated collagen. *New J. Phys.* **2011**, *13*, 065007.
- (56) Liimatainen, T. J.; Ylä-Herttua, S.; Hakumäki, J. M. ^1H NMR Spectroscopy study of lipid T_1 and T_2 Relaxation in BT4C rat gliomas in vivo. *Proceedings of the International Society of Magnetic Resonance Medicine* **2004**, *11*, 610.
- (57) Rakow-Penner, R.; Daniel, B.; Yu, H.; Sawyer-Glover, A.; Glover, G. H. Relaxation times of breast tissue at 1.5T and 3T measured using IDEAL. *J. Magn. Reson. Imaging* **2006**, *23*, 87–91.
- (58) Sehy, J. V.; Ackerman, J. J. H.; Neil, J. J. J. Water and lipid MRI of the *Xenopus* oocyte. *Magn. Reson. Med.* **2001**, *46*, 900–906.
- (59) Opstad, K. S.; Griffiths, J. R.; Bell, B. A.; Howe, F. A. Apparent T_2 relaxation times of lipid and macromolecules: A study of high-grade tumor spectra. *J. Magn. Reson. Imaging* **2008**, *27*, 178–184.
- (60) Gambarota, G.; Tanner, M.; van der Graat, M.; Mulker, R.; Newbould, R. D. Fast T_2 relaxometry in ^1H -MRS of hepatic water and fat using short TR at 3T. *Proceedings of the International Society of Magnetic Resonance Medicine* **2004**, *19*, 2997.
- (61) Bortolotti, V.; Fantazzini, P.; Gombia, M.; Greco, D.; Rinaldin, G.; Sykora, S. PERFIDI filters to suppress and/or quantify relaxation time components in multicomponent systems: An example for fat-water systems. *J. Magn. Reson.* **2010**, *206*, 219–226.
- (62) Hughes, T. P. Skeletal density and growth form of corals. *Mar. Ecol.: Prog. Ser.* **1987**, *35*, 259–266.
- (63) Jokiel, P. L.; Coles, S. L. Response of Hawaiian and other Indo-Pacific reef corals to elevated temperature. *Coral Reefs* **1990**, *4*, 155–162.
- (64) Al-Horani, F. A.; Ferdelman, T.; Al-Moghrabi, S. M.; De Beer, D. Spatial distribution of calcification and photosynthesis in the scleractinian coral *Galaxea fascicularis*. *Coral Reefs* **2005**, *24*, 173–180.
- (65) Madin, J. S.; Hughes, T. P.; Connolly, S. R. Calcification, storm damage and population resilience of tabular corals under climate change. *PLoS One* **2012**, *7*, e46637.
- (66) Reyes-Nivia, C.; Diaz-Pulido, G.; Kline, D.; Hoegh-Guldberg, O.; Dove, S. Ocean acidification and warming scenarios increase microbioerosion of coral skeletons. *Global Change Biology* **2013**, *19*, 1919–1929.

**Chapter 4:
Different sensitivity among
Mediterranean scleractinian corals to
seasonal temperatures and enhanced
CO₂ along a natural pH gradient**

Manuscript in preparation

Different sensitivity among Mediterranean scleractinian corals to seasonal temperatures and enhanced CO₂ along a natural pH gradient

Fiorella Prada^a, Erik Caroselli^a, Bruno Capaccioni^b, Oren Levy^c, Giuseppe Falini^d, Zvy Dubinsky^c, Stefano Goffredo^a

^aMarine Science Group, Department of Biological, Geological and Environmental Sciences, Section of Biology, Alma Mater Studiorum – University of Bologna, Via Selmi 3, I-40126 Bologna, Italy

^bDepartment of Biological, Geological and Environmental Sciences, Section of Geology, Alma Mater Studiorum – University of Bologna, Piazza di Porta S. Donato 1, I-40127 Bologna, Italy

^cThe Mina and Everard Goodman Faculty of Life Sciences, Bar-Ilan University, 52900 Ramat-Gan, Israel

^dDepartment of Chemistry “G. Ciamician”, Alma Mater Studiorum – University of Bologna, Via Selmi 2, I-40126 Bologna, Italy

*Corresponding authors:

Stefano Goffredo - E-mail: stefano.goffredo@marinesciencegroup.org; s.goffredo@unibo.it; sgoff@tin.it, Tel. +39 051 2094244, Fax +39 051 2094286.

Abstract

Global climate change is a threat to marine biota because increased atmospheric CO₂ is causing ocean warming, acidification, hypercapnia, decreased carbonate saturation and hypoxia. Ocean acidification (OA) has raised particular concerns about its effects on marine organisms and ecosystems reliant on the generation and accumulation of calcium carbonate (CaCO₃) shells, skeletons, and/or structures. Here we assessed the effects of *in situ* exposure to different pH conditions on the mortality and growth (extension and net calcification rates) of three Mediterranean scleractinian corals; the solitary zooxanthellate *Balanophyllia europaea*, the solitary non-zooxanthellate *Leptopsammia pruvoti* and the colonial non-zooxanthellate *Astroides calycularis*. The corals were transplanted in proximity of a volcanic vent where water is naturally acidified to levels matching different IPCC scenarios. In all three species, high temperature exacerbated the negative effect of lowered pH on mortality. The growth of the zooxanthellate species did not react to reduced pH, while in the two non-zooxanthellate species it was negatively affected, indicating that zooxanthellate species may be more resistant in a high CO₂ world than their non-zooxanthellate counterparts. These results suggest different levels of resilience/resistance to climate change among coral species, probably related to different modes of nutrition and/or biomineralization processes. Natural CO₂-leaking marine sites like the one used in this study can provide essential information on the combined effects of ocean acidification and global warming on Mediterranean scleractinian corals, which may help understand to which extent corals inhabiting shallower ranges will be threatened in the next century.

Keywords: zooxanthellate corals, non-zooxanthellate corals, ocean warming, ocean acidification, CO₂ vents, mortality, growth

Introduction

Anthropogenic CO₂ emissions have severe environmental impacts, often summarized under the term “global climate change”. In the marine realm, two of the main forces causing significant changes are ocean warming (OW) and ocean acidification (OA), both largely driven by the burning of fossil fuels that has led to the current dramatic rise in sea surface temperature (SST) and carbon dioxide partial pressure ($p\text{CO}_2$), respectively. During the last 2-3 decades, an increase of at least 0.3-0.4°C has been recorded in mean annual SST across much of the global tropics and subtropics (1). Projections of future climatic change estimate a 0.3-4.8°C average increase in surface air temperature, and a 0.6-2.0°C average increase in surface ocean temperature by the end of 2100 (2), posing a great threat for marine organisms who are likely to be more sensitive to climate change than their terrestrial counterparts (3). In temperate areas, the effect of temperature warming is expected to be even greater. For instance, the Mediterranean Sea, which can be regarded as a miniature ocean that is expected to react faster to global change compared to the open ocean (4), is already showing warming rates three times higher than the global ocean (5). Investigations conducted along an 850-km latitudinal gradient on Western Italian coasts on the zooxanthellate dendrophylliid *Balanophyllia europaea*, which is endemic to the Mediterranean sea (6), have shown that with increasing temperature there is a decrease of the skeletal density (7), determined by an increase of porosity (8), in particular, an increase of the larger pores in the pore-space (9). Temperature negatively affects also population abundance (7), structure stability (10) and calcification (11). On the other hand, the non-zooxanthellate Mediterranean scleractinian coral *Leptopsammia pruvoti* seems to be tolerant to the same temperature range experienced by *B. europaea* (7,12,13).

In response to the increasing amount of anthropogenic CO₂ dissolved in the oceans, the concentration of protons (H⁺) has increased as well, leading to a decline in seawater pH (14,15). During preindustrial times the global mean pH at sea surface was 8.2. Since then, this value has decreased by 0.1 units, and at the current rate of CO₂ uptake, the average surface ocean pH will drop by further 0.06-0.32 units by the end of 2100 (2). OA is a global phenomenon, but its impact varies locally. For instance, the Mediterranean Sea has experienced a pH decrease of up to 0.14 units since the pre-industrial era (16), larger than the global average surface ocean pH decrease of 0.1 pH units (15). Understanding how enhanced acidity has already affected and how it will affect Mediterranean Sea ecosystems and their key taxa is then urgent and crucial.

OW and OA are expected to cause a significant decrease in coral growth rates and, consequently, affect the stability of reef ecosystems (17). However, the sensitivity of marine calcifiers to acidification varies among taxa and some species may increase calcification rates with increasing CO₂ levels (18,19). Yet, studies on the response of calcification to OA have been conducted on a limited number of organisms (19-22). In addition, the interactive effects of elevated *p*CO₂ and temperature have been poorly investigated (23,24). Therefore, multifactor long-term experiments are essential to investigate the synergistic or antagonistic responses of corals to elevated *p*CO₂ and temperature, and to provide a more accurate projection of their future impacts.

In this study, we investigated the effects of *in situ* exposure to different pH conditions on the mortality and growth (extension and net calcification rates) of Mediterranean scleractinian corals transplanted to a volcanic CO₂ vent area with seawater pH values matching different IPCC scenarios for the current century (2). We compared (*i*) the solitary zooxanthellate *B. europaea*

(Risso, 1826) (Fig. 1a), (ii) the solitary non-zooxanthellate *L. pruvoti* Lacaze-Duthiers, 1897 (Fig. 1b) and (iii) the colonial non-zooxanthellate *Astroides calycularis* (Pallas, 1766) (Fig. 1c).

The following hypothesis were tested:

- solitary/zooxanthellate, solitary/non-zooxanthellate and colonial/non-zooxanthellate corals may respond differently, indicating different sensitivities between species.
- seasonal temperature may affect the degree to which acidification alters the response of these organisms.

Materials and Methods

Study site.

The Island of Panarea belongs to the Aeolian Archipelago (Italy), located in the southern Tyrrhenian Sea in the Mediterranean (Fig. 2). At 10 m depth a crater 20 x 14 m wide generates a stable and sustained column of bubbles (mainly CO₂: 25), at ambient temperature, which generates a natural CO₂ gradient that extends for ~34 m, where normal pH conditions are restored.

Carbonate chemistry.

Four sampling Sites were selected along the CO₂ gradient (Fig. 3): a control site (Site 1), intermediate CO₂ (Site 2 and Site 3), and high CO₂ (Site 4). Temperature, salinity and pH (NBS scale) were measured at each Site during several surveys between July 2010 and May 2013 with a multi-parametric probe (600R, YSI Incorporated, USA) powered from a small boat and operated by SCUBA divers. Bottom water samples for determination of total alkalinity (TA) were collected at each Site using sterile 120 ml syringes (two replicates for each Site). After each

dive, the syringe samples were immediately transferred in labelled 100 ml amber glass bottles, saturated with mercuric chloride (HgCl_2) to avoid biological alteration, and stored in darkness at 4°C . TA was measured by Gran titration, using a 702 SM Titrino (Metrohm AG). Certified reference materials (Batch 121 and 132) from the Andrew Dickson Laboratory at UC San Diego were used to ascertain the quality of results obtained. Additional temperature data were recorded every three hours by sensors (Thermochron iButton, DS1921G, Maxim Integrated Products, USA) attached in each Site from July 2010 to May 2013. Measured pH was converted to the total scale using CO2SYS software (28). Mean pH (back-transformed hydrogen ion concentrations) was calculated for each Site. The pH, TA, salinity and temperature were used to calculate carbonate system parameters using the software CO2SYS with referenced dissociation constants (29-31).

Vent gas.

Gas was sampled during five surveys (June 2011, August 2011, December 2011, April 2012, May 2013) using vial glass samplers with a screw cap. The vials were carried capped underwater and were previously filled with deionized water to prevent implosion. At the sampling point, they were placed upside-down on the vents to be purged. Gas samples were collected using 50-mL thorion-tapped glass tubes, partially filled with 20-mL of a 0.15M $\text{Cd}(\text{OH})_2$ and 4N NaOH suspension, connected to a plastic funnel positioned over the rising bubbles. To avoid contamination by seawater, the silicon connection between the funnel and the collecting glass tube was filled with Milli-Q water and isolated from seawater by a plastic plug. The plug was removed only after the complete evacuation of seawater by the gases contained in the funnel. Uncondensable gases were collected in the headspace. Inorganic residual gas compounds were

analysed using a thermal conductivity chromatograph at the Laboratory of Fluid and Rock Geochemistry of the University of Florence. Methane content was analysed with a flame ionization detector and ion chromatography was used to analyse inert gases (32). Water samples were also collected and tested for dissolved H₂S with Cd-precipitation and ion chromatography (33).

Field transplantation and biotic measurements.

During several expeditions (July 2010, September 2010, November 2010, March 2011, June 2011, August 2011, December 2011 and April 2012), specimens of *B. europaea*, *L. pruvoti* and *A. calycularis* were sampled at ~2 km away from the vent area and transplanted in the four Sites (Fig. 3). The same number of corals was randomly assigned to each of the four Sites. Colonies of *A. calycularis* were fixed with cable ties onto plastic grids, while *B. europaea* and *L. pruvoti* polyps were glued with a bicomponent epoxy coral glue (Milliput, Wales, UK) onto ceramic tiles. Polyps of *L. pruvoti* were placed upside-down under plastic cages to mimic their natural orientation in overhangs and caves. Mortality rate (% month⁻¹: polyp mortality rate for the three species, and tissue mortality rate only for the colonial species) and extension rate (% month⁻¹: linear extension for *B. europaea* and *L. pruvoti* and tissue area extension for *A. calycularis*) were assed by means of digital photographs and image analyses software (NIKON NIS-Elements D 3.1). Coral net calcification rate (mg CaCO₃ g⁻¹ month⁻¹) was measured using the buoyant weight technique (34). Buoyant weight was converted into dry weight according to the equation:

$$\text{Dry weight} = \text{Buoyant weight} / (1 - D_{\text{water}} / D_{\text{skeleton}})$$

where D_{water} is the density of the water in which the sample was weighed (calculated from the water temperature and salinity) and $D_{skeleton}$ the density of aragonite (2.93 g cm^{-3}). Net calcification was calculated as the change in dry weight before and after each experimental period, normalized to the initial weight and expressed as monthly variation.

Statistical analyses.

One-way analysis of variance (ANOVA) was used to compare environmental and biological data among Sites. Levene's test was used for testing homogeneity, and Shapiro–Wilk's test for testing normality of variance. When data failed the tests for homogeneity and normality, the non-parametric Kruskal-Wallis rank test was used. For each experimental period, Spearman's rank correlation coefficient was used to calculate the significance of the correlations between biological parameters and pH. Linear regressions of mortality rates, linear extension rates and net calcification rates of all species with pH were also calculated to examine the effects of increased CO₂ on biological parameters. The slopes of all linear regressions were compared with an F- test in order to look for differences between periods. All analyses were performed using SPSS v.20.

Results

Seawater CO₂ system.

The study site was characterized by cool gaseous emissions comprising 98-99% CO₂, 0.2-0.3% N₂, 0.01-0.02% O₂, 0.003-0.005% Ar, 0.001-0.002% CH₄, 0.3-0.6% H₂S. Water dissolved H₂S was below detection limit (0.1 mg/l). Over the study period (July 2010-May 2013), water temperature, salinity and total alkalinity were homogeneous among Sites (Kruskal-Wallis test, $p > 0.05$), whereas pH, pCO₂, HCO₃⁻, CO₃²⁻, DIC and Ω_{arag} were significantly different (Kruskal-

Wallis test, $p < 0.001$). Each Site was characterized by a distinct carbonate chemistry (Table 1). Mean seawater pH decreased along the CO₂ gradient from an average value of 8.1 in Site 1 to 7.4 in Site 4 (Table 1; Fig. 3).

Biotic response.

In the period December 2011-April 2012 the experimental setup was almost entirely lost due to violent storms and strong waves, thus only *B. europaea* transplants were found and measured.

In periods December 2011-April 2012, November 2010-March 2011 and March-June 2011, when average seawater temperature was between 15.1°C and 16.3°C, polyp mortality rate was homogeneous among Sites in all species (Table 2-4; Kruskal-Wallis test, $p > 0.05$). In periods June-August 2011 and August-December 2011, when average seawater temperature was between 23.9°C and 24.2°C, polyp mortality rate was still homogeneous among Sites in *B. europaea* (Table 2; Kruskal-Wallis test/ANOVA, $p > 0.05$), while it was significantly different in *L. pruvoti* (Table 3; Kruskal-Wallis test/ANOVA, $p < 0.05$ and $p < 0.01$) and in *A. calycularis* (Table 4; Kruskal-Wallis test/ANOVA, $p < 0.001$). The increase of polyp mortality rate with decreasing pH was significant in both periods, with pH explaining 59-76% of its variance in *L. pruvoti* and 24-34% in *A. calycularis*. Linear regression showed a slope of -17 in June-August 2011 and -22 in August-December 2011 in *L. pruvoti*, and of -37 and -130 respectively, in *A. calycularis*, suggesting a 17% to 22% increase for *L. pruvoti* and a 37% to 130% increase for *A. calycularis* in polyp mortality rate for each 1-unit decrease in pH. In July-September 2010, when average seawater temperature was 26.2°C, polyp mortality rate was significantly different among Sites in all species (Table 2-4; Kruskal-Wallis test/ANOVA, $p < 0.001$ in *B. europaea* and *A. calycularis* and $p < 0.05$ in *L. pruvoti*). pH showed significant correlations, explaining 85% of

polyp mortality rate variance in *B. europaea*, 81% in *L. pruvoti* and 13% in *A. calycularis* (Table 2-4; Fig. S1). Linear regression showed a slope of -108 in *B. europaea*, -58 in *L. pruvoti* and -8 in *A. calycularis* suggesting for every 1-unit decrease in pH an increase of 108% in *B. europaea*, 58% in *L. pruvoti* and 8% in *A. calycularis* in polyp mortality. Tissue mortality rate in the colonial *A. calycularis* was significantly different among Sites in all periods (Table 4; Kruskal-Wallis test/ANOVA, $p < 0.01$ and $p < 0.001$). In November 2010-March 2011 and March-June 2011, when average seawater temperature was between 15.9°C and 16.3°C, tissue mortality increased significantly with decreasing pH, explaining 15-18% of its variance (Table 4; Fig. S1). In June-August 2011, August-December 2011 and July-September 2010, when average temperature was between 23.9°C and 26.3°C, tissue mortality rate increased significantly with decreasing pH, 23-71% of its variance being explained by the variation of pH (Table 4; Fig. S1). Slopes among all periods were significantly different (F-test, $P < 0.001$). Linear regression between tissue mortality and pH showed a slope of approximately -18 in November 2010-March 2011 and March-June 2011, indicating an 18% increase in tissue mortality every 1-unit decrease in pH, and a slope from -41 to -127 between June-August 2011 and July-September 2010, which correspond to a 41% to 127% increase in tissue mortality every 1-unit decrease in pH.

Linear extension rate was either not significantly different among Sites or showed no relationship with pH in *B. europaea*, in any of the periods (Table 2; Fig. S2). Linear extension rate in *L. pruvoti* and area extension rate in *A. calycularis* was significantly different among Sites in all periods. In *L. pruvoti* linear extension rate decreased significantly with decreasing pH in November 2010-March 2011, with pH explaining 11% of its variance, in June-August 2011, with pH explaining 20% of its variance and in July-September 2010 when pH explained 42% of its variance. Slopes among periods were significantly different (F-test, $P < 0.001$). In November

2010-March 2011 the slope was 4, in June-August 2011 the slope was 8 and in July-September 2010 the slope was 13, suggesting a decrease of extension rate of 4%, 8% and 13%, respectively, per 1-unit decrease of pH (Table 3; Fig. S2). In *A. calycularis*, area extension rate was significantly different among Sites in all periods analyzed (Table 4; Kruskal-Wallis test/ANOVA, $p < 0.001$). In all periods, pH correlated positively with area extension rate, explaining 10% of its variance in November 2010-March 2011, 18% in March June, 21% in June-August, 23% in August-December 2011 and 69% in July-September 2010 (Table 4; Fig. S2). Slopes between periods were significantly different (F-test, $P < 0.001$). Linear regression in November 2010-March 2011 showed a slope of 17, in March-June 2011 a slope of 19, in June-August 2011 a slope of 42, in August-December 2011 a slope of 139 and in July-September 2010 a slope of 95, indicating a decrease of area extension rate of 17%, 19%, 42%, 139% and 95%, respectively, per 1-unit decrease of pH (Table 4; Fig. S2).

Net calcification rate was either not significantly different among Sites (Table 2; Kruskal-Wallis test/ANOVA, $p > 0.05$), or did not correlate with pH in *B. europaea*, in all periods analyzed. In *L. pruvoti*, net calcification rate was significantly different among Sites in March-June 2011 (Table 3; Kruskal-Wallis test/ANOVA, $p < 0.01$) and June-August 2011 (Table 3; Kruskal-Wallis test/ANOVA, $p < 0.05$) and correlated positively with pH only in June-August 2011, with pH explaining 33% of its variance. Linear regression showed a slope of 171, indicating that each 1-unit decrease in pH was associated with a 171 ($\text{mg CaCO}_3 \text{ g}^{-1} \text{ month}^{-1}$) decrease in net calcification rate (Table 3). In *A. calycularis*, net calcification rate was significantly different among Sites in all periods analyzed (Table 4; Kruskal-Wallis test/ANOVA, $p < 0.05$ and $p < 0.001$). Net calcification rate correlated positively with pH in all periods, with pH explaining 43% of its variance in November 2010-March 2011, 29% in March-

June 2011, and 57% in June-August 2011 (Table 4; Fig. S3). Slopes between periods were not significantly different (F-test, $P > 0.05$). Linear regression shows in November 2010-March 2011 a slope of 190, in March-June 2011 a slope of 88 and in June-August a slope of 134, suggesting a decrease of net calcification rate of 190 ($\text{mg CaCO}_3 \text{ g}^{-1} \text{ month}^{-1}$), 88 ($\text{mg CaCO}_3 \text{ g}^{-1} \text{ month}^{-1}$) and 134 ($\text{mg CaCO}_3 \text{ g}^{-1} \text{ month}^{-1}$), respectively, per 1-unit decrease of pH (Table 4; Fig. S3).

Discussion

Seawater temperature, salinity and irradiance did not differ among Sites. There is no evidence to suspect a difference in the corals' food availability among Sites because Site 1 was only 34 m away from Site 4 and at approximately the same depth (Fig. 3). Therefore, differences in seawater carbonate chemistry provide the most likely explanation for the differences we observed in mortality and growth of the corals.

In the colder periods, when average temperature ranged from 15 to 16 °C, no significant changes were observed in polyp mortality with pH, for any of the species, while tissue mortality in the colonial *A. calycularis* increased with decreasing pH in both periods analyzed. In the warmer periods, when average temperature was approximately 24°C, polyp mortality increased with decreasing pH in *L. pruvoti* and *A. calycularis* and then, when average temperature reached 26°C, also in *B. europaea*. When temperature ranged from 24°C to 26°C, tissue mortality in *A. calycularis* increased with decreasing pH, and this increase was much more pronounced than in the colder months. When temperature ranged from 15°C to 16°C, the slopes indicated an 18% increase every 1-unit decrease in pH, while between 24°C and 26 °C the slopes indicated a 41% to 127% increase in tissue mortality per 1-unit decrease in pH in the warmer periods. From these results, there seems to be a synergistic interaction between high temperature and low pH in

determining the mortality of these organisms. While increased atmospheric $p\text{CO}_2$ is responsible for OA, it is also causing an increase in global seawater temperature. In the Mediterranean Sea, increased seawater temperature has determined longer stratification periods associated with mass mortality events (36, 37). The first well-documented Mediterranean multispecies mass mortality events were during the summers 1999 and 2003. They affected at least 30-40 hard-substrate invertebrate species over several hundred kilometers of coastline between the Tyrrhenian Sea in Italy and the Gulf of Lions in France with some places in Spain also affected (37-40). In both years, a positive correlation was observed between mortality rates and exposure to heat stress (38), indicating that shallow water corals are living, at least in the North Mediterranean, near their upper thermal limits during summer (41, 42). Since the frequency of abnormally warm summers is expected to increase in the next century, as a result of climate change, such mortality events in summer may also become more frequent as a direct response to elevated temperatures. Given the projected decrease of seawater pH, these mass mortality events could be exacerbated by the combination of high temperatures and low pH. Studies like this one, assessing the synergistic interaction between low pH and elevated temperatures, are essential to detect possible interactions between multiple stressors and establish to which extent corals inhabiting shallower ranges will be threatened by climate change.

Growth was investigated both as linear extension/area extension rate and net calcification rate. Linear extension rate was not affected by pH in *B. europaea*, in any of the periods. In *L. pruvoti*, in the colder periods, linear extension rate was either lightly affected or not affected by pH. Except for the period August-December 2011, when linear extension rate in *L. pruvoti* was homogeneous among Sites, the negative effect of pH on linear extension rate was more marked in the warmer periods, when the slopes indicated a decrease of extension rate from 8% to 13% in

against a 4% decrease per 1-unit decrease of pH in the colder period. In *A. calycularis*, area extension decreased with decreasing pH in all periods, and this decrease was greater in the warmer periods, when average temperature ranged from 24 to 26 °C, compared to colder ones, when average temperature ranged from 15 to 16 °C. In the warmer periods, the slopes suggested a decrease of area extension from 42% to 139%, and in the colder periods a decrease of 17% to 19% per 1-unit decrease of pH.

In *B. europaea* calcification was not affected by pH in any period. In *L. pruvoti* calcification was not affected by pH in the colder periods, while in *A. calycularis* it decreased with decreasing pH. In the warmer period, calcification decreased with decreasing pH in *L. pruvoti* and *A. calycularis*. In *A. calycularis* the negative effect of pH on calcification wasn't actually more pronounced in the warmer period compared to the colder ones but the average pH at which negative calcification (dissolution) occurred shifted towards higher values as temperature increased, indicating an increased vulnerability to low pH at higher temperatures. In fact, in November 2010-March 2011 (average temperature 15.9 °C), dissolution began at pH 7.8, in March-June 2011 (average temperature 16.3 °C) dissolution began at pH 8.0 and in June-August 2011 (average temperature 23.9 °C) dissolution began at pH 8.1 (Fig. S3). The different response to temperature stress among *B. europaea*, *L. pruvoti* and *A. calycularis* may suggest a different susceptibility to temperature, perhaps due to different protective mechanisms (e.g. stress proteins, antioxidant enzymes: 43). A previous study reported that live samples of *Cladocora caespitosa* transplanted at CO₂ vents underwent evident marks of dissolution with increased CO₂ whereas transplanted *B. europaea* samples were apparently unaffected, perhaps because *C. caespitosa* has large parts of its skeleton exposed, while *B. europaea* has a skeleton that is completely covered in tissue (44). However, this is unlikely the only explanation since in

our study we observed that *L. pruvoti* was clearly more sensitive than *B. europaea*, showing a significant decrease in calcification with increasing acidity between June and August, and both species have skeletons totally covered with tissue. A possible explanation could be that the symbiosis with the zooxanthellae in *B. europaea* could make it more tolerant than the non-zooxanthellate *L. pruvoti*, in a hypercapnic (elevated CO₂) environment. In zooxanthellate corals, calcification is tightly linked to photosynthesis by the symbiotic zooxanthellae (45-47). The glycerol and oxygen produced by the symbionts facilitate calcification through mitochondrial respiration and ATP production, which could be used for ion transport (45,48). CO₂ uptake by photosynthesis is also thought to stimulate calcification by changing the equilibrium of dissolved inorganic carbon (DIC) in coral tissue, although the mechanisms are unresolved (45). Thus, high CO₂ levels could enhance coral calcification (49), which may help compensate for the negative effect of low pH seawater, maintaining same levels of net calcification along the pH gradient. However, this does not explain the sensitivity observed in *C. caespitosa* (44). The method used in this study measured net calcification (gross calcification minus dissolution) and did not allow the discrimination between gross calcification and dissolution. More experiments are necessary in order to discriminate between the two processes by using methods such as the ⁴⁵Ca uptake (50). Another possible explanation could depend on differences in the porosity of the skeletons of these two species. *L. pruvoti* skeleton is more porous than the one of *B. europaea* (8,9). In shallow water sediments, the magnitude of dissolution is controlled by a number of parameters that are highly variable, such as organic matter content, mineral composition, grain size distribution, permeability, and porosity (51). Porosity-permeability relationships show the general trend of increasing permeability with increasing porosity (52,53). This means that a greater amount of skeleton would be exposed to low pH water making it more susceptible to the

corrosiveness of acidic seawater. However, the dynamics of water diffusion inside the skeleton of living corals should be studied to verify this hypothesis.

In conclusion, the present study indicated that in all three species, high temperature exacerbates the negative relationship between mortality and pH, with the highest mortalities in the warmest periods. While the growth of the zooxanthellate *B. europaea* did not react to pH, the growth of the two non-zooxanthellate species *L. pruvoti* and *A. calycularis* was negatively affected by low pH, showing an increased sensitivity to acidic condition with increasing temperature. The fact that *B. europaea* specimens naturally occurring around the vent area were not found below mean pH_{TS} 7.7 could depend on the increased metabolic costs related to high CO_2 levels in the oligotrophic, food-limited conditions of the Tyrrhenian Sea, combined with the elevated competition with non-calcifying seaweeds (54-59), which were abundant close to the crater. The sensitivity to enhanced acidity of corals that were transplanted along the natural CO_2 gradient increased when the water was warmest, indicating that OA will probably exacerbate the temperature driven mass benthic mortality events that have hit the Mediterranean Sea during summer periods in the last 30 years (38,60). Moreover, the envisaged increase in seawater temperature may aggravate the negative effects of lowered pH on calcification of asymbiotic corals, while symbiotic species may be relatively less sensitive due to the increased photosynthesis at high CO_2 .

Acknowledgements

I. Berman-Frank helped with alkalinity measurements. B. Basile, F. Sesso, and Eolo Sub diving center assisted in the field. F. Sesso provided the pictures of live specimens. F. Gizzi and G. Polimeni helped during preparation and participated to field surveys. The Marine Science Group and Scientific Diving School supplied scientific, technical, and logistical support. The research

leading to these results was funded by the ERC under the EU FP7 grant agreement n° [249930-CoralWarm: Corals and global warming: the Mediterranean versus the Red Sea]. The experiments comply with current Italian law.

References

1. Kleypas JA, Danabasoglu G, Lough JM (2008) Potential role of the ocean thermostat in determining regional differences in coral reef bleaching events. *Geophys Res Lett* 35:L03613.
2. IPCC (2013) in *Climate Change 2013: The Physical Science Basis. Contribution of Working Group I to the Fifth Assessment Report of the Intergovernmental Panel on Climate Change*, eds Stocker TF, et al. (Cambridge University Press, Cambridge).
3. Richardson AJ, Poloczanska ES (2008) Under-resourced, under threat. *Science* 320:1294-1295.
4. Bethoux JP, Gentili B, Morin P, Nicolas E, Pierre C, Ruiz-Pino D (1999) The Mediterranean Sea: a miniature ocean for climatic and environmental studies and a key for the climatic functioning of the North Atlantic. *Progr Oceanogr* 44:131-146.
5. Field CB, Barros V, Stocker TF, Dahe Q (2012) Managing the Risks of Extreme Events and Disasters to Advance Climate Change Adaptation: Special Report of the Intergovernmental Panel on Climate Change. Cambridge University Press, Cambridge.
6. Zibrowius H (1980) Les scléactiniaires de la Méditerranée et de l'Atlantique nord-oriental. *Mem Inst Oceanogr (Monaco)* 11:1-284

7. Goffredo S, Caroselli E, Pignotti E, Mattioli G, Zaccanti F (2007) Variation in biometry and population density of solitary corals with environmental factors in the Mediterranean Sea. *Mar Biol* 152:351-361.
8. Caroselli E, Prada F, Pasquini L, Nonnis Marzano F, Zaccanti F, Falini G, Levy O, Dubinsky Z, Goffredo S (2011) Environmental implications of skeletal micro-density and porosity variation in two scleractinian corals. *Zoology* 114:255-264.
9. Fantazzini P, Mengoli S, Evangelisti S, Pasquini L, Mariani M, Brizi L, Goffredo S, Caroselli E, Prada F, Falini G, Levy O, Dubinsky Z (2013) Time-Domain NMR study of Mediterranean scleractinian corals reveals skeletal-porosity sensitivity to environmental changes. *Environ Sci Technol* 47:12679-12686.
10. Goffredo S, Caroselli E, Mattioli G, Pignotti E, Zaccanti F (2008) Relationships between growth, population structure and sea surface temperature in the temperate solitary coral *Balanophyllia europaea* (Scleractinia, Dendrophylliidae). *Coral Reefs* 27:623-632.
11. Goffredo S, Caroselli E, Mattioli G, Pignotti E, Dubinsky Z, Zaccanti F (2009) Inferred level of calcification decreases along an increasing temperature gradient in a Mediterranean endemic coral. *Limnol Oceanogr* 54:930-937.
12. Caroselli E, Mattioli G, Levy O, Falini G, Dubinsky Z, Goffredo S (2012) Inferred calcification rate of a Mediterranean azooxanthellate coral is uncoupled with sea surface temperature along an 8° latitudinal gradient. *Front Zool* 9:32.
13. Caroselli E, Zaccanti F, Mattioli G, Falini G, Levy O, Dubinsky Z, Goffredo S (2012) Growth and demography of the solitary scleractinian coral *Leptopsammia pruvoti* along a sea surface temperature gradient in the Mediterranean Sea. *PLoS One* 7:e37848.

14. Sabine CL, Feely RA, Gruber N, Key RM, Lee K, et al. 2004. The oceanic sink for anthropogenic CO₂. *Science* 305:367-371.
15. Orr JC, et al. (2005) Anthropogenic ocean acidification over the twenty-first century and its impact on calcifying organisms. *Nature* 437:681-686.
16. Touratier F, Goyet C (2011) Impact of the Eastern Mediterranean Transient on the distribution of anthropogenic CO₂ and first estimate of acidification for the Mediterranean Sea. *Deep Sea Res Part 1 Oceanogr Res Pap* 58:1-15.
17. Hoegh-Guldberg O, et al. (2007) Coral reefs under rapid climate change and ocean acidification. *Science* 318:1737-1742.
18. Iglesias-Rodriguez MD, et al (2008) Phytoplankton calcification in a high-CO₂ world. *Science* 320:336–340.
19. Ries JB, Cohen AL, McCorkle DC (2009) Marine calcifiers exhibit mixed responses to CO₂-induced ocean acidification. *Geology* 37:1131-1134.
20. Doney SC, Fabry VJ, Feely RA, Kleypas J A (2009) Ocean Acidification: The Other CO₂ Problem. *Annu Rev Mar Sci* 1:169-192.
21. Guinotte JM, Fabry VJ (2008) Ocean acidification and its potential effects on marine ecosystems. *Ann N Y Acad Sci* 1134:320-342.
22. Movilla J, et al (2012) Calcification reduction and recovery in native and non-native Mediterranean corals in response to ocean acidification. *J Exp Mar Biol Ecol* 438:144-153.
23. Reynaud S, Leclercq N, Romaine-Lioud S, Ferrier-Pagés C, Jaubert J, Gattuso JP (2003) Interacting effects of CO₂ partial pressure and temperature on photosynthesis and calcification in a scleractinian coral. *Glob Chang Biol* 9:1660-1668.

24. Langdon C, Atkinson MJ (2005) Effect of elevated pCO₂ on photosynthesis and calcification of corals and interactions with seasonal change in temperature / irradiance and nutrient enrichment. *J Geophys Res* 110:C09S07.
25. Capaccioni B, Tassi F, Vaselli D, Tedesco D, Poreda R (2007) Submarine gas burst at Panarea Island (Southern Italy) on 3 November 2002: a magmatic versus hydrothermal episode. *J Geophys Res* 112:B05201.
28. Lewis E, Wallace DWR (1998) Program developed for CO₂ system calculations, ORNL/CDIAC-105 Carbon dioxide information analysis center, Oak Ridge National Laboratory (US Department of Energy, Washington, DC).
29. Mehrbach C, Culberson CH, Hawley JE, Pytkowicz RM (1973) Measurement of the apparent dissociation constants of carbonic acid in seawater at atmospheric pressure. *Limnol Oceanogr* 18:897-907.
30. Dickson AG, Millero FJ (1987) A comparison of the equilibrium constants for the dissociation of carbonic acid in seawater media. *Deep-Sea Res A* 34:1733-1743.
31. Dickson AG (1990) Thermodynamics of the dissociation of boric acid in synthetic sea water from 273.15 to 298.15 K. *Deep-Sea Res A* 37:755–766.
32. Capaccioni B, Tassi F, Vaselli D, Tedesco D, Rossi PL (2005) The November 2002 degassing event at Panarea Island (Italy): the results of a 5 months geochemical monitoring program. *Annals of Geophysics* 48:755-765.
33. Montegrossi G, Tassi F, Vaselli O, Bidini E, Minissale A (2006) A new, rapid and reliable method for the determination of reduced sulphur (S²⁻) species in natural water discharges. *Appl Geochem* 21:849-857.
34. Davies PS (1989) Short-term growth measurements of corals using an accurate buoyant weighing technique. *Mar Biol* 101:389-395.

35. Altman DG (1991) Practical Statistics for Medical Research. Chapman & Hall, London.
36. Coma R, Ribes M, Serrano E, Jiménez E, Salat J, Pascual J (2009) Global warming-enhanced stratification and mass mortality events in the Mediterranean. *Proc Natl Acad Sci U S A* 106:6176-6181.
37. Garrabou J, et al. (2009). Mass mortality in Northwestern Mediterranean rocky benthic communities: effects of the 2003 heat wave. *Glob Chang Biol* 15:1090-1103.
38. Cerrano C, et al. (2000) A catastrophic mass-mortality episode of gorgonians and other organisms in the Ligurian Sea (North-western Mediterranean), summer 1999. *Ecol Lett* 3:284-293.
39. Garrabou J, Perez T, Sartoretto S, Harmelin JG (2001) Mass mortality event in red coral *Corallium rubrum* populations in the Provence region (France, NW Mediterranean). *Mar Ecol Progr Ser* 217:263-272.
40. Linares C, et al. (2005) Immediate and delayed effects of a mass mortality event on gorgonian population dynamics and benthic community structure in the NW Mediterranean Sea. *Mar Ecol Progr Ser* 305:127-137.
41. Rodolfo-Metalpa R, Reynaud S, Allemand D, Ferrier-Pagès C (2008) Temporal and depth response of two temperate corals, *Cladocora caespitosa* and *Oculina patagonica* from the North Mediterranean Sea. *Mar Ecol Prog Ser* 369:103-114.
42. Rodolfo-Metalpa R, Richard C, Allemand D, Ferrier-Pagès C (2006) Growth and photosynthesis of two Mediterranean corals *Cladocora caespitosa* and *Oculina patagonica* under normal and elevated temperatures. *J Exp Biol* 209:4546-4556.
43. Brown BE (1997) Coral bleaching: causes and consequences. *Coral Reefs* 16:S129-S138.

44. Rodolfo-Metalpa R, et al. (2011) Coral and mollusc resistance to ocean acidification adversely affected by warming. *Nat Clim Chang* 1:308-31.
45. Allemand D, Ferrier-Pagès C, Furla P, Houlbrèque F, Puverel S, Reynaud S, Tambutté É, Tambutté S, Zoccola D (2004) Biomineralisation in reef-building corals: from molecular mechanisms to environmental control. *C. R. Palevol* 3:453-467.
46. Muscatine L (1990) The role of symbiotic algae in carbon and energy flux in reef corals. *Coral Reefs* 25:75-87.
47. Yellowlees D, Rees TAV, Leggat W (2008) Metabolic interactions between algal symbionts and invertebrate hosts. *Plant Cell Environ* 31:679–694.
48. Colombo-Pallotta MF, Rodriguez-Román A, Iglesias-Prieto R (2010) Calcification in bleached and unbleached 5 *Montastraea faveolata*: evaluating the role of oxygen and glycerol. *Coral Reefs* 29:899–907.
49. Holcomb M, McCorkle DC, Cohen AL (2010) Long-term effects of nutrient and CO₂ enrichment on the temperate coral *Astrangia poculata* (Ellis and Solander, 1786). *J Exp Mar Biol Ecol* 386:27-33.
50. Tambutté E, Allemand D, Bourge J, Gattuso JP, Jaubert J (1995) An improved ⁴⁵Ca protocol for investigating physiological mechanisms in coral calcification. *Mar Biol* 122:453-459.
51. Andersson AA, Gledhill D (2013) Ocean acidification and coral reefs: Effects on breakdown, dissolution, and net ecosystem calcification. *Annu Rev Mar Sci* 5:1.1-1.28.
52. Montes F, Haselbach L (2006) Measuring hydraulic conductivity in pervious concrete. *Environ Eng Sci* 23:960–9.

53. Neithalath N, Sumanasooriya MS, Deo O (2010) Characterizing pore volume, sizes, and connectivity in previous concretes for permeability prediction. *Materials characterization* 61:802-813.
54. Povero P, Hopkins TS, Fabiano M (1990) Oxygen and nutrient observations in the southern Tyrrhenian Sea. *Oceanologica Acta* 13:299-305.
55. Ribera d'Alcalà M, Brunet C, Conversano F, Corato F, Lavezza R (2009). Nutrient and pigment distributions in the southern Tyrrhenian Sea during mid-summer and late fall 2005. *Deep Sea Research Part II: Topical Studies in Oceanography* 56:676-686.
56. Fabricius KE, et al. (2011) Losers and winners in coral reefs acclimatized to elevated carbon dioxide concentrations. *Nat Clim Chang* 1:165-169.
57. Hall-Spencer JM, et al. (2008) Volcanic carbon dioxide vents show ecosystem effects of ocean acidification. *Nature* 454:96-99.
58. Porzio L, Buia MC, Hall-Spencer JM (2011) Effects of ocean acidification on macroalgal communities. *J Exp Mar Biol Ecol* 400:278-287.
59. Diaz-Pulido G, Gouezo M, Tilbrook B, Dove S, Anthony K (2011) High CO₂ enhances the competitive strength of seaweeds over corals. *Ecol Lett* 14:156-162.
60. Pérez T et al. (2000) Mortalité massive d'invertébrés marins: un évènement sans précédent en Méditerranée nord-occidentale. *C R Acad Sc Paris, Sc Vie* 323:853-865.

Tables

Table 1. Seawater carbonate chemistry for each transplantation Site. The pH, temperature (T), total alkalinity (TA) and salinity (Sal) were used to calculate all the other parameters using CO2SYS software with referenced dissociation constants (29-31). Mean pH values were calculated after conversion of data to hydrogen ion concentrations. Values are means with 95% CIs in brackets.

Measured Parameters					
	pH (total scale)	T (°C)	TA ($\mu\text{mol kg}^{-1}$)	Sal (‰)	
Site 1	8.1 (8.0-8.1)	19.2 (19.0-19.3)	2438 (2405-2572)	37 (36-37)	
Site 2	7.9 (7.8-7.9)	19.5 (19.3-19.7)	2429 (2384-2474)	37 (36-37)	
Site 3	7.7 (7.7-7.8)	19.5 (19.3-19.7)	2426 (2386-2466)	37 (36-37)	
Site 4	7.4 (7.3-7.5)	19.3 (19.2-19.5)	2395 (2366-2423)	37 (36-37)	

Calculated Parameters					
	pCO ₂ (μatm)	HCO ₃ ⁻ ($\mu\text{mol kg}^{-1}$)	CO ₃ ²⁻ ($\mu\text{mol kg}^{-1}$)	DIC ($\mu\text{mol kg}^{-1}$)	Ω_{arag}
Site 1	391 (358-424)	1869 (1836-1903)	232 (218-246)	2114 (2093-2135)	3.6 (3.4-3.8)
Site 2	672 (614-730)	2030 (2000-2059)	163 (151-175)	2214 (2195-2234)	2.5 (2.3-2.7)
Site 3	907 (751-1063)	2073 (2045-2101)	144 (132-156)	2246 (2225-2267)	2.2 (2.0-2.4)
Site 4	1944 (1580-2309)	2159 (2132-2185)	96 (85-107)	2317 (2291-2343)	1.4 (1.3-1.6)

Temperature ($n = 2580$ per Site) was recorded from May to September 2012 and from November 2012 to April 2013. pH ($n = 103$ -110 per Site) and salinity ($n = 107$ -110 per Site) were measured in July 2010, September 2010, November 2010, March 2011, June 2011, July-August 2011, November-December 2011, April-May 2012, June 2012 and May 2013. TA ($n = 14$ per Site) was measured in September 2010, November 2010, March 2011, June 2011, July-August 2011, November-December 2011, April-May 2012, June 2012 and May 2013. DIC: dissolved inorganic carbon.

Table 2. *Balanophyllia europaea*. Kruskal-Wallis rank test/ANOVA, linear regression and correlation analyses between pH and polyp mortality rate, linear extension rate and net calcification rate in the four transplantation Sites. Polyp mortality rate and linear extension rate were measured in 6 experimental periods and calcification rate in 4 experimental periods, from July 2010 and April 2012. Experimental periods are arranged in order of increasing temperature. Temperature (T: $n = 2580$ per Site), shown as mean and 95% CIs in brackets, was recorded from May to September 2012 and from November 2012 to April 2013. Regression parameters are shown only where the relationship is significant.

Experimental Period	T (°C)	Biological Parameter	N	K-W/ANOVA	Slope (SE)	Intercept (SE)	r_s^2	r_s
December 2011-April 2012	15.1 (15.1-15.2)	Polyp mortality rate (% month ⁻¹)	9	NS	-	-	-	-
		Linear extension rate (% month ⁻¹)	44	NS	-	-	-	-
		Net calcification rate (mg CaCO ₃ g ⁻¹ month ⁻¹)	18	*	-	-	0.028	0.168
November 2010-March 2011	15.9 (15.8-15.9)	Polyp mortality rate (% month ⁻¹)	12	NS	-	-	-	-
		Linear extension rate (% month ⁻¹)	78	***	-	-	0.001	0.029
		Net calcification rate (mg CaCO ₃ g ⁻¹ month ⁻¹)	24	NS	-	-	-	-
March-June 2011	16.3 (16.3-16.4)	Polyp mortality rate (% month ⁻¹)	12	NS	-	-	-	-
		Linear extension rate (% month ⁻¹)	71	***	-	-	0.045	0.211
		Net calcification rate (mg CaCO ₃ g ⁻¹ month ⁻¹)	20	NS	-	-	-	-
June-August 2011	23.9 (23.8-24.0)	Polyp mortality rate (% month ⁻¹)	12	NS	-	-	-	-
		Linear extension rate (% month ⁻¹)	66	NS	-	-	-	-
		Net calcification rate (mg CaCO ₃ g ⁻¹ month ⁻¹)	21	NS	-	-	-	-
August-December 2011	24.2 (20.7-27.8)	Polyp mortality rate (% month ⁻¹)	12	NS	-	-	-	-
		Linear extension rate (% month ⁻¹)	49	NS	-	-	-	-
July-September 2010	26.2 (26.1-26.3)	Polyp mortality rate (% month ⁻¹)	9	***	-108.084 (16.900)	882.498 (133.388)	0.848	-0.921***
		Linear extension rate (% month ⁻¹)	35	***	-	-	0.052	0.227

N, number of polyps for linear extension rate and net calcification rate and number of tiles for polyp mortality rate; K-W/ANOVA, significance of the Kruskal-Wallis test/ANOVA; r_s^2 , Spearman's determination coefficient; r_s , Spearman's correlation coefficient; * $p < 0.05$; ** $p < 0.010$; *** $p < 0.001$; NS, not significant.

Table 3. *Leptopsammia pruvoti*. Kruskal-Wallis rank test/ANOVA, linear regression and correlation analyses between pH and polyp mortality rate, linear extension rate and net calcification rate in the four transplantation Sites. Polyp mortality rate and linear extension rate were measured in 5 experimental periods and net calcification rate in 3 experimental periods from July 2010 to December 2011. Experimental periods are arranged in order of increasing temperature. Temperature (T: $n = 2580$ per Site), shown as mean and 95% CIs in brackets, was recorded from May to September 2012 and from November 2012 to April 2013. Regression parameters are shown only where the relationship is significant.

Experimental Period	T (°C)	Biological Parameter	N	K-W/ANOVA	Slope (SE)	Intercept (SE)	r_s^2	r_s
November 2010-March 2011	15.9 (15.8-15.9)	Polyp mortality rate (% month ⁻¹)	12	NS	-	-	-	-
		Linear extension rate (% month ⁻¹)	58	**	3.534 (1.537)	-27.569 (11.943)	0.112	0.335*
		Net calcification rate (mg CaCO ₃ g ⁻¹ month ⁻¹)	21	NS	-	-	-	-
March-June 2011	16.3 (16.3-16.4)	Polyp mortality rate (% month ⁻¹)	12	NS	-	-	-	-
		Linear extension rate (% month ⁻¹)	70	***	-	-	0.017	0.132
		Net calcification rate (mg CaCO ₃ g ⁻¹ month ⁻¹)	21	**	-	-	0.047	-0.216
June-August 2011	23.9 (23.8-24.0)	Polyp mortality rate (% month ⁻¹)	12	*	-16.839 (4.509)	133.539 (35.054)	0.585	-0.765**
		Linear extension rate (% month ⁻¹)	74	***	7.716 (1.851)	-61.837 (14.443)	0.199	0.446***
		Net calcification rate (mg CaCO ₃ g ⁻¹ month ⁻¹)	22	*	171.436 (63.386)	-1404.377 (494.799)	0.325	0.570**
August-December 2011	24.2 (20.7-27.8)	Polyp mortality rate (% month ⁻¹)	9	**	-21.658 (3.781)	178.369 (29.274)	0.762	-0.873**
		Linear extension rate (% month ⁻¹)	34	NS	-	-	-	-
July-September 2010	26.2 (26.1-26.3)	Polyp mortality (% month ⁻¹)	9	*	-58.296 (15.922)	475.172 (125.696)	0.810	-0.900***
		Linear extension rate (% month ⁻¹)	54	***	12.883 (2.114)	-106.955 (16.750)	0.417	0.646***

N, number of polyps for extension rate and net calcification rate and number of tiles for polyp mortality rate; K-W/ANOVA, significance of the Kruskal-Wallis test/ANOVA; r_s^2 , Spearman's determination coefficient; r_s , Spearman's correlation coefficient; * $p < 0.05$; ** $p < 0.010$; *** $p < 0.001$; NS, not significant.

Table 4. *Astroides calycularis*. Kruskal-Wallis rank test/ANOVA, linear regression and correlation analyses between pH and polyp mortality rate, tissue mortality rate, area extension rate and net calcification rate in the four transplantation Sites. Polyp mortality rate, tissue mortality rate and area extension rate were measured in 5 experimental periods and net calcification rate in 3 experimental periods from July 2010 to December 2011. Experimental periods are arranged in order of increasing temperature. Temperature (T: $n = 2580$ per Site), shown as mean and 95% CIs in brackets, was recorded from May to September 2012 and from November 2012 to April 2013.

Experimental Period	T (°C)	Biological Parameter	N	K-W/ANOVA	Slope (SE)	Intercept (SE)	r_s^2	r_s
November 2010-March 2011	15.9 (15.8-15.9)	Polyp mortality rate (% month ⁻¹)	45	NS	-	-	-	-
		Tissue mortality rate (% month ⁻¹)	45	***	-18.382 (3.014)	148.232 (23.492)	0.154	-0.393**
		Area extension rate (% month ⁻¹)	45	***	17.341 (5.071)	-137.812 (39.523)	0.101	0.318*
		Net calcification rate (mg CaCO ₃ g ⁻¹ month ⁻¹)	20	*	190.189 (53.034)	-1479.633 (414.015)	0.429	0.655**
March-June 2011	16.3 (16.3-16.4)	Polyp mortality rate (% month ⁻¹)	46	NS	-	-	-	-
		Tissue mortality rate (% month ⁻¹)	46	**	-18.192 (4.754)	153.065 (36.984)	0.177	-0.421**
		Area extension rate (% month ⁻¹)	46	***	19.213 (5.295)	-160.321 (41.191)	0.179	0.423**
		Net calcification rate (mg CaCO ₃ g ⁻¹ month ⁻¹)	15	***	88.539 (17.704)	-709.439 (138.043)	0.278	0.527*
June-August 2011	23.9 (23.8-24.0)	Polyp mortality rate (% month ⁻¹)	44	***	-37.233 (6.891)	301.003 (53.889)	0.339	-0.582***
		Tissue mortality rate (% month ⁻¹)	44	***	-41.138 (8.965)	344.767 (70.109)	0.334	-0.578***
		Area extension rate (% month ⁻¹)	44	***	41.984 (9.051)	-351.404 (70.783)	0.206	0.454**
		Net calcification rate (mg CaCO ₃ g ⁻¹ month ⁻¹)	12	***	133.840 (22.819)	-1078.656 (178.855)	0.572	0.756**
August-December 2011	24.2 (20.7-27.8)	Polyp mortality rate (% month ⁻¹)	52	***	-130.138 (12.497)	1045.149 (97.186)	0.242	-0.492***
		Tissue mortality rate (% month ⁻¹)	52	***	-126.994 (13.604)	1020.471 (105.794)	0.225	-0.474***
		Area extension rate (% month ⁻¹)	52	***	139.136 (16.351)	-1110.483 (127.154)	0.229	0.479***
July-September 2010	26.2 (26.1-26.3)	Polyp mortality rate (% month ⁻¹)	39	***	-8.416 (3.503)	69.296 (27.635)	0.125	-0.353*
		Tissue mortality rate (% month ⁻¹)	39	***	-59.889 (7.173)	483.653 (56.589)	0.706	-0.840***
		Area extension rate (% month ⁻¹)	39	***	95.451 (11.251)	-760.374 (88.763)	0.691	0.831***

N, number of colonies; K-W/ANOVA, significance of the Kruskal-Wallis test/ANOVA; r_s^2 , Spearman's determination coefficient; r_s , Spearman's correlation coefficient; * $p < 0.05$; ** $p < 0.010$; *** $p < 0.001$; NS, not significant.

Figure legends

Figure 1. Living specimens of a) *Balanophyllia europaea*, b) *Leptopsammia pruvoti*, c) *Astroides calycularis*.

Figure 2. Map of the study site off Panarea Island (Aeolian Archipelago) with a close-up on the location of the vent area, SE of Bottaro, where corals were transplanted.

Figure 3. Bathymetric profile of the four Sites, shown in the pictures, with the associated mean pH_{TS} and Ω_{arag} .

Figures

Figure 1

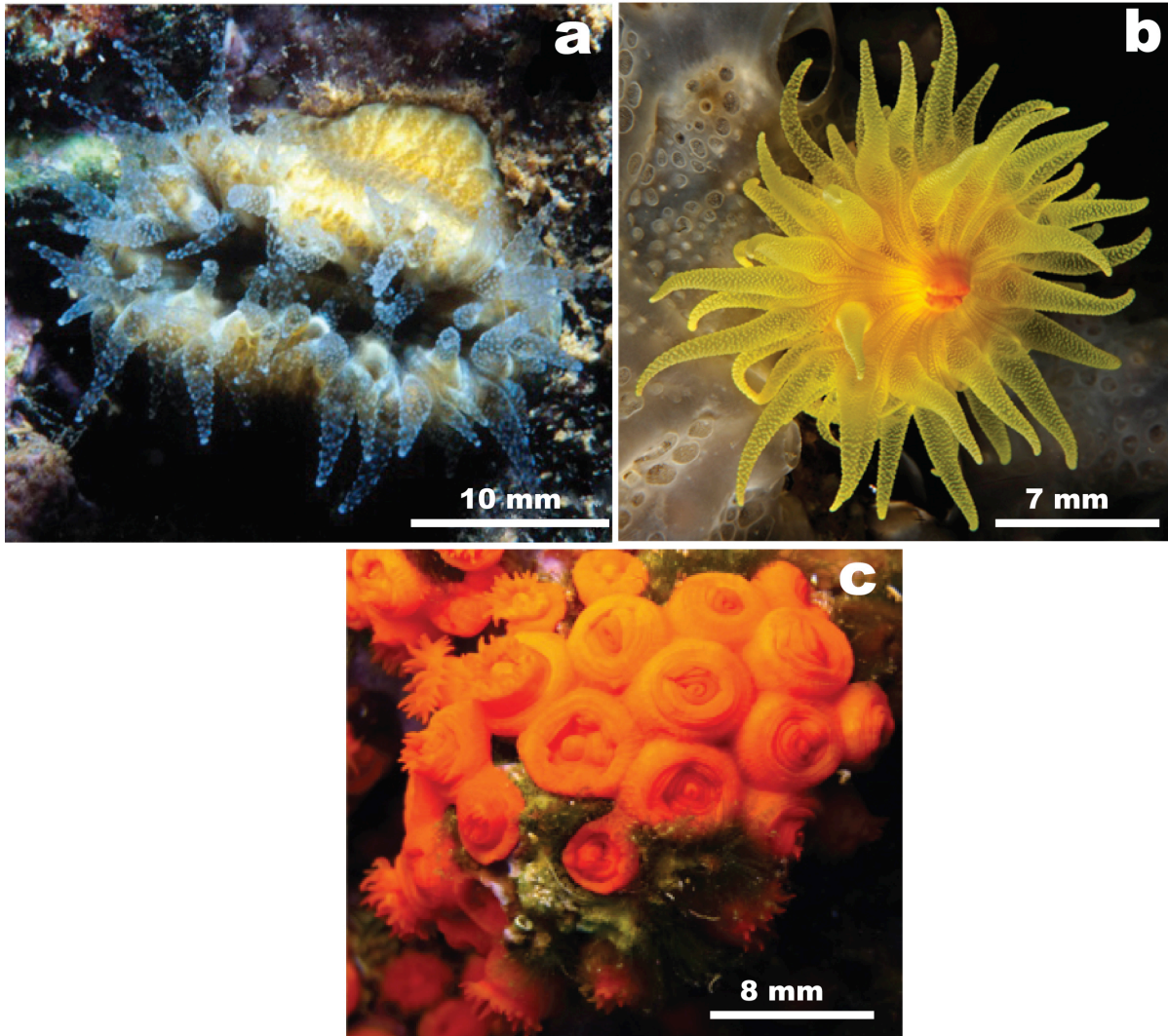


Figure 2

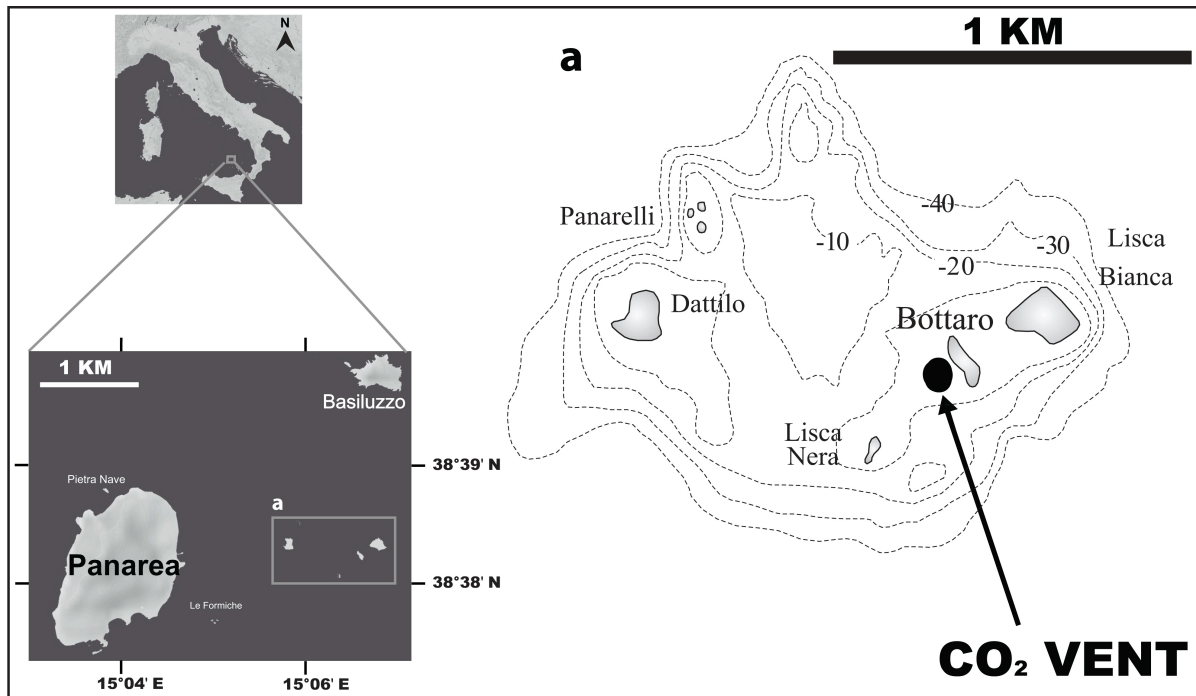
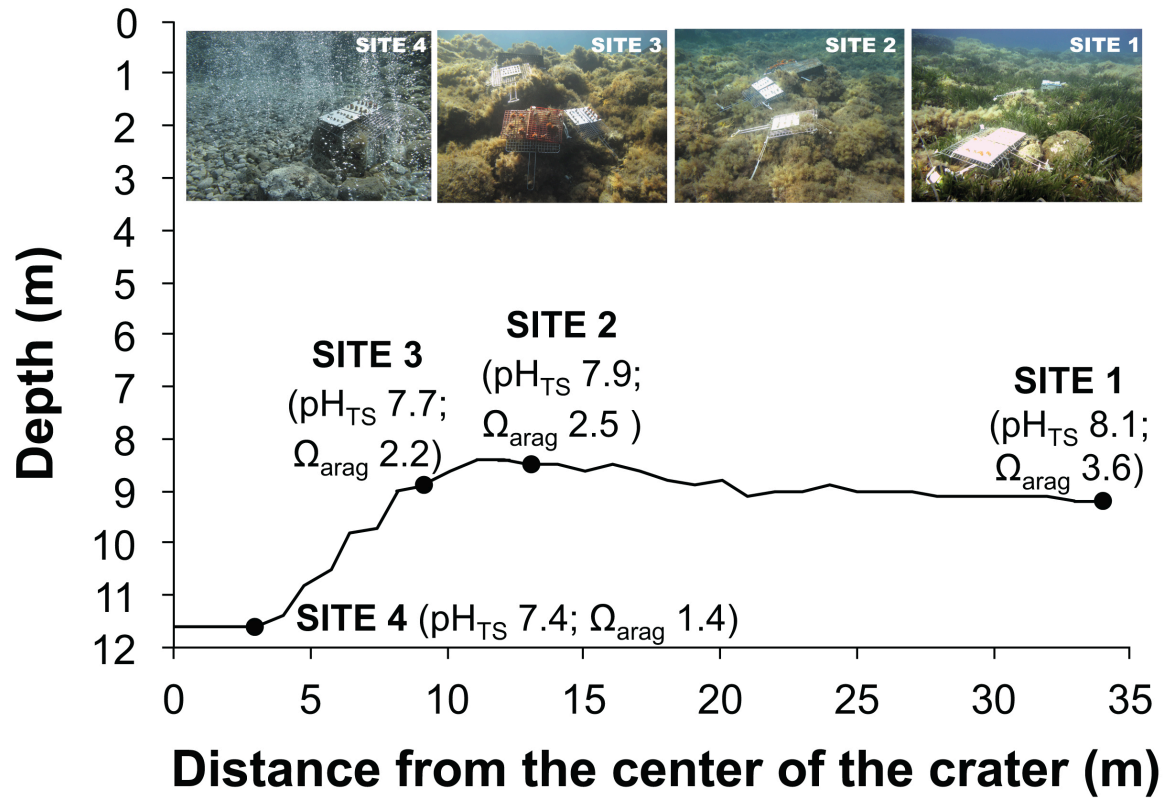
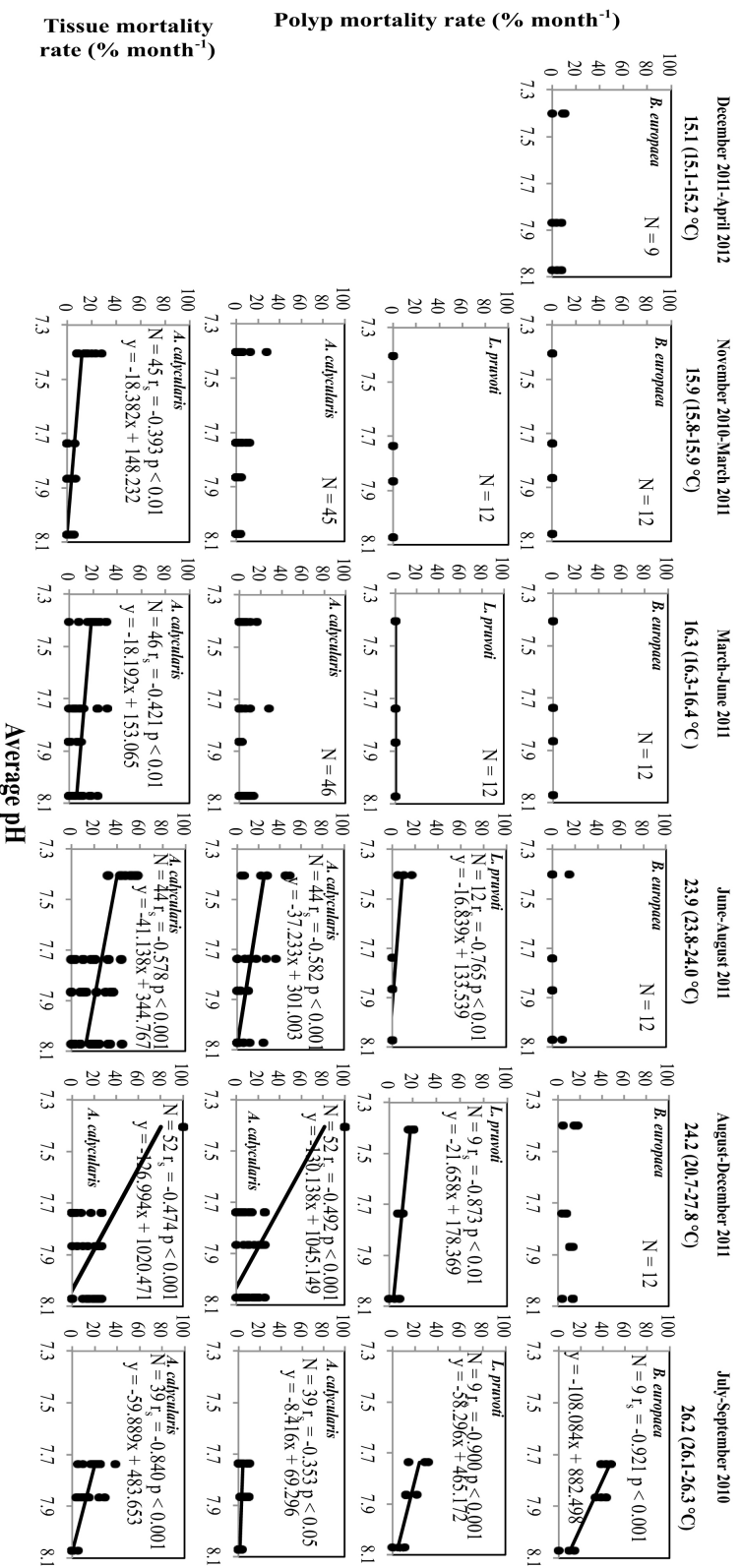


Figure 3



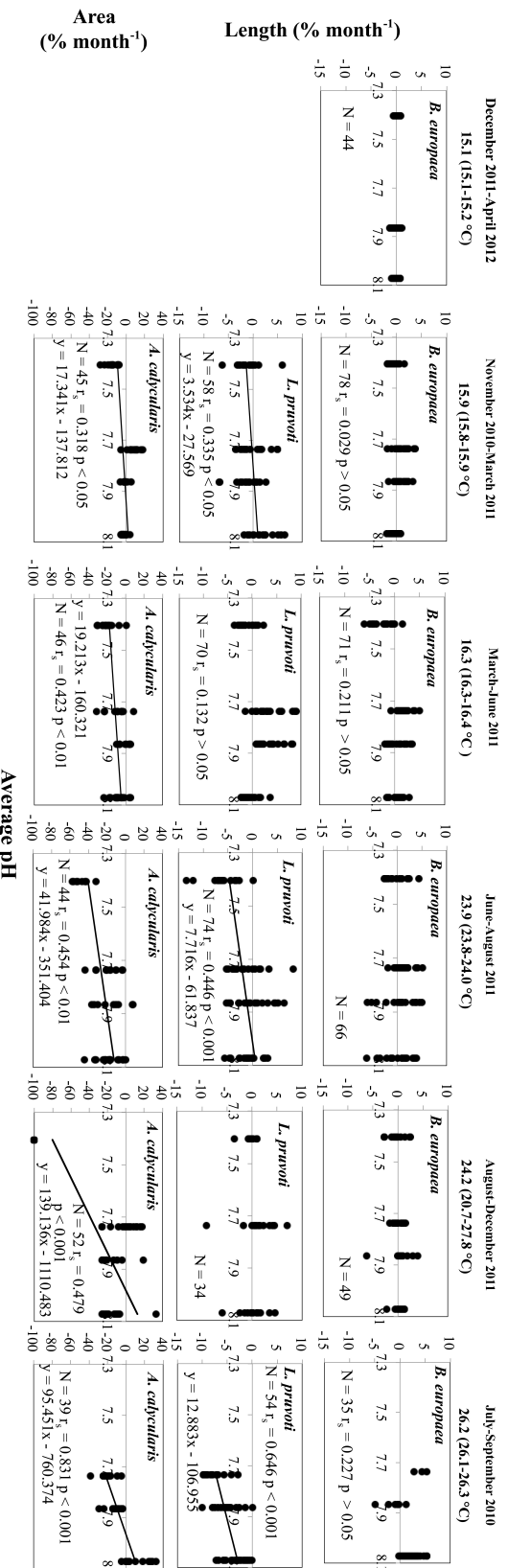
Supplementary Figures

Fig. S1. Variation in polyp mortality rate for *B. europaea*, *L. pruvoti* and *A. cadyceularis* and tissue mortality rate for the latter with average pH of each site (N = 103-110 per site; measured between July 2010 and May 2013), in 6 experimental periods from July 2010 to April 2012. Experimental periods are arranged in order of increasing temperature. Temperature data ($n = 2580$ per site), shown as mean and 95% CIs in brackets, was recorded every three hours by data loggers placed in each site from May to September 2012 and from November 2012 to April 2013.



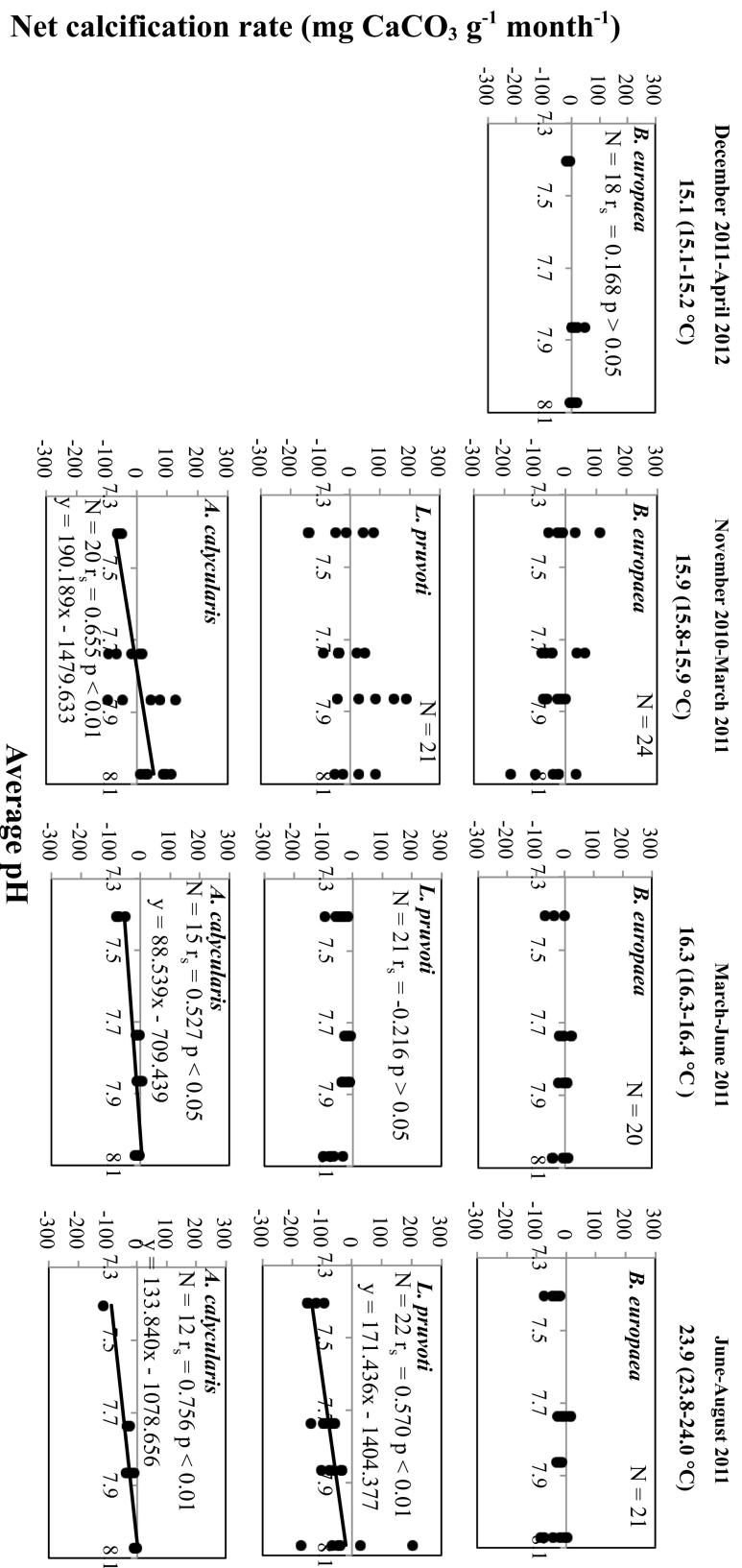
N, number of tiles for *B. europaea* and *L. pruvoti*, and number of colonies for *A. cadyceularis*; r, Spearman's correlation coefficient.

Fig. S2. Variation in linear extension rate for *B. europaea*, *L. pruvoti* and area extension rate for *A. calycularis* with average pH of each site (N = 103-110 per site, measured between July 2010 and May 2013), in 6 experimental periods from July 2010 to April 2012. Experimental periods are arranged in order of increasing temperature. Temperature data ($n = 2580$ per site), shown as mean and 95% CIs in brackets, was recorded every three hours by data loggers placed in each site from May to September 2012 and from November 2012 to April 2013.



N, number of polyps for *B. europaea* and *L. pruvoti*, and number of colonies for *A. calycularis*; r_s , Spearman's correlation coefficient

Fig. S3. Variation in net calcification rate for *B. europaea*, *L. pruvoti* and *A. calycularis* with average pH of each site (N = 103-110 per site; measured between July 2010 and May 2013), in 4 experimental periods from November 2010 to April 2012. Experimental periods are arranged in order of increasing temperature. Temperature data ($n = 2580$ per site), shown as mean and 95% CIs in brackets, was recorded every three hours by data loggers placed in each site from May to September 2012 and from November 2012 to April 2013.



N, number of polyps for *B. europaea* and *L. pruvoti*, and number of colonies for *A. calycularis*; r_s , Spearman's correlation coefficient

**Chapter 5:
Biomineralization control related to
population density under ocean
acidification**

Submitted to Nature Climate Change

Biom mineralization control related to population density under ocean acidification

Stefano Goffredo^{a*}, Fiorella Prada^a, Erik Caroselli^a, Bruno Capaccioni^b, Francesco Zaccanti^a, Luca Pasquini^c, Paola Fantazzini^{c,d}, Simona Fermani^e, Michela Reggi^e, Oren Levy^f, Katharina E. Fabricius^g, Zvy Dubinsky^f, Giuseppe Falini^{e*}

^a Marine Science Group, Department of Biological, Geological and Environmental Sciences, Section of Biology, Alma Mater Studiorum – University of Bologna, Via Selmi 3, 40126 Bologna, Italy

^b Department of Biological, Geological and Environmental Sciences, Section of Geology, Alma Mater Studiorum – University of Bologna, Piazza di Porta S. Donato 1, 40127 Bologna, Italy

^c Department of Physics and Astronomy, Alma Mater Studiorum – University of Bologna, Viale Berti Pichat 6/2, 40127 Bologna, Italy

^d Centro Enrico Fermi, Rome, Italy

^e Department of Chemistry “G. Ciamician”, Alma Mater Studiorum – University of Bologna, Via Selmi 2, 40126 Bologna, Italy

^f The Mina and Everard Goodman Faculty of Life Sciences, Bar–Ilan University, 52900 Ramat–Gan, Israel

^g Australian Institute of Marine Science, PMB 3, Townsville 4810, Queensland, Australia

*Corresponding authors:

Stefano Goffredo - E-mail: stefano.goffredo@marinesciencegroup.org; s.goffredo@unibo.it; sgoff@tin.it, Tel. +39 051 2094244, Fax +39 051 2094286.

Giuseppe Falini - E-mail: giuseppe.falini@unibo.it, Tel. +39 051 2099484.

Anthropogenic CO₂ is a major driver of current environmental change in most ecosystems¹, and the related ocean acidification (OA) is threatening marine biota². With increasing pCO₂, calcification rates of several species decrease³, although cases of up-regulation are observed⁴. Here, we show that biological control over mineralization relates to species abundance along a natural pH gradient. As pCO₂ increased, the mineralogy of a scleractinian coral (*Balanophyllia europaea*) and a mollusc (*Vermetus triqueter*) did not change. In contrast, two calcifying algae (*Padina pavonica* and *Acetabularia acetabulum*) reduced and changed mineralization with increasing pCO₂, from aragonite to the less soluble calcium sulphates and whewellite, respectively. As pCO₂ increased, the coral and mollusc abundance was severely reduced, with both species disappearing at pH < 7.8. Conversely, the two calcifying and a non-calcifying algae (*Lobophora variegata*) showed less severe or no reductions with increasing pCO₂, and were all found at the lowest pH site. The mineralization response to decreasing pH suggests a link with the degree of control over the biomineralization process by the organism, as only species with lower control managed to thrive in the lowest pH.

Several studies on the influence of pH on crystallography and texture of calcified regions are *ex situ*, short-term experiments on isolated organisms⁵, providing important information, but unrepresentative of natural ecosystems and failing to assess long-term effects⁶. There is a great need of long-term analyses on OA effects on marine ecosystems acclimated to high pCO₂, as found around CO₂ vents. Vents are not ideal predictors of future oceans, owing to pH variability, proximity of unaffected populations, and co-varying environmental parameters⁷. However, vents acidify seawater on sufficiently large temporal and spatial scales to integrate ecosystem processes⁶, acting as “natural laboratories”. In Papua New Guinea vents, reductions in coral diversity, recruitment, abundance, and shifts in competitive interactions are found⁸. In Mediterranean vents, decreased diversity, biomass,

trophic complexity, and abundance in many calcifying and non-calcifying organisms, and increases in macroalgae and seagrasses are observed^{7,9,10}.

We assessed, along a natural pH gradient, the effect of pCO₂ on the mineralization and abundances of the aragonitic scleractinian *B. europaea*, the aragonitic tube-forming gastropod *V. triqueter*, the brown alga *P. pavonica*, which deposits aragonite on the surface of thalli, the green alga *A. acetabulum*, whose cups' outer surfaces are calcified with aragonite and a small amount of whewellite, and the non-mineralized brown alga *L. variegata*. The mineralization is biologically controlled in *V. triqueter* (i.e., mineral is deposited in confined nucleation sites under complete biological control with minimal environmental effects), biologically induced in *P. pavonica* and *A. acetabulum* (i.e., it is strongly affected by the environment with minimal biological control), while *B. europaea* may represent an intermediate and still controversial situation¹¹. We aimed to assess, for the first time, changes in the mineralization and abundance of species along a pCO₂ gradient in relation to their control over biomineralization.

Seawater chemistry

Mean pH, CO₂, saturation of calcite (Ω_{calc}), and of aragonite (Ω_{arag}) differed among Sites (Kruskal-Wallis test/ANOVA, $p < 0.001$). The median pH values were 8.1 (Site 1), 7.9 (Site 2), 7.8 (Site 3) and 7.7 (Site 4), with increasing variability towards Site 4 (Fig. 1; Fig. S1; Table S1).

Mineralogy

Aragonite was the only mineral phase in *B. europaea* skeletons (Fig. S2). Organic matrix (OM) content was homogeneous among Sites (Kruskal-Wallis test, $p > 0.05$; Fig. S3; Table 1). Skeletal texture displayed fibers evolving from a center of calcification (Fig. S4),

but the morphology of these centers, and fiber thickness (600 ± 200 nm) were not related to $p\text{CO}_2$ (Fig. S5). Hardness was homogeneous among sample regions and study Sites (5100 ± 600 MPa). The elastic Young's modulus decreased (i.e., the skeleton became less stiff) along the aboral to oral direction and was lower at Sites 2 and 3 than at Site 1 (Table S2). Crystal quality and fiber thickness usually increases when crystallization occurs under lower supersaturation¹². While a reduction of precipitation rate with $p\text{CO}_2$ could increase crystal quality, other mechanisms could involve OM molecules. Corals appear to maintain a high pH at the nucleation sites within the calcicoblastic layer, possibly expending significant amount of energy¹³. This is supported by the lack of increase in aragonite fiber thickness with decreasing seawater Ω_{arag} , which would be expected if Ω_{arag} of the calcification site decreased¹². The reduction of skeletal stiffness with declining pH is likely associated with an increase in porosity, as confirmed by preliminary Nuclear Magnetic Resonance analyses. *B. europaea* skeletons have already been found to increase their porosity in stress conditions, such as increasing temperature¹⁴.

The apical regions of *V. triqueter* shell-tubes of similar diameter (~ 5 mm) were analysed. Aragonite was the only mineral phase (Fig. S2). Shell-tubes from Site 1 had four layers with different crystal texture and variable relative thickness among samples (Fig. 2). The first two layers were prismatic, with the second one made of regular prisms with square section (500 nm side). The third was cross-lamellar with regular fibers 500 nm thick. The fourth external layer was spherulitic, with several bores and channels (Fig. 2). In one of six samples from Site 2, and in four of six from Site 3, the two internal layers were not present. Different hardness and elastic Young's modulus were associated with different textures, without significant variations among Sites (Table S2). OM content was homogeneous among Sites (Kruskal-Wallis test, $p > 0.05$; Table 1; Fig. S3). The unaffected mineralogy of *V. triqueter* shell-tubes is possibly due to the exquisite control of biological macromolecules on

mollusc mineralization, which occurs in confined sites resulting in complex crystalline textures (Fig. 2). During shell-tube growth, the external layers are the first to be deposited, followed by the internal ones¹¹. A pH reduction can reduce the growth rates (calcification) of mollusc shells¹⁵, which likely explains the absence of the internal layers in shell-tubes from the most acidic Sites.

Padina pavonica thallus tips from Site 1 were mainly aragonitic with traces of hydrate calcium sulphate salts (CSh). Aragonite concentration decreased with increasing pCO₂, and almost only CSh was observed at Site 4 (Fig. S2). The presence of CSh was investigated in detail by further tests and considerations (see Supplementary Information). The overall mineral content differed among Sites (Kruskal-Wallis test, $p < 0.05$; Table 1, Fig. S3), and declined with increasing pCO₂ (Spearman's rho of the correlation with pH = 0.592, $p < 0.01$). In all samples, many aragonite needle-like crystals were aggregated or merged forming bundles. CSh crystals appeared as prisms or tablets (Fig. 3, Fig. S6). The decalcification left the thalli free of mineral deposits (Fig. S6). In *P. pavonica*, CSh increased with increasing pCO₂. Some stabilization of CSh minerals by algal molecules^{16,17}, probably polysaccharides, is expected, as CSh is soluble in seawater converting to gypsum.

Acetabularia acetabulum was mainly aragonitic, with minor presence of whewellite (calcium oxalate; Fig. S2). All samples contained about 10% (w/w) of water. The content of mineral phases, estimated after pyrolysis and release of water, differed among Sites (Kruskal-Wallis test, $p < 0.01$; Table 1 and Fig. S3) and declined with increasing pCO₂ (Spearman's rho of the correlation with pH = 0.555, $p < 0.01$). The aragonite/whewellite ratio decreased with increasing pCO₂. Globular granules of amorphous material rich in Ca and S were observed on the surface of needle-like aragonite aggregates at Sites 1-4 (Fig. 3 and Fig. S6). Whewellite was the only phase detected at Site 4 (Fig. S2; Fig. 3), where it appeared as prisms. After decalcification, the cup surface was free of mineral deposits (Fig. S6). In line

with a mainly chemical mineralization control¹⁷, increasing pCO₂ did not affect deposition of whewellite in *A. acetabulum*. The persistence of amorphous globular particles rich of calcium and sulphur was unexpectedly observed when aragonite disappeared. This phase, soluble in acetic acid solution, may be the result of interactions between Ca ions and the sulphonated groups of polysaccharides, overexpressed by the algae as a response to acidification¹⁷.

Within each sample, *P. pavonica* and *A. acetabulum* showed a marked reduction of mineralized areas with increasing pCO₂ (Fig. 4). Their aragonite content decreased with decreasing Ω_{arag} . At a Ω_{arag} of 1.5, aragonite was not observed, probably because this saturation level is too low to sustain its nucleation process. The observed changes in morphology of aragonite crystals (Fig. 3) are associated with seawater chemistry¹⁸.

Abundance

Percent cover of all species, except *A. acetabulum*, differed among Sites (Kruskal-Wallis test, $p < 0.001$), and decreased with increasing pCO₂ (Table S3). *B. europaea* and *V. triqueter* were not found at Site 4 (pH = 7.7, $\Omega_{\text{arag}} = 1.5$; Fig. 1). Densities of *A. acetabulum* were homogeneous among Sites (Kruskal-Wallis test, $p > 0.05$). This suggests that *P. pavonica* and *A. acetabulum* are not obligate calcifiers, persisting in high pCO₂ where also the non-calcifying species *L. variegata* survives (Fig. 1).

A changing benthic community was associated with the pCO₂ gradient (Supplementary Video). The coverage of a coral, a mollusc, and two macroalgae, one of which is a calcifier, declined with increasing pCO₂ (Fig. 1). This is in agreement with previous investigations at CO₂ vents, documenting dramatic reductions in calcifying macroalgal abundance^{7,8}.

Calcifying organisms seem the most sensitive to elevated pCO₂¹⁹, even if their response is not consistent^{8,15,20}. *A. acetabulum*, *B. europaea* and *V. triqueter* were previously found only outside vent areas, at a pH_{T_S} of 8.14⁷. Instead, in our survey, *B. europaea* and *V. triqueter*

survived up to pH_{TS} 7.8 and algal species up to pH_{TS} 7.7 (Fig. 1). The response of macroalgae to pCO_2 is expected to vary among species. As an example, increased cover with decreasing pH was observed for *Padina spp* at CO_2 seeps in Vulcano and Papua New Guinea²¹, and for *L. variegata* at CO_2 seeps in Ischia¹⁰, which contrasts with our data. The responses of non-calcifying macroalgae to elevated pCO_2 is variable²², depending on energy availability²³. The nature of CO_2 -induced shifts in macroalgal community structure is likely to vary depending on other environmental factors, such as nutrient availability, temperature and solar radiation²⁴. For instance, *L. variegata* were sampled in Ischia at 1 m depth and in our study at 8-12 m. Growth of the brown alga *Dictyota ciliolata* decreases with decreasing light intensity²⁵. In the brown alga *Fucus vesiculosus*, photosynthesis and growth decrease with increasing depth²⁶ from 1 to 6 m. At the high light of the shallow Ischia site, *L. variegata* may compensate for the negative effect of lowered pH through enhanced growth.

Relationships with the control over the biomineralization process

We related, for the first time, the biological control over biomineralization with changes in the abundance of organisms along natural pCO_2 gradients. The content of biomineralized products decreased with increasing pCO_2 only in the two calcifying algal species (with a weak control over their biomineralization), but the two species with stronger biomineralization control (*B. europaea* and *V. triqueter*) tolerated less severe pCO_2 increases (pH 7.8) than the algae (pH ≤ 7.7). Moreover, the more tolerant algae continued to grow despite their biomineralization products being profoundly altered by pCO_2 . Even if biomineralization in algae is only induced¹⁷, we can't exclude that the switch from aragonite to other biominerals may represent a phenomenon of phenotypic plasticity²⁷, which is increasingly being found to strongly contribute to persistence in the face of climate change²⁸. The control over biomineralization may not be the only cause of the observed differences,

since while the coral and the mollusc have a biology completely dependent on calcification, the algae don't. Moreover, the algae may benefit from pCO₂ increase in terms of photosynthesis, while the coral may be less dependent on the photosynthetic process and the mollusc does not photosynthesize. This study adds new evidence to field studies on OA effects^{4,9,29,30}, all indicating major ecological shifts as CO₂ rises. It documented that (i) the mineralization response to OA seems connected with the organisms' control of biomineralization, (ii) increasing pCO₂ profoundly affects the abundance of many benthic organisms, and (iii) only the species with weaker control were observed at the lowest pH.

Methods

Study site. Fieldwork was conducted at Panarea, Italy (Supplementary Video; Fig. S1), where hydrothermally stable CO₂ emissions acidify seawater, generating a pH gradient (see Supplementary Information for details).

Carbonate chemistry. Four sampling Sites were selected (Figs. 1 and S1): a control site (Site 1), two intermediate pCO₂ (Site 2 and Site 3), and high pCO₂ (Site 4). pH (NBS scale), temperature, and salinity were measured at each Site during several surveys between July 2010 and May 2013 with a multi-parametric probe (600R, YSI Incorporated, USA) powered from a small boat and operated by SCUBA divers. Bottom water samples for determination of total alkalinity (TA) were collected and analysed using standard methods (see Supplementary Information for details). Additional temperature data were recorded every three hours by sensors (Thermochron iButton, DS1921G, Maxim Integrated Products, USA) attached in each Site from July 2010 to May 2013. Measured pH was converted to the total scale using CO2SYS software. Median pH (back-transformed hydrogen ion concentrations) were

calculated for each Site. The pH, TA, salinity and temperature were used to calculate other carbonate system parameters using the software CO2SYS (Supplementary Information).

Benthic survey. Photographs of benthos (5 to 10 per site, 50 x 50 cm for the animals, 21.0 x 29.7 cm for the algae) were used to measure the percent cover of *B. europaea*, *V. triqueter*, *P. pavonica*, *A. acetabulum* and *L. variegata* at each Site. See Supplementary Information for details.

Vent gas. Gas was sampled during five surveys (June 2011-May 2013) and analysed at the Laboratory of Fluid and Rock Geochemistry of the University of Florence using standard methods (Supplementary Information). Water samples were collected and tested for dissolved H₂S (Supplementary Information).

Statistical analyses. Analysis of variance (ANOVA) and the post-hoc Fisher LSD test were used to test for differences among Sites using arcsine and log-transformation for percent cover and environmental data, respectively, when necessary. Else, the non-parametric Kruskal-Wallis and Spearman's rank correlation coefficients were used. All analyses were performed using SPSS v.20.

Biom mineralization. Samples were randomly collected by SCUBA divers at all Sites and were prepared for analyses with standard methods (Supplementary Information). Microscopic observations, mechanical, and spectroscopic measurements required the preparation of cross sections of the samples (Supplementary Information). X-ray powder diffraction (XRD) and Fourier transform infrared spectroscopy (FTIR) patterns on small amounts of powdered samples were collected using standard methods (Supplementary Information). Attenuated Total Reflection FTIR (FTIR ATR) spectra of sample cross sections were acquired with

standard methods (Supplementary Information). The organic matter content in the sample was determined by thermo-gravimetric analysis (TGA; Supplementary Information).

Microstructures were observed using optical and scanning electronic microscopes (SEM; Supplementary Information). The mechanical properties of shell-tubes and skeletons were measured with standard nanoindentation techniques (Supplementary Information).

Correspondence and requests for materials should be addressed to Stefano Goffredo and Giuseppe Falini.

Acknowledgements

I. Berman-Frank helped with alkalinity measurements. B. Basile, F. Sesso, and Eolo Sub diving center assisted in the field. F. Gizzi and G. Polimeni helped during preparation and participated in field surveys. The Marine Science Group and Scientific Diving School supplied scientific, technical, and logistical support. The research leading to these results has received funding from the European Research Council under the European Union's Seventh Framework Programme (FP/2007-2013) / ERC Grant Agreement n. [249930 - CoralWarm].

Author Contributions

S. G., Z. D., and G. F. conceived and designed research. S. G., F. P., E. C., and B. C. collected the samples. L. P., S. F., M. R., and G. F. performed the experiments. S. G., F. P., E. C., B. C., L. P., P. F., M. R., and G. F. analysed the data. All authors wrote the manuscript and participated in the scientific discussion.

References

1. IPCC. *IPCC Special Report on Renewable Energy Sources and Climate Change Mitigation* (Cambridge University Press, 2011).
2. Orr, J. C. *et al.* Anthropogenic ocean acidification over the twenty-first century and its impact on calcifying organisms. *Nature* **437**, 681-686 (2005).
3. Fabry, V. J., Seibel, B. A., Feely, R. A. & Orr, J. C. Impacts of ocean acidification on marine fauna and ecosystem processes. *ICES J. Mar. Sci.* **65**, 414-432 (2008).
4. Rodolfo-Metalpa, R., Martin, S., Ferrier-Pages, C. & Gattuso, J. P. Response of Mediterranean corals to ocean acidification. *Biogeosciences Discuss.* **6**, 7103-7131 (2010).
5. Hahn, S. *et al.* Marine bivalve shell geochemistry and ultrastructure from modern low pH environments: environmental effect versus experimental bias. *Biogeosciences* **9**, 1897–1914 (2012).
6. Barry, J. P., Hall-Spencer, J. M. & Tyrrell, T. *Guide to Best Practices for Ocean Acidification Research and Data Reporting* (Publications Office of the European Union, 2010).
7. Hall-Spencer, J. M. *et al.* Volcanic carbon dioxide vents show ecosystem effects of ocean acidification. *Nature* **454**, 96-99 (2008).
8. Fabricius, K. E. *et al.* Losers and winners in coral reefs acclimatized to elevated carbon dioxide concentrations. *Nat. Clim. Chang.* **1**, 165-169 (2011).
9. Cigliano, M., Gambi, M. C., Rodolfo-Metalpa, R., Patti, F. P. & Hall-Spencer, J. M. Effects of ocean acidification on invertebrate settlement at volcanic CO₂ vents. *Mar. Biol.* **157**, 2489-2502 (2010).
10. Porzio, L., Buia, M. C. & Hall-Spencer, J. M. Effects of ocean acidification on macroalgal communities. *J. Exp. Mar. Biol. Ecol.* **400**, 278-287 (2011).
11. Lowenstam, H. A. & Weiner, S. *On Biomineralization* (Oxford University Press, 1989).

12. Holcomb, M., Cohen, A. L., Gabitov, R. I. & Hutter, J. L. Compositional and morphological features of aragonite precipitated experimentally from seawater and biogenically by corals. *Geochim. Cosmochim. Acta* **73**, 4166-4179 (2009).
13. Venn, A. A. *et al.* Impact of seawater acidification on pH at the tissue–skeleton interface and calcification in reef corals. *Proc. Natl. Acad. Sci. USA* **110**, 1634-1639 (2013).
14. Fantazzini, P. *et al.* A time-domain nuclear magnetic resonance study of Mediterranean scleractinian corals reveals skeletal-porosity sensitivity to environmental changes. *Environ. Sci. Technol.* **47**, 12679–12686 (2013).
15. Ries, J. B., Cohen, A. L. & McCorkle, D. C. Marine calcifiers exhibit mixed responses to CO₂-induced ocean acidification. *Geology* **37**, 1131-1134 (2009).
16. McCandless, E. L. & Craigie, J. S. Sulfated polysaccharides in red and brown algae. *Ann. Rev. Plant Physiol.* **30**, 41-53 (1979).
17. Mann, S., Webb, J. & Williams, R. J. P. (1989) *Biomineralization: Chemical and Biochemical Perspectives*. (VCH Verlagsgesellschaft, 1989).
18. Robbins, L. L., Knorr, P. O. & Hallock, P. Response of *Halimeda* to ocean acidification: field and laboratory evidence. *Biogeosciences Discuss.* **6**, 4895-4918 (2009).
19. Kroeker, K. J., Kordas, R. L., Crim, R. N. & Singh, G. G. Meta-analysis reveals negative yet variable effects of ocean acidification on marine organisms. *Ecol. Lett.* **13**, 1419–1434 (2010).
20. Fabry, V. J. Marine calcifiers in a high-CO₂ ocean. *Science* **320**, 1020–1022 (2008).
21. Johnson, V. R., Russell, B. D., Fabricius, K. E., Brownlee, C. & Hall-Spencer, J. M. Temperate and tropical brown macroalgae thrive, despite decalcification, along natural CO₂ gradients. *Glob. Change Biol.* **18**, 2792-2803 (2012).
22. Cornwall, C. E. *et al.* Carbon-use strategies in macroalgae: differential responses to lowered pH and implications for ocean acidification. *J. Phycol.* **48**, 137–144 (2012).

23. Hofmann, L. C., Straub, S. & Bischof, K. Competition between calcifying and noncalcifying temperate marine macroalgae under elevated CO₂ levels. *Mar. Ecol. Prog. Ser.* **464**, 89 (2012).
24. Sarker, M. Y., Bartsch, I., Olischläger, M., Gutow, L. & Wiencke, C. Combined effects of CO₂, temperature, irradiance and time on the physiological performance of *Chondrus crispus* (Rhodophyta). *Bot. Mar.* **56**, 63-74 (2013).
25. Cronin, G. & Hay, M. E. Effects of light and nutrient availability on the growth, secondary chemistry, and resistance to herbivory of two brown seaweeds. *Oikos* **77**, 93-106 (1996).
26. Rohde, S., Hiebenthal, C., Wahl, M., Karez, R. & Bischof, K. Decreased depth distribution of *Fucus vesiculosus* (Phaeophyceae) in the Western Baltic: effects of light deficiency and epibionts on growth and photosynthesis. *Eur. J. Phycol.* **43**, 143-150 (2008).
27. Munday, P. L., Warner, R. R., Monro, K., Pandolfi, J. M. & Marshall, D. J. Predicting evolutionary responses to climate change in the sea. *Ecol. Lett.* **16**, 1488-1500 (2013).
28. Anderson, J. T., Inouye, D. W., McKinney, A. M., Colautti, R. I. & Mitchell-Olds, T. Phenotypic plasticity and adaptive evolution contribute to advancing flowering phenology in response to climate change. *Proc. R. Soc. B-Biol. Sci.* **279**, 3843-3852 (2012).
29. Dias, B. B., Hart, M. B., Smart, C. W. & Hall-Spencer, J. M. Modern seawater acidification: The response of foraminifera to high-CO₂ conditions in the Mediterranean Sea. *J. Geol. Soc.* **167**, 843-846 (2010).
30. Calosi, P., *et al.* Distribution of sea urchins living near shallow water CO₂ vents is dependent upon species acid-base and ion-regulatory abilities. *Mar. Pollut. Bull.* **73**, 470-484 (2013).

Competing Financial Interests

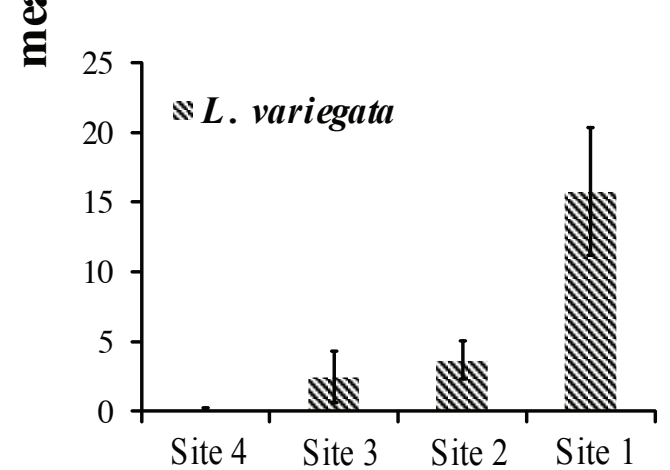
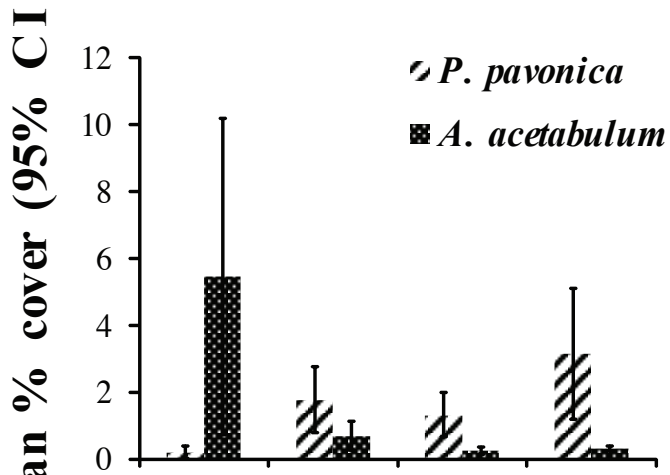
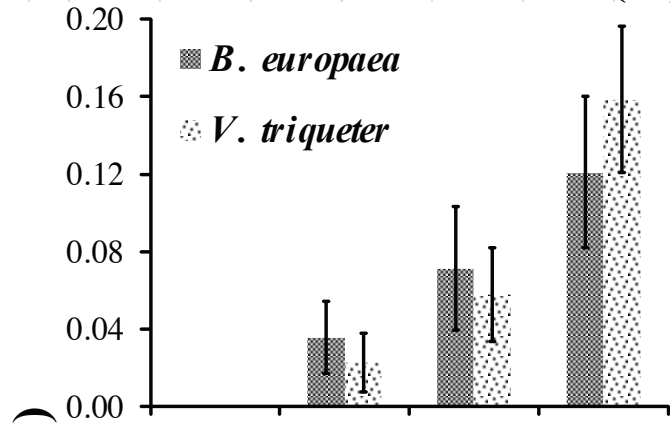
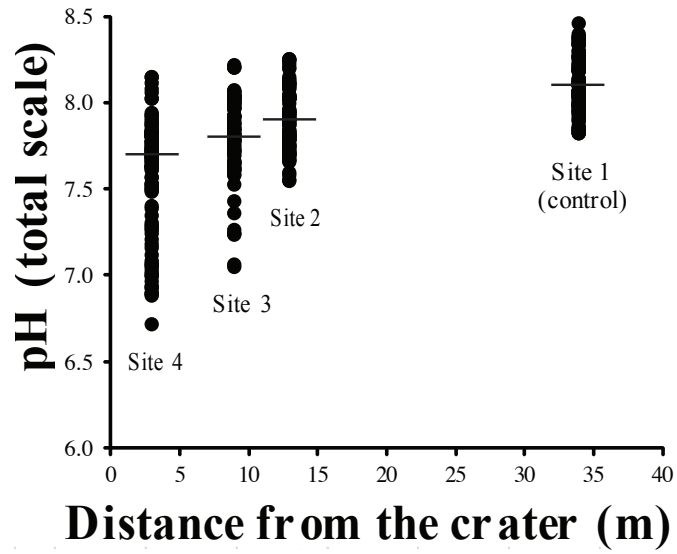
The authors declare no competing financial interests.

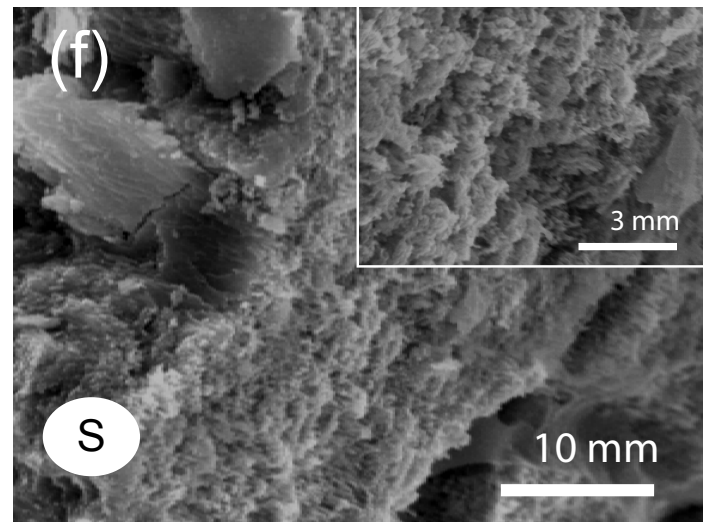
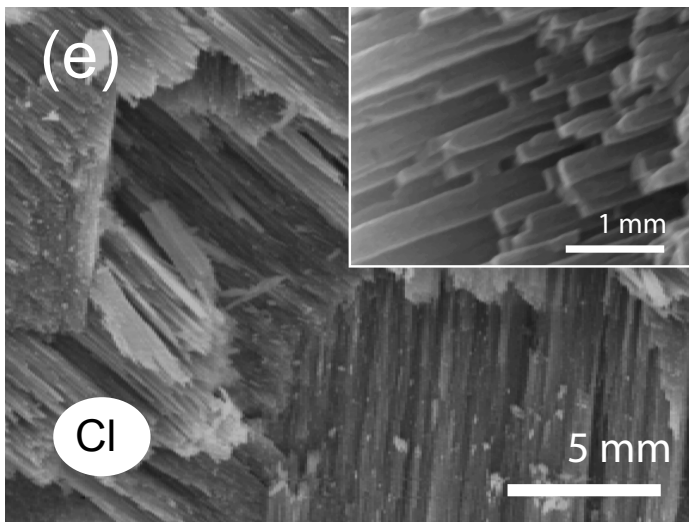
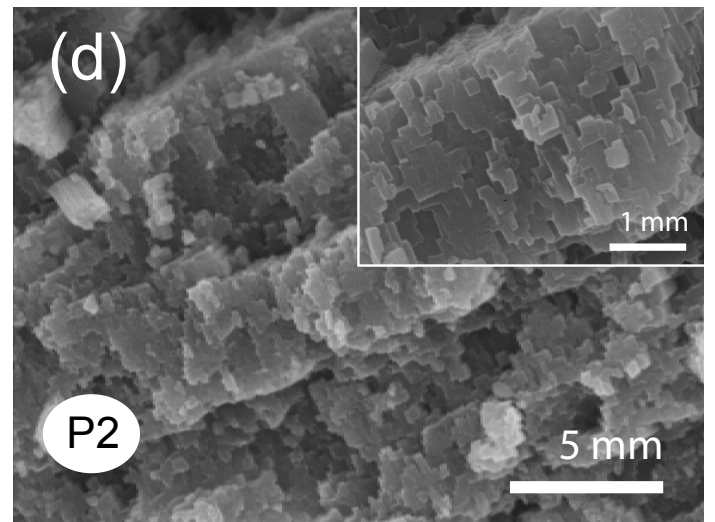
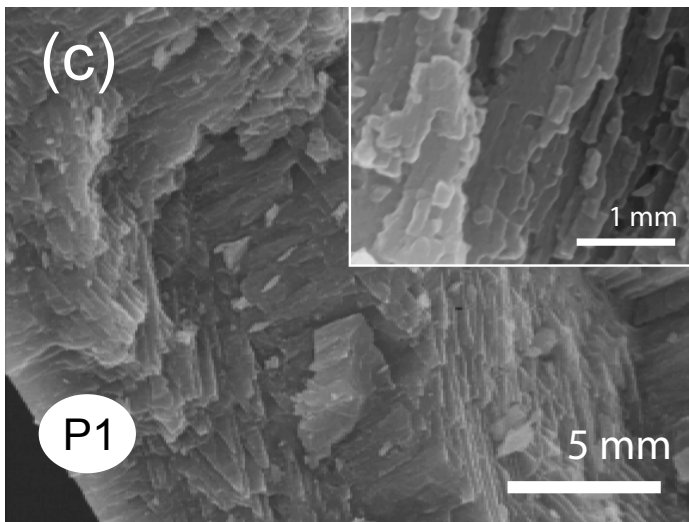
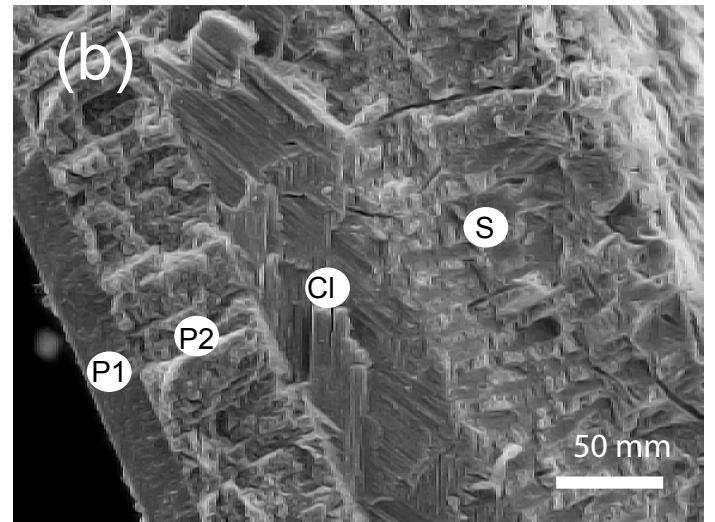
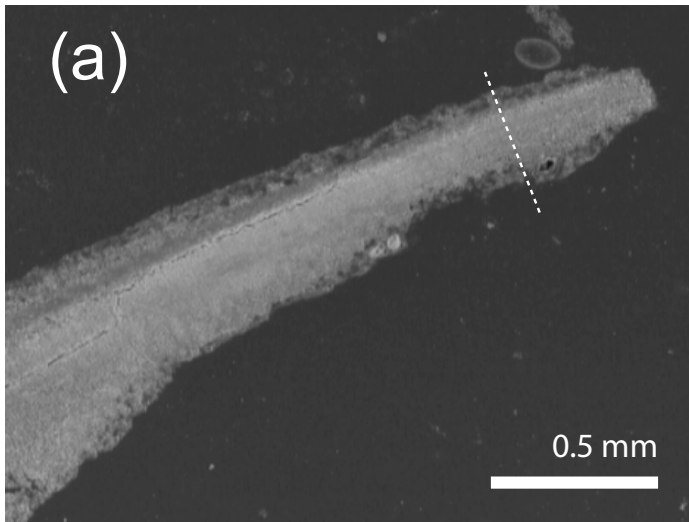
Fig. 1. Range in pH_{TS} and mean percentage cover of *Balanophyllia europaea*, *Vermetus triqueter*, *Padina pavonica*, *Acetabularia acetabulum* and *Lobophora variegata* along the pCO_2 gradient. pH measures were 103-110 per site. Horizontal bars indicate the median pH. Error bars are 95% confidence intervals.

Fig. 2. a) SEM image of the upper rim of *Vermetus triqueter* shell-tubes highlighting a transect from the inside (P1) to outside (S) the shell-tube (dotted line). b) Shell-tubes in Site 1 consisted of four layers (P1, P2, Cl, S); c) first prismatic layer (P1); d) second prismatic layer (P2), with square cross-sections; e) cross-lamellar layer (Cl); f) spherulitic layer (S) containing bores and channels. The first two layers were not present in one sample from Site 2 and in most of the samples from Site 3.

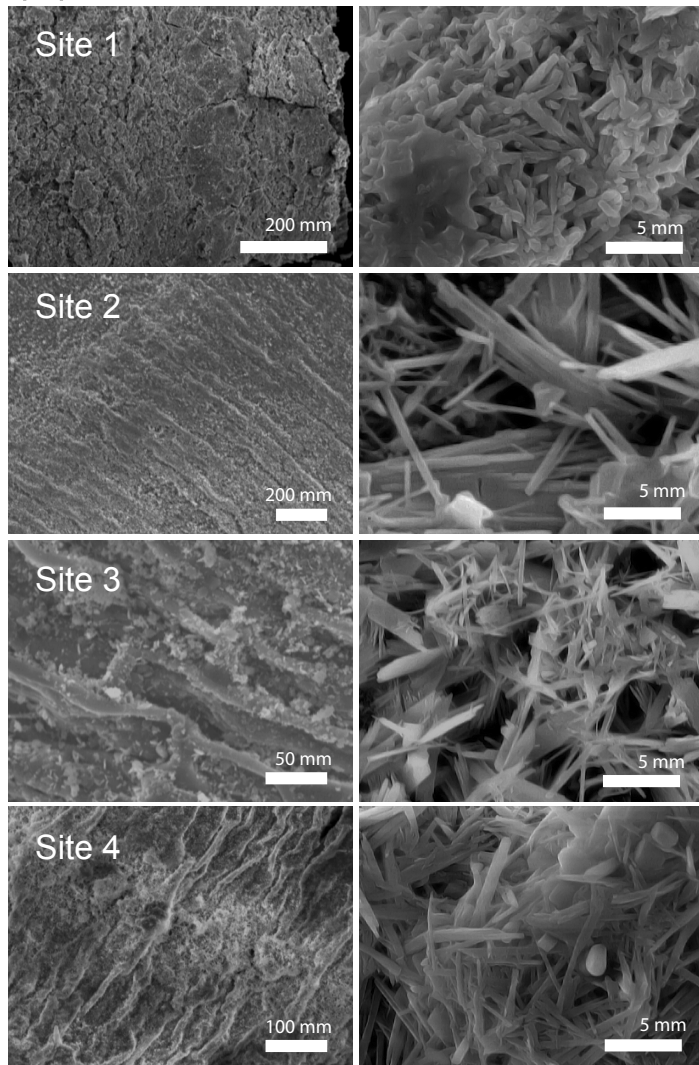
Fig. 3. SEM images of *Padina pavonica* thalli and *Acetabularia acetabulum* cups. Left column: low magnification, right column: high magnification images. *P. pavonica* became less mineralized with increasing pCO_2 . The aggregation and shape of aragonite crystals was lightly affected by pCO_2 . In *A. acetabulum*, needle-like crystals of aragonite (An) were above and among the globular aggregates (Ga). The amount of biomineralized material was reduced with increasing pCO_2 , while the center of the cup became more populated by spherical aggregates. Aragonite needles are shown in the inset for Site 2 and 3, while whewellite is shown in the inset for Site 4.

Fig. 4. *In situ* pictures of *Padina pavonica* and *Acetabularia acetabulum* at Sites 1 and 4, showing the reduction of calcified material (white areas) with increasing pCO_2 .

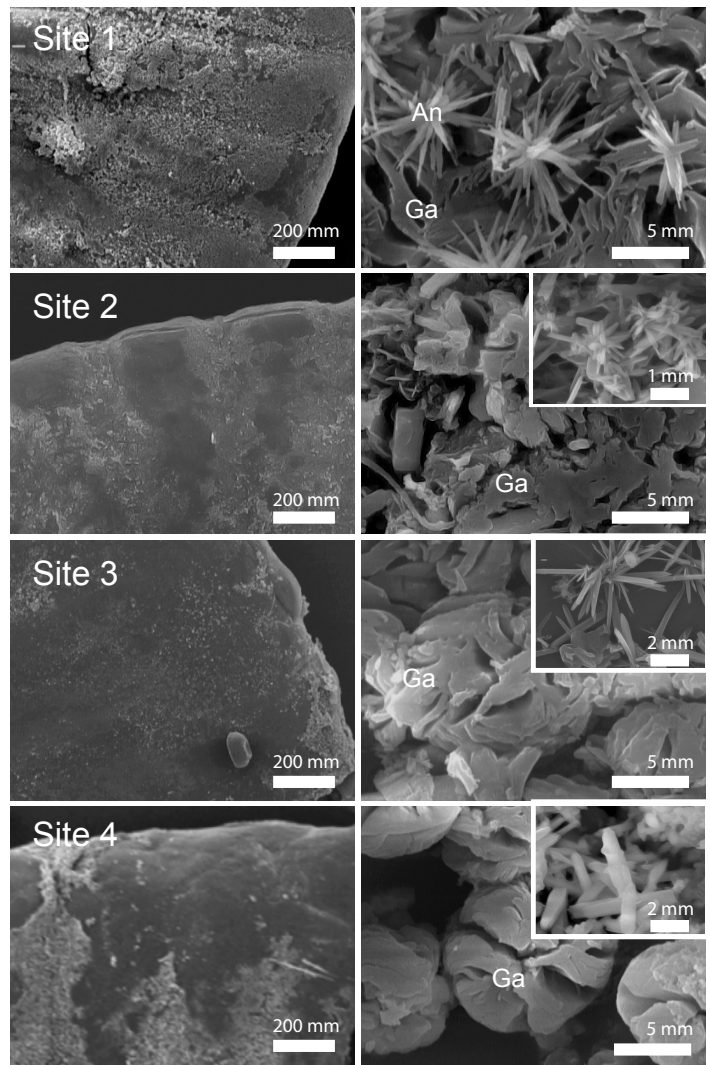




(a) *Padina pavonica*



(b) *Acetabularia acetabulum*



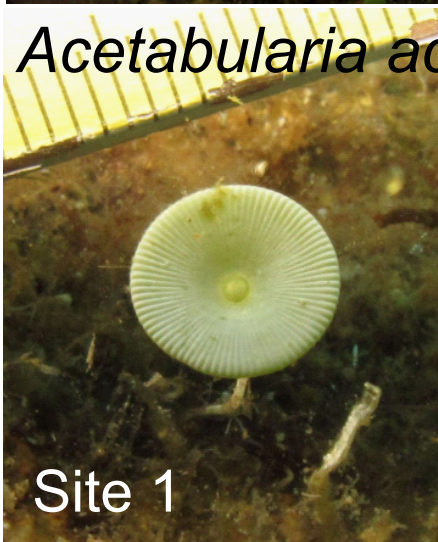
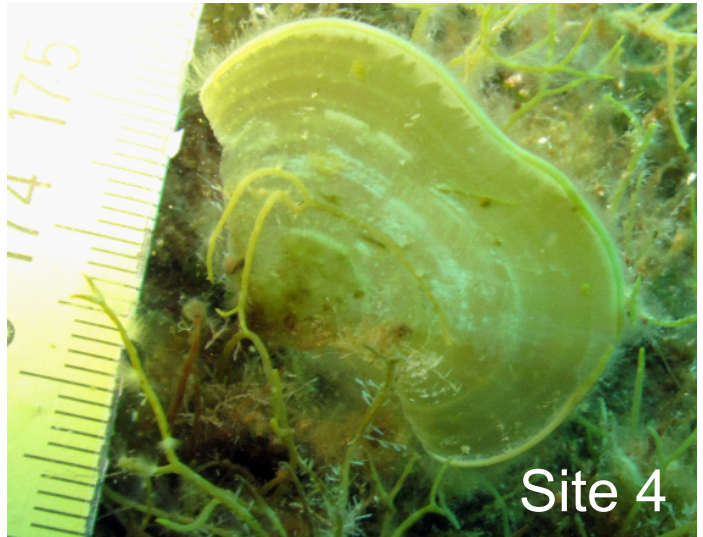


Table 1 Summary of the main effects of OA on the mineral distribution and content in the calcified organisms at increasing proximity to the CO₂ seep (declining pH). Uncertainties are one standard deviation.

	Median pH	Median Ω_{arag}	<i>Balanophyllia europaea</i>		<i>Vermetus triquetus</i>		<i>Patina pavonica</i>		<i>Acetabularia acetabulum</i>	
			min. phase	% min. phase [#]	min. phase	% min. phase [#]	min. phases	% min. phases	min. phases [*]	% min. phases
Site 1	8.1	3.6	A	97.4 ± 0.4	A	98.0 ± 0.5	A CSh [§]	73.9 ± 8.3	A Wh	42.9 ± 3.9
Site 2	7.9	2.4	A	97.80 ± 0.04	A	98.3 ± 0.2	A CSh	71.5 ± 10.6	A Wh	24.2 ± 6.9
Site 3	7.8	2.1	A	97.8 ± 0.2	A	98.1 ± 0.1	A CSh	59.6 ± 4.9	A Wh	22.7 ± 7.6
Site 4	7.7	1.5	-	-	-	-	A [§] CSh	61.6 ± 4.5	Wh	25.4 ± 8.0

A, Wh and CSh indicate aragonite, whewellite and monohydrate calcium sulphate salts. The % of mineral phase(s) is reported as mass ratio.

* Amorphous globular particles were also detected. [#] The content of organic matrix is the complement to 100 in *B. europaea* and *V. triquetus* where no significant amounts of water were detected in the skeletons and shell-tubes. *P. pavonica* and *A. acetabulum* contained a significant amount of bounded water and their percentage of organic matrix significantly increased with pCO₂. When two phases were present, the most abundant one is indicated in bold. [§]This phase was detected in traces.

Biom mineralization control related to population density under ocean acidification

Stefano Goffredo^{a*}, Fiorella Prada^a, Erik Caroselli^a, Bruno Capaccioni^b, Francesco Zaccanti^a, Luca Pasquini^c, Paola Fantazzini^{c,d}, Simona Fermani^e, Michela Reggi^e, Oren Levy^f, Katharina E. Fabricius^g, Zvy Dubinsky^f, Giuseppe Falini^{e*}

Supplementary Information

Supplementary results

Seawater chemistry of the Sites.

Vent gaseous emissions (flux = 1-30 L min⁻¹) contained 98-99% CO₂, 0.2-0.3% N₂, 0.01-0.02% O₂, 0.003-0.005% Ar, 0.001-0.002% CH₄, 0.3-0.6% H₂S by volume (detection limits: CO₂, N₂, O₂, and Ar: 0.1 ppm; CH₄: 1 ppb; H₂S: 1 ppm). Other contaminants (e.g. metals) can be excluded since the emission is exclusively gaseous at ambient temperature. Water dissolved H₂S was below detection limit (0.1 mg L⁻¹). The possible conversion of H₂S to sulphate ions would need catalytic activity of bacteria, whose presence in the bacterial mud on the bottom has irrelevant effects, since the sulphate content along the transect does not show significant variations with respect to normal seawater values (2777.5 mg L⁻¹). Moreover, the vent site is subject to strong currents^{S1} (mainly directed from North/West to South/East at speeds of 0.15-0.6 m sec⁻¹; all dives confirmed the trends highlighted in the reference, except one in which there was no current) which ensure a regular rapid water exchange and inhibit the establishment of a significant community of active bacteria. Finally, CO₂ dissolution and the effect of acidic dissociation is almost instantaneous and determines a significant lowering of pH (which has characteristic values of acidification by CO₂ and not by H₂S) and the establishment of the pH gradient.

Supplementary methods

Study site.

The Island of Panarea belongs to the Aeolian Archipelago (Italy), located in the southern Tyrrhenian Sea in the Mediterranean (Fig. S1), and is part of an active volcanic system^{S2}. In the main vent, a crater 20 x 14 m wide and 10 m deep generates a sustained column of bubbles from the seabed to the sea surface. The hydrothermal system of Panarea is characterized by very active discharges of hydrothermal water and gas from the seafloor at a shallow depth (up to 150 m)^{S3}. On the seafloor, at depths ranging from 8 to 40 m, in an area delimited by the islets of Dattilo, Bottaro, Lisca Nera and Lisca Bianca, there is a widespread presence of gas vents and hot water springs^{S4}. As reported, the hydrothermal activity at Panarea was limited to only light gas bubbling in the years of first investigations (mid-80's) and the system was considered almost static and interpreted as the declining activity of a cooling and extinct volcano^{S5}. During the night of the 3rd of November 2002, a sudden and huge outgassing phenomenon was observed on the sea surface near the islets of Bottaro and Lisca Bianca, off the eastern coast of Panarea^{S6}. Several active spots were identified by direct observations and bathymetric investigations^{S7}. After the crisis, investigations on the Panarea hydrothermal system have intensified and were performed by co-authors of this study^{S3,S5,S8-S10}. Between November 2002 and March 2003 the monitored submarine gas exhalations displayed a complex combination of temporal and spatial changes of their chemical compositions. The pre-2002 conditions were restored relatively rapidly, reaching a stationary hydrothermal condition starting from March 2003^{S11,S12}.

Carbonate chemistry.

Bottom water samples for determination of total alkalinity (TA) were collected at each site using sterile 120 ml syringes (two replicates for each site). After each dive upon return to the boat, the syringe samples were immediately transferred in labelled 100 ml amber glass bottles and immediately fixed with saturated mercuric chloride (HgCl_2) to avoid biological alteration, and stored in darkness at 4°C prior to measurement. TA was measured by Gran titration, using a 702 SM Titrino (Metrohm AG). Certified reference materials (Batch 121) from the Andrew Dickson Laboratory at UC San Diego were used to ascertain the quality of results obtained. The pH, TA, salinity and temperature were used to calculate other carbonate system parameters using the software CO2SYS with referenced dissociation constants^{S13-S15}.

Benthic surveys.

The percentage cover of all species was quantified at each site from 5-10 randomly placed quadrats, 2 m away from each other at a depth of 10-12 m. We used 50 * 50 cm quadrats for *Balanophyllia europaea* and *Vermetus triqueter* and 21.0 * 29.7 cm quadrats for *Padina pavonica*, *Acetabularia acetabulum* and *Lobophora variegata*. During each survey, photographs of each quadrat were taken using a Canon G11 camera with underwater housing. The photos were taken to fit the whole quadrat into one picture. The area of each organism within the quadrat was extracted by tracing its outline with a hand-controlled mouse on the digital image, with a digitizing software (NIS-Elements Microscope Imaging Software). The software can be used to calculate precise percentage cover in an area.

Vent gas.

Gas was sampled during five surveys (June 2011, August 2011, December 2011, April 2012, May 2013) by using a pre-weighted and pre-evacuated 50-ml thorion-tapped glass tubes, partially filled with 20 ml of a solution 0.15 M $\text{Cd}(\text{OH})_2$ and 4 M NaOH, connected to a plastic funnel positioned over the rising bubbles. To avoid contamination by seawater, the silicon connection between the funnel and the collecting glass tube was filled with Milli-Q water and isolated from seawater by a plastic plug. The plug was removed only after the complete evacuation of seawater by the gases contained in the funnel. Uncondensable gases were collected in the headspace. At the Laboratory of Fluid and Rock Geochemistry of the University of Florence, uncondensable gases were analysed with a gas-cromatograph (Shimadzu 15a), equipped with a Thermal Conductivity Detector. Methane was analyzed with a Flame Ionization Detector^{S11}. CO_2 and H_2S were trapped in the alkaline solution, the former dissolved as CO_3^{2-} and the latter precipitated as CdS. CO_2 was analysed by acidimetric titration with 0.5 N HCl solution while H_2S as SO_4^{2-} by ion chromatography after oxidation of CdS with H_2O_2 . Water samples were also collected and tested for dissolved H_2S by using $\text{Cd}(\text{OH})_2$ and ion chromatography^{S16}.

Biomineralization.

Sampling. After collection, all organism samples were rinsed with deionized water, cleaned from ground contaminations and stored in ethanol at 4°C . The skeletons of *B. europaea* and the shell-tubes of *V. triqueter* were cleaned from the live tissues by treatment with a 0.5% (v/v) sodium hypochlorite for 10 minutes^{S17}. The remaining skeletons and shell-tubes were then washed with deionized water and dried at room temperature. Each skeleton and shell-tube was inspected under a binocular microscope to remove fragments of rock and calcareous deposits produced by other organisms, such as serpulid tubes and bryozoan colonies. For some characterizations, the samples, or regions of them, were dusted using an agate mortar. Attention was paid to avoid high local increase of temperature. For microscopic observation and mechanical measurements, the samples

were embedded in resin (Technovit 5071, Buehler), and were then lightly polished using colloid alumina (average size of 1 μm , PACE Technologies). For spectroscopic measurements, the samples were sandwiched in a KBr disk and then polished normally to the disk surface. The demineralization process of the algae was carried out treating the samples with a 0.3% (v/v) acetic acid solution overnight.

A series of considerations and tests were applied to get confidence on the presence of hydrated calcium sulphate salts in the tip of the thallus of *P. pavonica*.

- i. *A. acetabulum* and *P. pavonica* were subject to the same procedure of sampling, cleaning and washing. Calcium sulphate salts were observed only on the surface of *P. pavonica*.
- ii. A set of samples after collection were stored in sea water instead that in ethanol. Also in these sample was observed the presence of calcium sulphates salts.
- iii. A third set of samples was stored in a saturated solution of calcium carbonate, but unfortunately the algae decomposed.
- iv. Upon drying of ethanol solution used to keep the algae, no detectable amounts of calcium sulphate were observed.

Despite all of the above facts we cannot completely exclude the possibility that the presence of calcium sulphate salts can be an unavoidable effect associated to the drying process, specific for *P. pavonica*.

X-ray powder diffraction. X-ray powder diffraction patterns of the samples were collected using a PanAnalytical X'Pert Pro equipped with X'Celerator detector powder diffractometer using $\text{Cu K}\alpha$ radiation generated at 40 kV and 40 mA. The diffraction patterns were collected within the 2Θ range from 10° to 60° or from 20° to 60° with a step size ($\Delta 2\Theta$) of 0.02° and a counting time of 1200 s. The X-ray powder diffraction patterns were analyzed using the X'Pert HighScore Plus software (PANalytical).

Fourier transform infrared spectroscopy. Low amount powder samples were analyzed by means of Fourier transform infrared (FTIR) spectroscopy analyses conducted by using a FTIR Nicolet 380 Thermo Electron Corporation, working in the range of wavenumbers $4000\text{--}400\text{ cm}^{-1}$ at a resolution of 2 cm^{-1} . Disk was obtained mixing a small amount ($<1\text{ mg}$) of sample with 100 mg of KBr and applying a pressure of 48.6 tsi (670.2 MPa) to the mixture using a hydraulic press.

Attenuated Total Reflection Fourier transform Infrared (FTIR ATR) spectra of sample cross sections were acquired in the range $4000\text{--}650\text{ cm}^{-1}$ with a Thermo-Nicolet Nexus 5700 spectrometer connected to a Thermo Continuum IR microscope, fitted with an MCT type A detector cooled by liquid nitrogen. Measurements were made with the microscope in reflection mode, using a $15\times$ Thermo-Electron Infinity Replachromat objective and a tube factor of $10\times$. A micro slide-on ATR with a silicon crystal (contact area diameter $120\text{ }\mu\text{m}$) was connected to the $15\times$ objective.

Thermal analyses. An estimation of the organic matter content in the sample was determined by thermo-gravimetric analysis (TGA) on a SDT Q600 simultaneous thermal analysis instrument (TA instrument). The analysis was performed under nitrogen flow from 30 to 120°C with a heating rate of $10^\circ\text{C min}^{-1}$, an isothermal at 120°C for 5 min, and another cycle from 120 to 600°C with the same heating rate. The reported values are the average of at least three independent measurements.

Microscopy. Several fractured and polished sections of samples were cut perpendicular to the surface. Polished sections and some fractures were etched with various acids and enzymes to reveal microstructural features. The optical microscope observations of samples were made with a Leica microscope equipped with a digital camera. The scanning electron microscopy (SEM) observations were conducted in a PhenomTM microscope (FEI) for uncoated samples and a Hitachi FEG 6400 microscope for samples after coating with gold. Presented images are representative of the entire population of each sample.

The aragonitic fiber diameter in the coral skeleton was measured from high magnification SEM images (see Fig. S5). About 20 fibers were measured from three different skeleton fragments for each site.

Mechanical analyses. The mechanical properties of coral skeletons and mollusc shell-tubes were measured using a Nanoindentation Tester, model NHT-TTX by CSM Instruments, equipped with a Berkovich diamond tip. The maximum applied load in the test was always 50 mN, corresponding to a penetration depth in the range from 700 to 900 nm. The instrumented (IT) values of the elastic Young's modulus (E_{IT}) and hardness (H_{IT}) were determined by Oliver-Pharr analysis of the load-depth curves^{S18}. The reported values are the average of at least 10 measurements.

Supplementary references

- S1. Aliani, S., Bortoluzzi, G., Caramanna, G. & Raffa, F. Seawater dynamics and environmental settings after November 2002 gas eruption off Bottaro (Panarea, Aeolian Islands, Mediterranean Sea). *Cont. Shelf Res.* **30**, 1338-1348 (2010).
- S2. De Astis, G., Ventura, G. & Vilardo, G. Geodynamic significance of the Aeolian volcanism (Southern Tyrrhenian Sea, Italy) in light of structural, seismological, and geochemical data. *Tectonics* **22**, 1040 (2003).
- S3. Gugliandolo, C., Italiano, F. & Maugeri, T. L. The submarine hydrothermal system of Panarea (Southern Italy): biogeochemical processes at the thermal fluids-sea bottom interface. *Ann. Geophys.-Italy* **49**, 783-792 (2006).
- S4. Gamberi, F., Marani, P. M. & Savelli, C. Tectonic, volcanic and hydrothermal features of submarine portion of Aeolian arc (Tyrrhenian Sea). *Mar. Geol.* **140**, 167-181 (1997).
- S5. Tassi, F. *et al.* Low-pH waters discharging from submarine vents at Panarea Island (Aeolian Islands, southern Italy) after the 2002 gas blast: Origin of hydrothermal fluids and implications for volcanic surveillance. *Appl. Geochem.* **24**, 246-254 (2009).
- S6. Esposito, A., Giordano, G. & Anzidei, M. The 2002-2003 submarine gas eruption at Panarea volcano (Aeolian Islands, Italy): Volcanology of the seafloor and implications for the hazard scenario. *Mar. Geol.* **227**, 119-134 (2006).
- S7. Anzidei, M., Esposito, A., Bortoluzzi, G. & De Giosa, F. The high resolution bathymetric map of the exhalative area of Panarea (Aeolian Islands, Italy). *Ann. Geophys.-Italy* **48**, 899-921 (2005).
- S8. Caracausi, A. *et al.* Changes in fluid geochemistry and physico-chemical conditions of geothermal systems caused by magmatic input: The recent abrupt outgassing off the island of Panarea (Aeolian Islands, Italy). *Geochim. Cosmochim. Acta* **69**, 3045-3059 (2005).
- S9. Chiodini, G. *et al.* *Relazione sulle Emissioni Gassose Antistanti l'Isola di Panarea, Novembre-Dicembre 2002* (Istituto Nazionale di Geofisica e Vulcanologia, 2003).
- S10. Chiodini, G. *et al.* Geochemistry of the submarine gaseous emissions of Panarea (Aeolian Islands, Southern Italy): magmatic vs. hydrothermal origin and implications for volcanic surveillance. *Pure Appl. Geophys.* **163**, 759-780 (2006).

- S11. Capaccioni, B., Tassi, F., Vaselli, D., Tedesco, D. & Rossi, P. L. The November 2002 degassing event at Panarea Island (Italy): the results of a 5 months geochemical monitoring program. *Ann. Geophys.-Italy* **48**, 755-765 (2005).
- S12. Capaccioni, B., Tassi, F., Vaselli, D., Tedesco, D. & Poreda, R. Submarine gas burst at Panarea Island (Southern Italy) on 3 November 2002: a magmatic versus hydrothermal episode. *J. Geophys. Res.* **112**, B05201 (2007).
- S13. Mehrbach, C., Culberson, C. H., Hawley, J. E. & Pytkowicz, R. M. Measurement of the apparent dissociation constants of carbonic acid in seawater at atmospheric pressure. *Limnol. Oceanogr.* **18**, 897-907 (1973).
- S14. Dickson, A. G. & Millero, F. J. A comparison of the equilibrium constants for the dissociation of carbonic acid in seawater media. *Deep-Sea Res. A* **34**, 1733-1743 (1987).
- S15. Dickson, A. G. Thermodynamics of the dissociation of boric acid in synthetic sea water from 273.15 to 298.15 K. *Deep-Sea Res. A* **37**, 755-766 (1990).
- S16. Montegrossi, G., Tassi, F., Vaselli, O., Bidini, E. & Minissale, A. A new, rapid and reliable method for the determination of reduced sulphur (S²⁻) species in natural water discharges. *Appl. Geochem.* **21**, 849-857 (2006).
- S17. Pingitore, N. E., et al. (1993) Dissolution kinetics of CaCO₃ in common laboratory solvents. *J. Sediment. Petrol.* **63**, 641-645.
- S18. Oliver, W. C. & Pharr, G. M. An improved technique for determining hardness and elastic modulus using load and displacement sensing indentation experiments. *J. Mater. Res.* **7**, 1564-1583 (1992).

Fig. S1. Map of vent site off Panarea Island (Aeolian Archipelago) and bathymetric profile of the experimental area. Underwater volcanic crater with localized CO₂ emissions a few tens of meters SE of Bottaro, one of the islets surrounding Panarea. Depth along the pCO₂ gradient goes from 11.6 m in the center of the crater to 9.2 m in the control site, at a distance of 34 m from the crater. pH values in brackets are expressed as medians at the total scale.

Fig. S2. Fourier transform infrared spectra (a, c, e, g) and X-ray powder diffraction patterns (b, d, f, h) from ground skeletons of *Balanophyllia europaea* (a, b) and ground shell-tubes of *Vermetus triqueter* (c, d) collected at Sites 1 to 3 along the pCO₂ gradient, and from ground samples of *Padina pavonica* (e, f) and *Acetabularia acetabulum* (g, h) collected at Sites 1 to 4. In (a-d) only absorption bands and diffraction peaks due to aragonite are observable. In *P. pavonica* (g, h) absorption bands and diffraction peaks due to aragonite (A) and mono hydrate calcium sulphate minerals (CSh) are marked. In *A. acetabulum* (e, f) only absorption bands and diffraction peaks due to aragonite (A) and whewellite (Wh) are observable. The diffraction peaks are indicated according to the Miller indices. Spectra are vertically offset to increase their readability.

Fig. S3. Percentage weight loss of the samples with increasing temperature (thermo gravimetric profiles, green curves) and their first derivate curves (blue curves). (a-c) skeletons of *Balanophyllia europaea* and (d-f) shell-tubes of *Vermetus triqueter* from Sites 1 to 3 along the pCO₂ gradient. (g-j) thalli of *Padina pavonica* and (k-n) cups of *Acetabularia acetabulum* from Sites 1-4. Each TGA profile shows two weight loss events: the first one, which occurs at lower temperature, can be associated to the release of bounded water molecules, while the second one is due to the pyrolysis of the organic matrix.

Fig. S4. SEM images of *Balanophyllia europaea* skeletons. Centers of calcification (indicated by arrows) and fibers were observed. Their size and shape were not related to pCO₂.

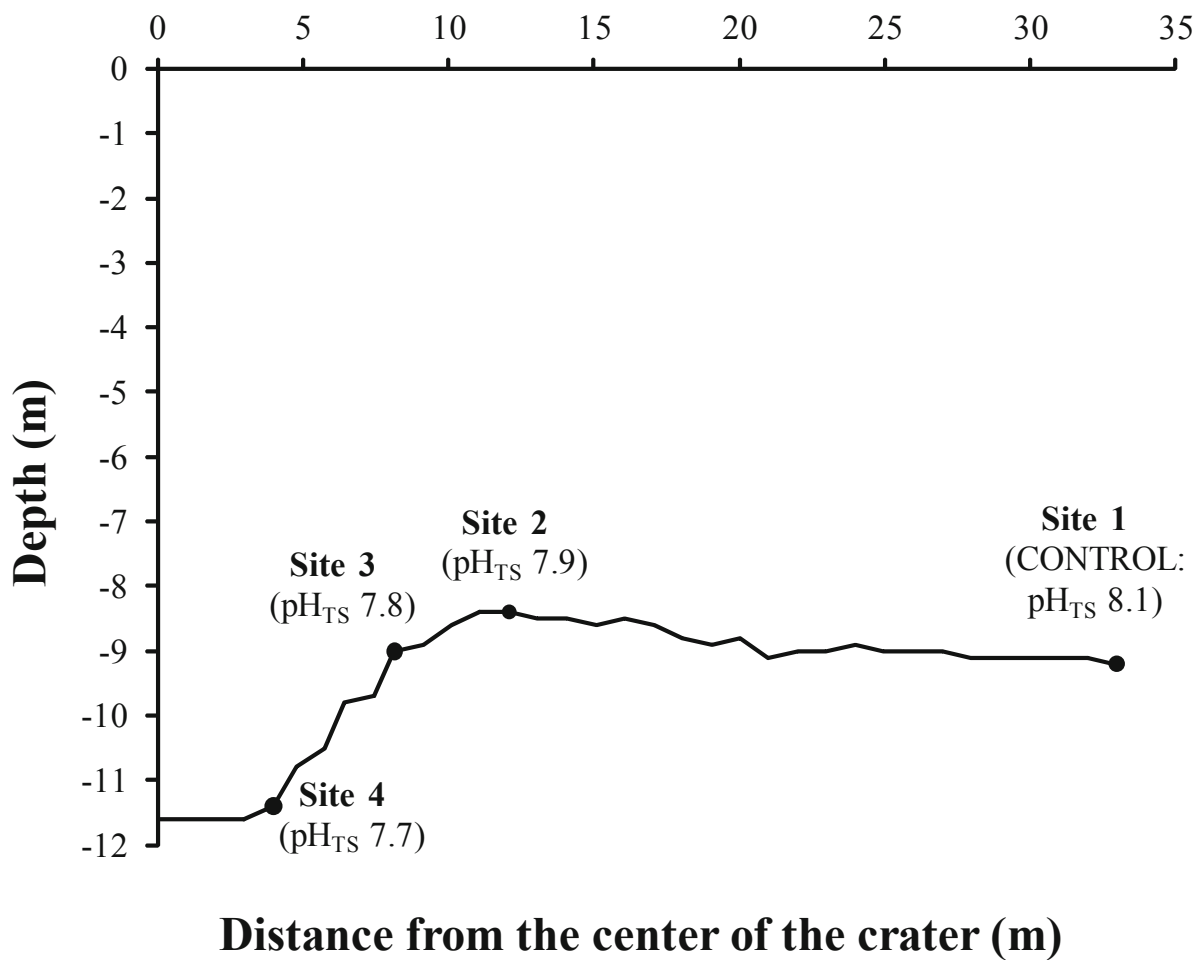
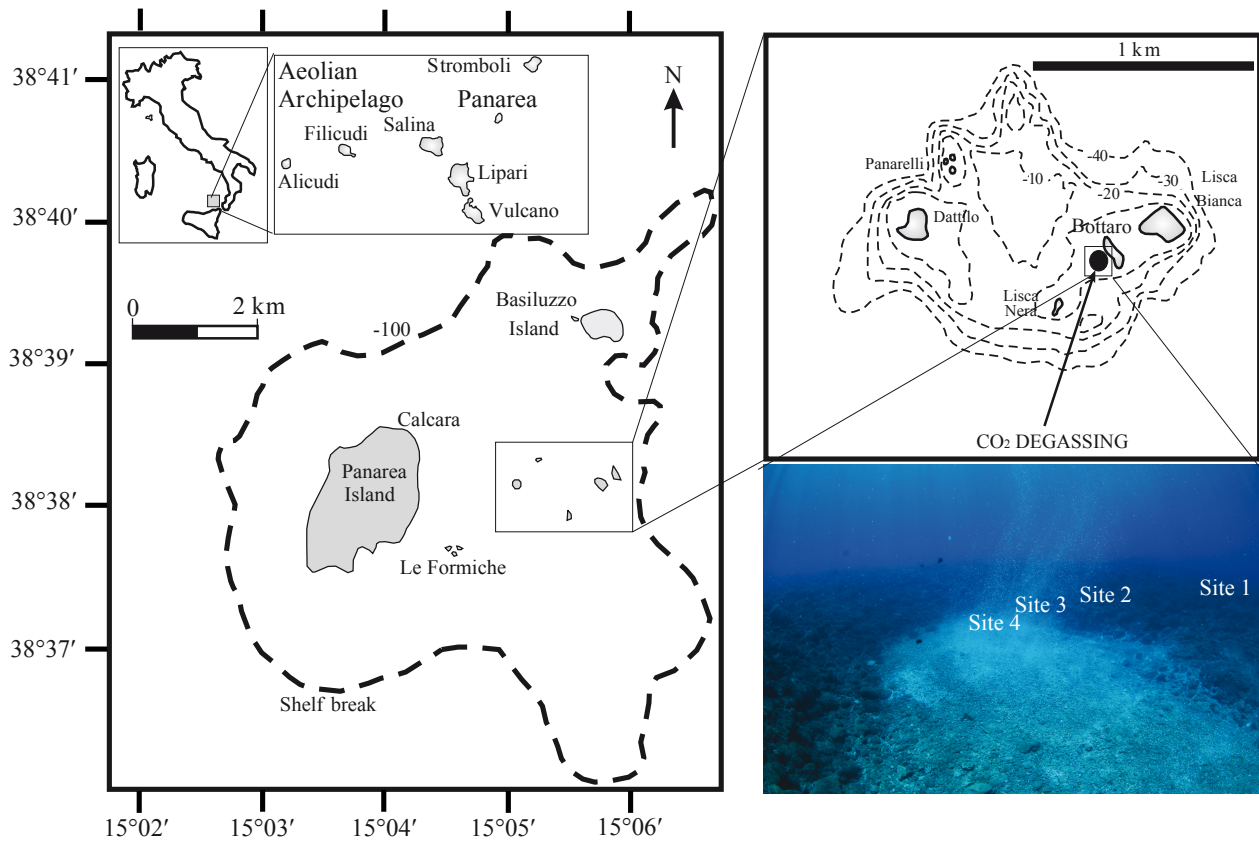
Fig. S5. SEM images of the cross sections of the tip regions of septa of *Balanophyllia europaea* skeletons collected at Sites 1 to 3 along the pCO₂ gradient. The two structural entities constituting the coral skeleton, centers of calcification and fibers, are illustrated in the left and right columns, respectively. The observed differences were not statistically significant.

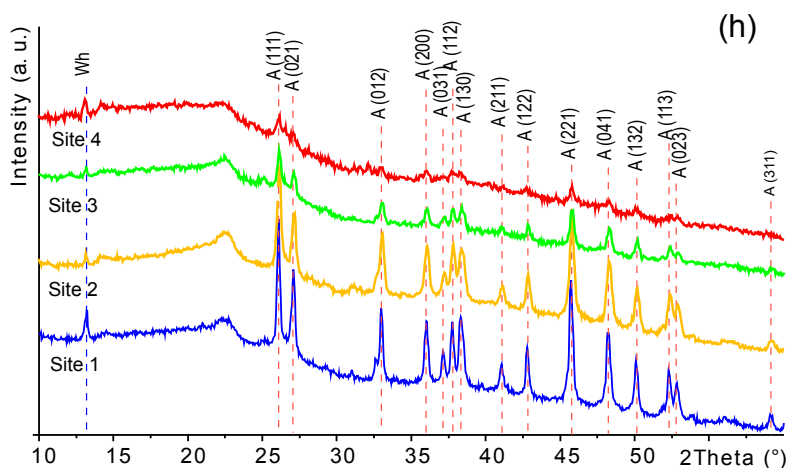
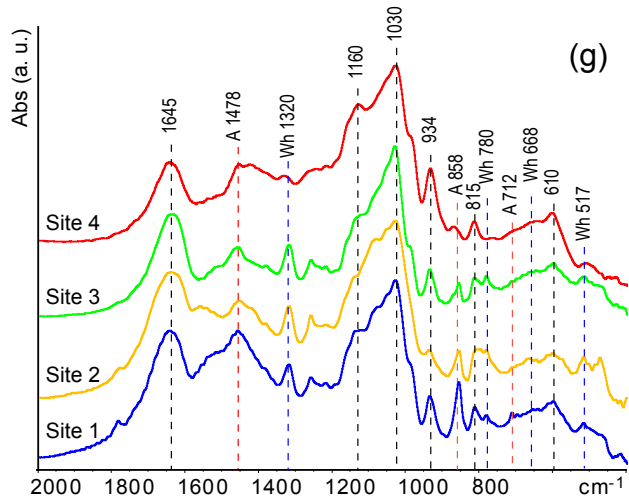
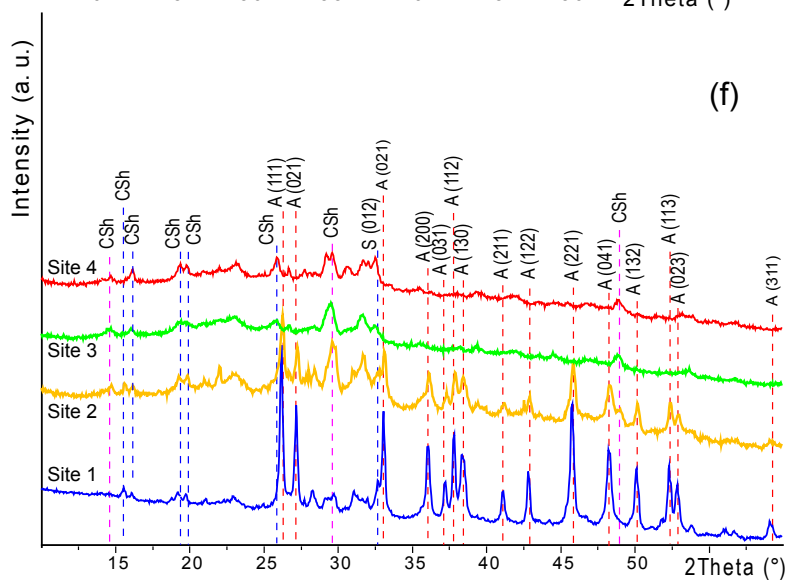
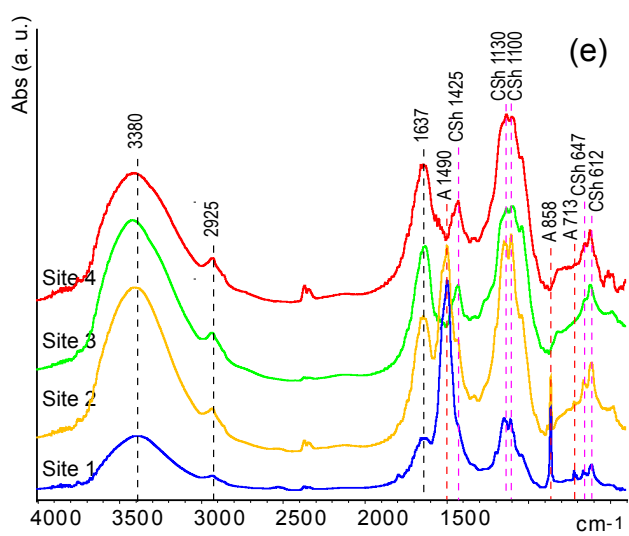
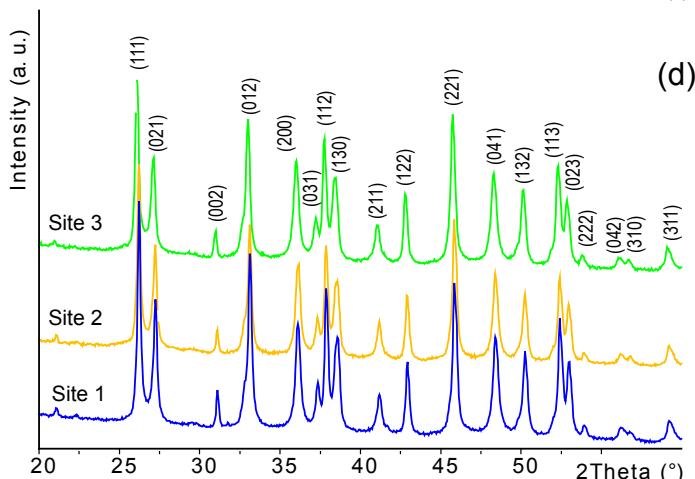
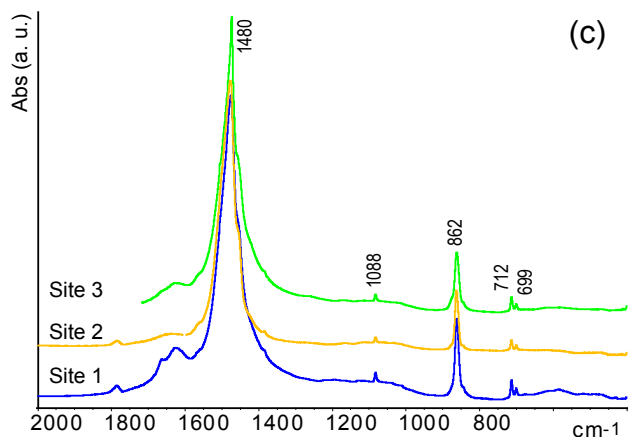
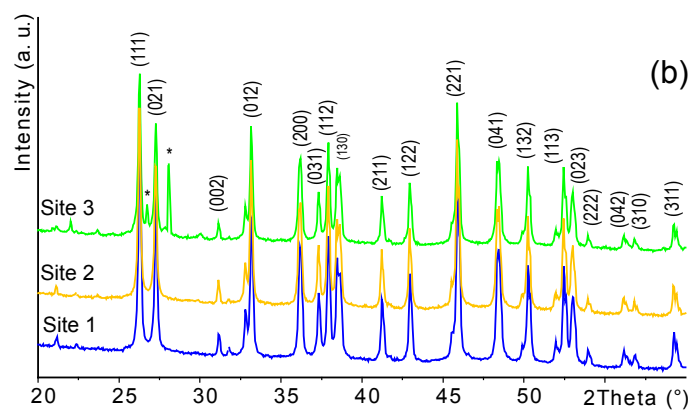
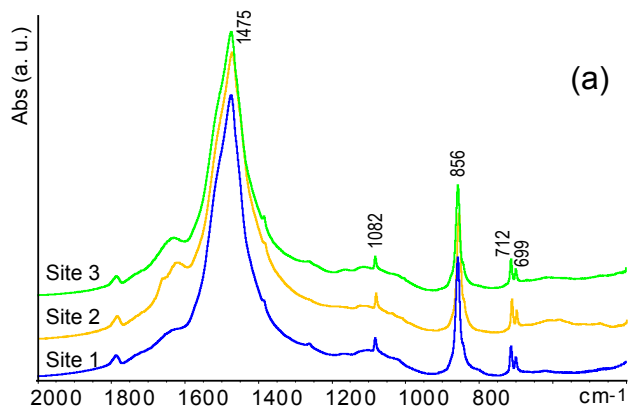
Fig. S6. First row Dry thalli of *Padina pavonica* (a) and dry cups of *Acetabularia acetabulum* (b) collected at Sites 1 to 4 along the pCO₂ gradient. The calcified regions appeared white, with the upward facing surfaces being more heavily calcified than the downward facing surfaces. SEM

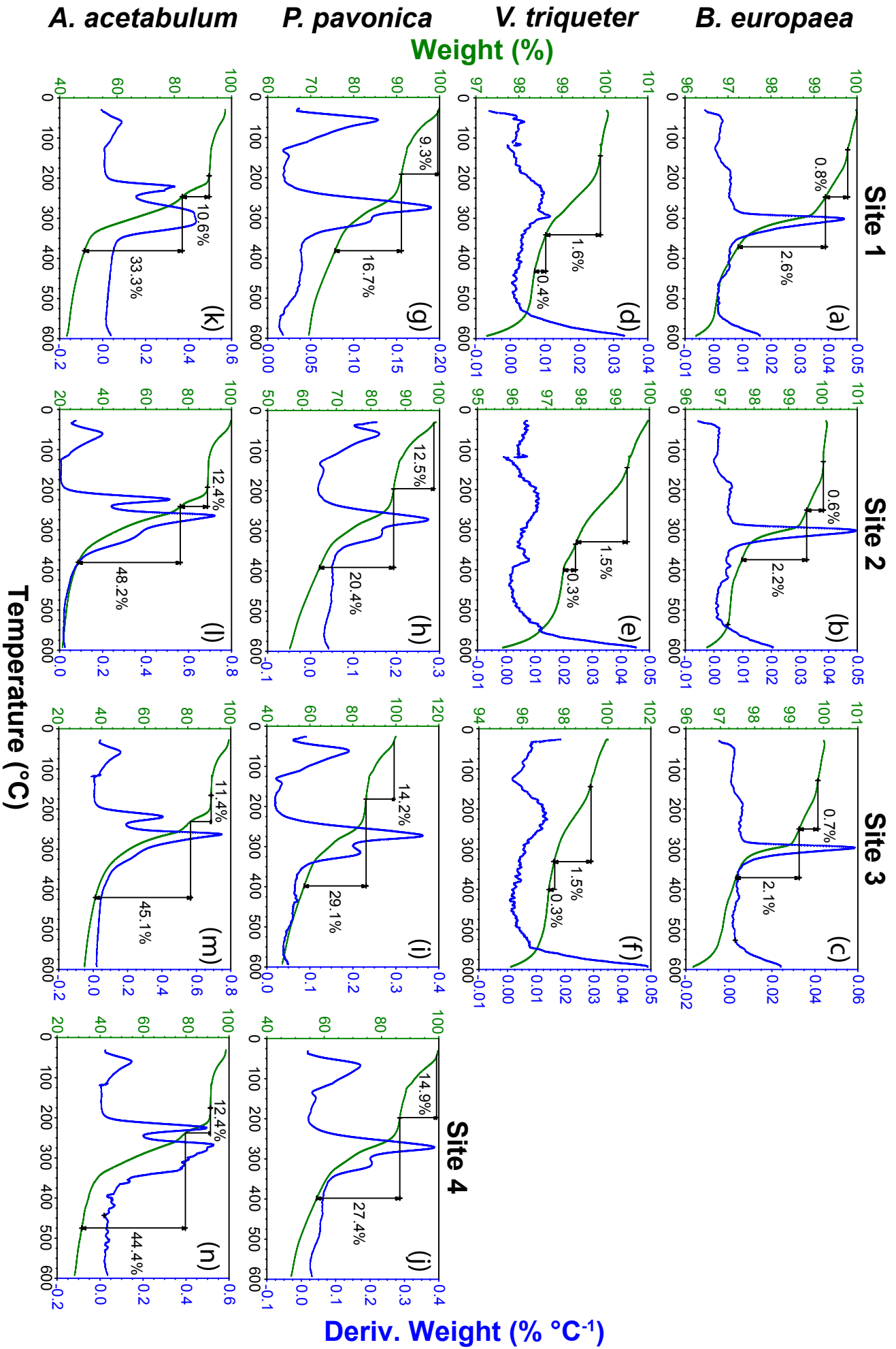
images (*first column*) of the cross sections of the thalli (a) and the cups (b) and corresponding ATR FTIR spectra (*second column*) at three points, the two surfaces (1, upward; 3, downward) and inside the algae (2), for each sample at each site. The dotted line in the ATR FTIR spectra indicate the band associated to aragonite. The image shows that the upward pointing face is more calcified than the downward facing surface and that mineral phases were not detected inside the algae thalli or cups. SEM images (*third column*) of the surface of the thalli (a) and cups (b) after overnight treatment with a 0.3% acetic acid solution and corresponding FTIR spectra (*fourth column*). The surfaces are completely free of mineral phases and FTIR spectra do not show any absorption band clearly associable to mineral phases.

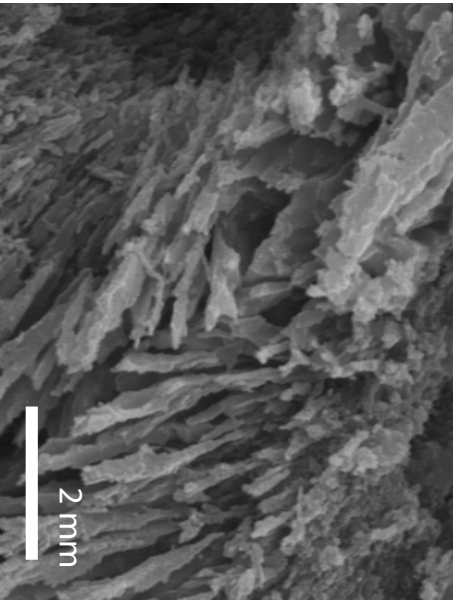
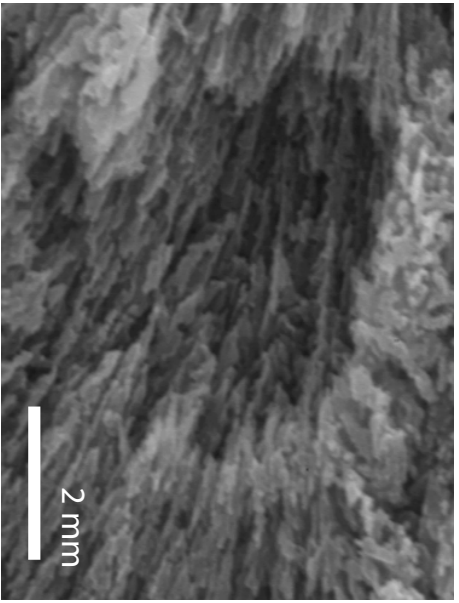
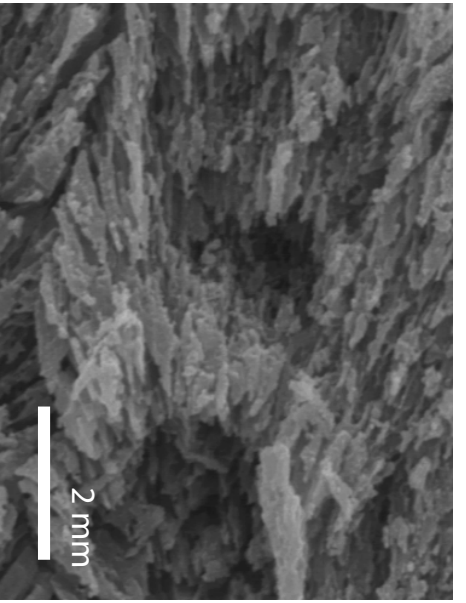
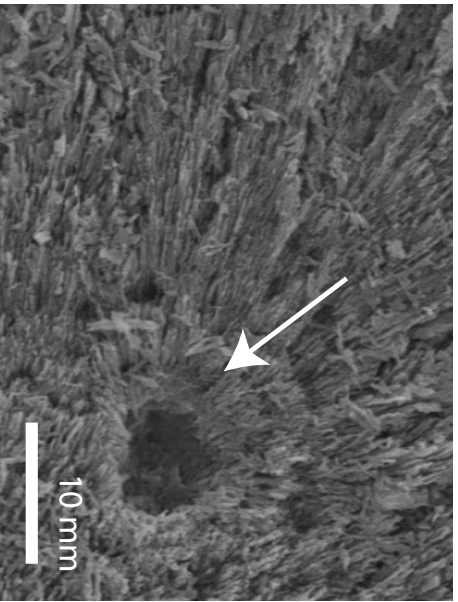
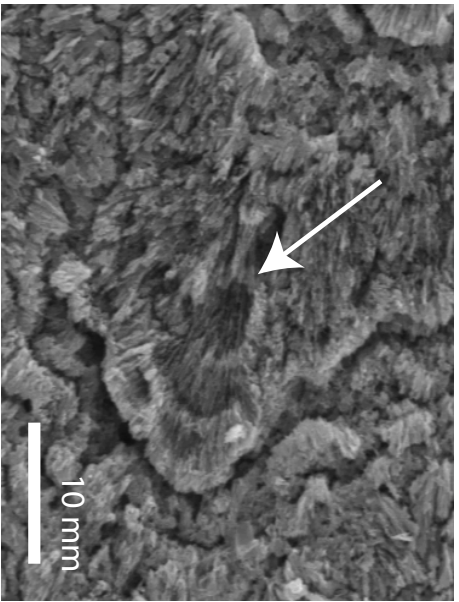
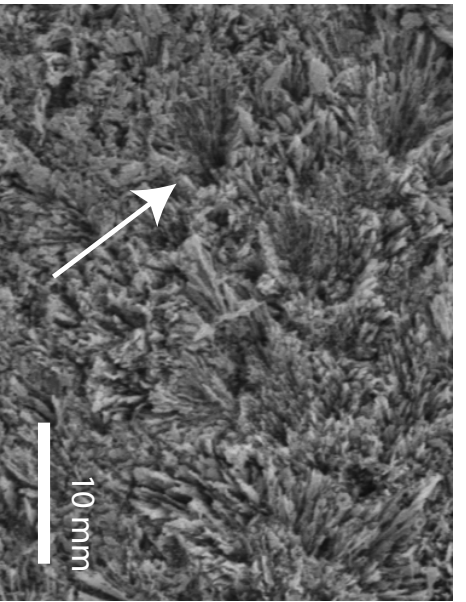
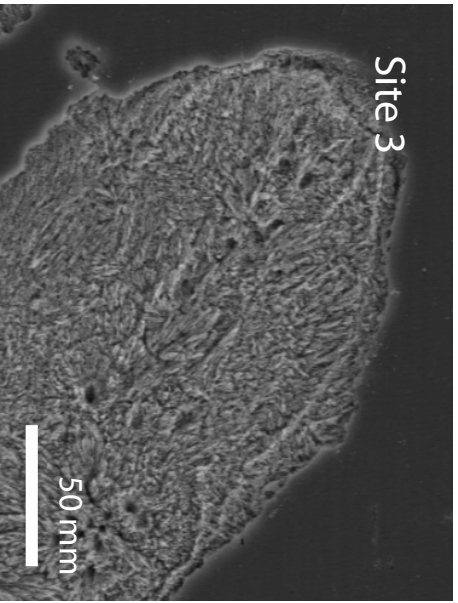
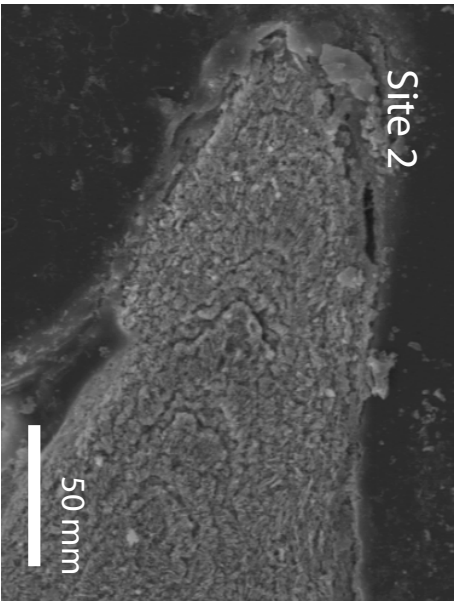
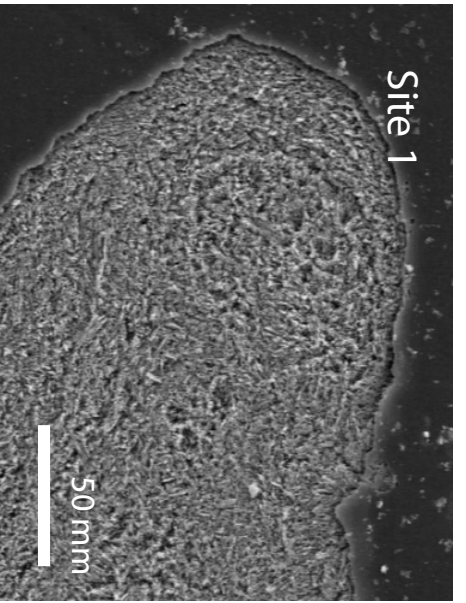
Supplementary video legend

Underwater video showing CO₂ degassing from the crater.









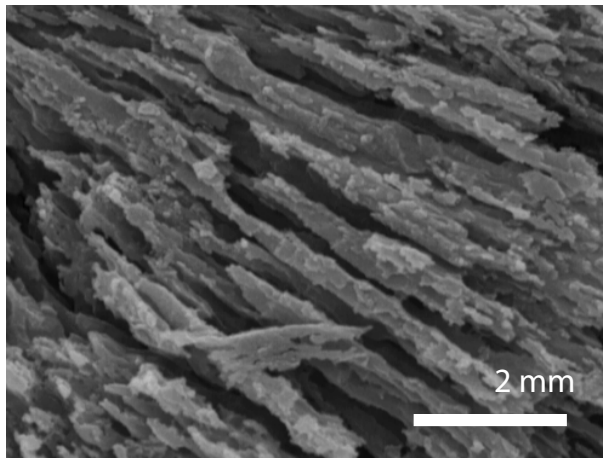
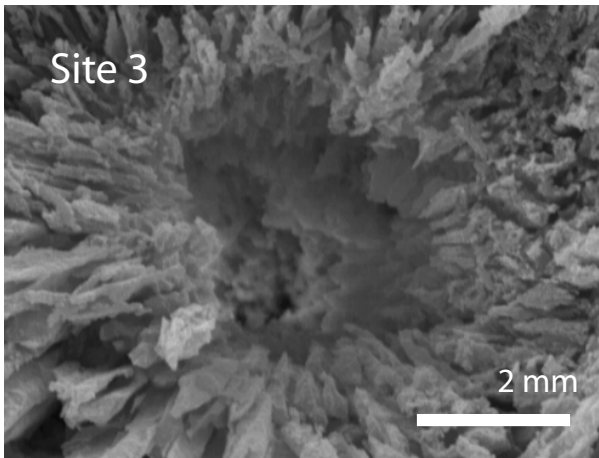
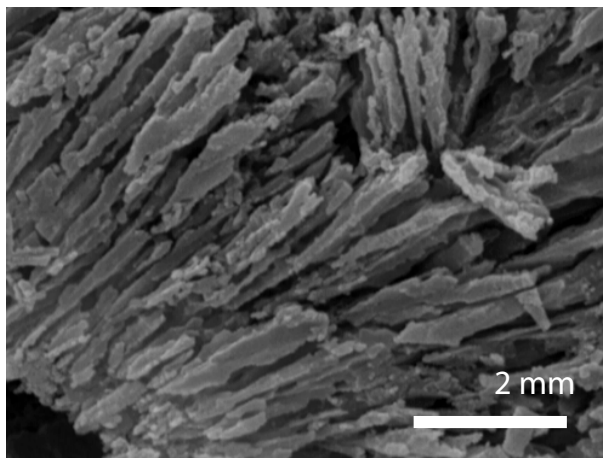
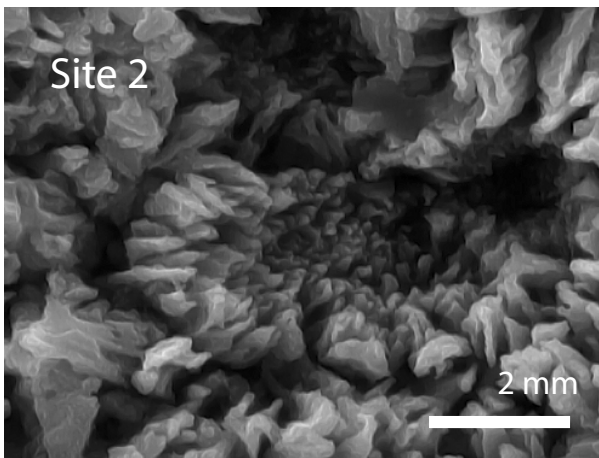
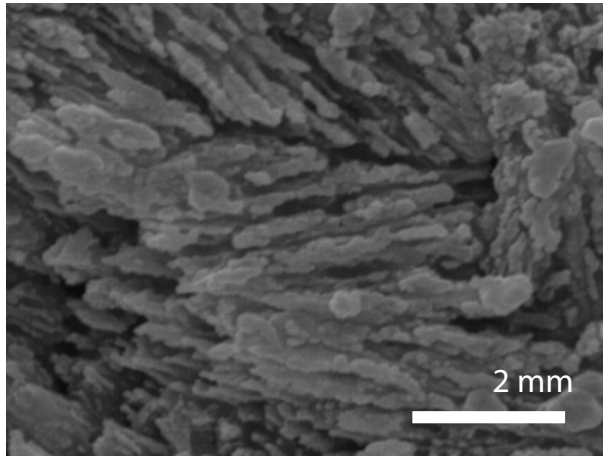
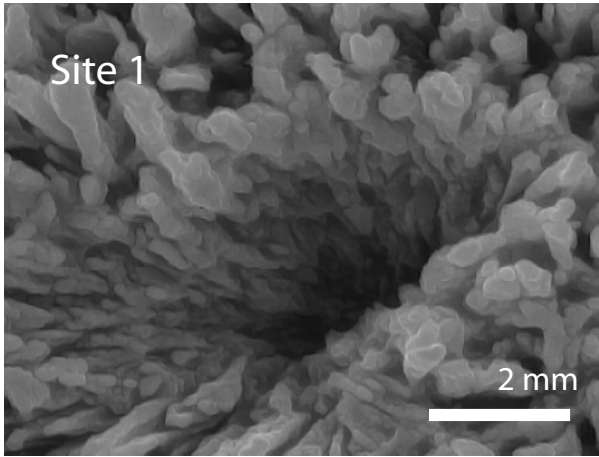


Table S1 Seawater carbonate chemistry measurements for each study Site off the Island of Panarea. Site 1 is the control and sites 2-4 are the elevated pCO₂ Sites. Temperature ($n = 2580$ per site) data were recorded every three hours by data loggers placed in each Site from May to September 2012 and from November 2012 to April 2013. pH ($n = 103$ -110 per Site) and salinity ($= 37\%$, $n = 107$ -110 per Site) were measured in July 2010, September 2010, November 2010, March 2011, June 2011, July-August 2011, November-December 2011, April-May 2012, June 2012 and May 2013 (over 36 days). TA (total alkalinity, $n = 8$ per Site) was measured in September 2010, November 2010, March 2011, June 2011, July-August 2011, November-December 2011, April-May 2012 and June 2012. The pH, temperature, salinity and total alkalinity (TA) were used to calculate carbonate system parameters (*) using CO2SYS software. DIC: dissolved inorganic carbon.

	pH range (total scale)	T (°C)	TA ($\mu\text{mol kg}^{-1}$)	*pCO ₂ (μatm)	*DIC ($\mu\text{mol kg}^{-1}$)	*CO ₃ ²⁻ ($\mu\text{mol kg}^{-1}$)	*HCO ₃ ⁻ ($\mu\text{mol kg}^{-1}$)	* Ω_{calc}	* Ω_{arag}	
Site 1	95%ile	8.4	27.0	2595	754	2323	358	2168	8.2	5.4
	Median	8.1	18.0	2457	405	2195	208	1974	4.9	3.2
	5%ile	7.8	13.5	2424	179	1974	129	1611	3.1	2.0
Site 2	95%ile	8.2	28.0	2603	1171	2430	275	2299	6.4	4.3
	Median	7.9	18.5	2455	652	2322	155	2144	3.6	2.4
	5%ile	7.7	14.0	2401	273	2142	91	1858	2.1	1.4
Site 3	95%ile	8.1	27.5	2573	2143	2457	237	2332	5.6	3.7
	Median	7.8	18.5	2450	715	2284	141	2119	3.3	2.2
	5%ile	7.3	14.0	2390	403	2133	54	1890	1.3	0.8
Site 4	95%ile	8.0	27.0	2551	6532	2613	199	2384	4.2	2.8
	Median	7.7	18.5	2415	1110	2326	96	2195	2.2	1.5
	5%ile	6.9	14.0	2357	445	2150	20	1938	0.5	0.3

Table S2. Hardness (HIT) and elastic Young's modulus (EIT) values calculated at an indentation depth of 200 nm, averaged over three different samples of the same type. At least 20 nanoindentation measurements were carried in each sample for each region. In *Balanophyllia europaea*, the measurements were carried out at three points along the aboral – oral direction (aboral, middle, oral). In *Vernmetus triquetus*, the measurements were carried out within each region defining its diverse texture: prismatic, cross lamellar, and spherulitic. The ranges shown are one standard deviation.

		<i>B. europaea</i>			<i>V. triquetus</i>		
		aboral	middle	oral	prismatic	cross lamellar	spherulitic
Site 1	HIT (MPa)	5100 ± 500	5100 ± 500	5100 ± 500	4600 ± 400	4600 ± 400	4000 ± 350
	EIT (GPa)	80 ± 3	71 ± 3	60 ± 5	91 ± 3	81 ± 2	74 ± 4
Site 2	HIT (MPa)	5200 ± 600	5200 ± 600	5200 ± 600	4700 ± 400	4700 ± 400	4000 ± 350
	EIT (GPa)	71 ± 3	61 ± 4	44 ± 6	89 ± 3	80 ± 3	73 ± 4
Site 3	HIT (MPa)	5000 ± 500	5000 ± 500	5000 ± 500	-	4300 ± 400	4000 ± 350
	EIT (GPa)	70 ± 3	63 ± 3	49 ± 5	-	80 ± 2	73 ± 4

Table S3 Correlation analysis between % cover of *Balanophyllia europaea*, *Vermetus triqueter*, *Padina pavonica* and *Lobophora variegata* and pH at four Sites along a natural pCO₂ gradient. Percentage cover of *Acetabularia acetabulum* was homogeneous among Sites.

Species	<i>n</i>	rho	<i>r_s²</i>
<i>B. europaea</i>	110	0.588***	0.346
<i>V. triqueter</i>	139	0.626***	0.392
<i>P. pavonica</i>	105	0.434***	0.188
<i>L. variegata</i>	53	0.858***	0.736

n, number of quadrats; rho, Spearman's correlation coefficient, *r_s²*, Spearman's determination coefficient; *** *p* < 0.001.

**Chapter 6:
Skeletal porosity of a coral living in a
natural model of ocean acidification
increases with CO₂**

Manuscript in preparation

Skeletal porosity of a coral living in a natural model of ocean acidification increases with CO₂

Paola Fantazzini^{*a,b,c}, Stefano Mengoli^c, Manuel Mariani^{a,b}, Leonardo Brizi^{a,b}, Luca Pasquini^a, Giuseppe Falini^d, Stefano Goffredo^e, Erik Caroselli^e, Fiorella Prada^e, Oren Levy^f, Zvy Dubinsky^f

^a Department of Physics and Astronomy, Alma Mater Studiorum - University of Bologna, Viale Berti Pichat 6/2, 40127 Bologna, Italy

^b Centro Enrico Fermi, Roma, Italy

^c Management Department, Alma Mater Studiorum - University of Bologna, Via Capo di Lucca 34, 40126 Bologna, Italy

^d Department of Chemistry “G. Ciamician”, Alma Mater Studiorum – University of Bologna, Via Selmi 2, 40126 Bologna, Italy

^e Marine Science Group, Department of Biological, Geological and Environmental Sciences, Section of Biology, Alma Mater Studiorum – University of Bologna, Via Selmi 3, 40126 Bologna, Italy

^f The Mina and Everard Goodman Faculty of Life Sciences, Bar-Ilan University, Ramat-Gan, 52900 Israel.

*Corresponding author: Paola Fantazzini; tel: +390512095119; fax: +390512095047; paola.fantazzini@unibo.it

Abstract

Global environmental changes, including ocean acidification, have been identified as a major threat to scleractinian corals. In particular, the potential effects of a lowering pH on tropical coral reefs have received special attention. Only a few studies have focused on testing the effects of ocean acidification in corals from the Mediterranean Sea, despite the fact that this basin is especially sensitive to increasing atmospheric CO₂. In this context, we investigated the response to ocean acidification of *Balanophyllia europaea*, a scleractinian zooxanthellate coral endemic to the Mediterranean Sea. We analyzed for the first time with time-domain nuclear magnetic resonance (TD-NMR) the porosity and pore-space structure of *B. europaea* specimens collected along a natural CO₂ gradient. Off the Island of Panarea (Southern Italy), an underwater extinct volcanic crater generates the gradient through emissions of carbon dioxide from the sea floor, at ambient seawater temperatures, which naturally lowers the pH of the surrounding seawater. These areas of acidified seawater provide natural laboratories in which to study the long-term biological response to rising CO₂ levels. The NMR results indicate that the increase of CO₂ has effects on the coral skeleton. The major effect is the increase in porosity with increasing CO₂ accompanied by an increase in macroporosity, meaning an increase of the fraction of the largest pores in the pore-space. In our natural model of OA, the increased values of porosity, and macroporosity with CO₂ observed in *B. europaea* predict that lowered pH could significantly reduce the resistance of this zooxanthellate species to mechanical stresses, which might have serious consequences for its survivorship in the envisaged acidified seawater of the next decades.

Introduction

Surface ocean CO₂ partial pressure (pCO₂) is expected to rise in proportion with the atmospheric CO₂ increase due to the oceanic uptake of anthropogenic CO₂ (Sabine et al. 2004). When CO₂ is absorbed by seawater, chemical reactions occur that lower seawater pH, carbonate ion (CO₃²⁻) concentration, and saturation states of the biologically important calcium carbonate (CaCO₃) minerals calcite (Ω_{calc}) and aragonite (Ω_{arag}), in the process commonly referred to as Ocean Acidification (OA; Orr et al. 2005).

There is a great concern and debate about coral reefs survival under the envisaged scenarios of global climate change (Dove et al. 2013; J.M. Pandolfi et al. 2011; Hoegh-Guldberg et al. 2007). Coral reefs are not only one of the most biodiverse ecosystems, but they are also important for human society and economy (Hoegh-Guldberg et al. 2007), and marine organisms are likely to be more sensitive to climate change than their terrestrial counterparts (Richardson and Poloczanska 2008). In the marine realm, two of the main forces causing significant changes are global warming and OA, both largely driven by the burning of fossil fuels since the second industrial revolution that has caused the current dramatic rise in atmospheric CO₂ partial pressure (Solomon et al. 2007).

The importance of understanding effects of OA has recently increased, since global warming and OA are coupled, and it has been hypothesized that OA has the potential to exacerbate the effects of anthropogenic warming (Six et al. 2013).

During preindustrial times the global mean pH at sea surface was 8.2. Since then, this value has decreased already by 0.1 units, and at the current rate of CO₂ uptake, the average surface ocean pH will likely drop to 7.8 by the end of 2100 (Solomon et al. 2007). Although OA acts at a global scale, its impact varies locally. In the case of the Mediterranean Sea, a recent study estimated a pH decrease of up to 0.14 units since the pre-industrial era (Touratier and Goyet 2011), larger than the global averaged surface ocean pH decrease of 0.1 pH units (Orr et al. 2005), making it one of the world's hotspots for OA (Yilmaz et al. 2008; Calvo et al. 2011; Ziveri 2012). It is consequently important to understand how anthropogenic CO₂ has already affected and how it will affect Mediterranean Sea ecosystems and their key species.

A study performed along a temperature gradient in the western Italian coast (Caroselli et al. 2011) has shown that porosity increases with temperature for the zooxanthellate (i.e. symbiotic with unicellular algae named zooxanthellae) coral *Balanophyllia europaea* (Risso, 1826), but not for the azooxanthellate coral *Leptopsammia pruvoti* Lacaze-Duthiers, 1897. The increase in porosity for the zooxanthellate coral has been ascribed to the inhibition of the photosynthesis at elevated temperatures (Al-Horani 2005; Jokieli and Coles 1990), causing the

attenuation of calcification (Jokiel and Coles 1990), with possible negative consequences also on space colonization (Goffredo et al. 2007, 2009). These results have been confirmed by a study where the pore-space structure of the coral skeleton was studied by Time-Domain Nuclear Magnetic Resonance (TD-NMR) (Fantazzini et al. 2013). It has been shown that the increase in porosity with temperature was largely due to an increase of the larger pores in the pore-space. The negative correlations between temperature and various biological parameters generate concern for the future of the Mediterranean endemic *B. europaea*, with respect to future global warming scenarios (Goffredo et al. 2007, 2008, 2009; Caroselli et al. 2011).

In a study (Goffredo et al. submitted), different species were collected in an area close to Panarea Island, where hydrothermally stable CO₂ emissions generate a pH gradient that can be considered as a natural model for the study of ocean acidification effects on benthic biota and ecosystems in their natural setting (Fig.1). The study was conducted to relate the control over the biomineralization process with the population density. The data indicate a decrease in the abundance of *B. europaea* (Fig.2), without any change of skeletal CaCO₃ phase composition, atomic order, organic matrix content, aragonite fiber thickness, and hardness. Corals were not found at the highest CO₂ levels (pH 7.4).

In order to understand the effects of CO₂-driven acidity on the population density decrease of *B. europaea*, this study is focused on the analysis of the structure of the pore-space of the skeleton by means of TD-NMR analysis on specimens collected along the pH gradient. Not only porosity (pore-volume to sample-volume ratio) but also pore-size distribution of mineralized tissues strongly influence the skeletal resistance to natural and anthropogenic breakage. TD-NMR and in particular Magnetic Resonance Relaxometry of ¹H nuclei of water saturating the pore-space, has the advantage, compared to other methods, to give information on porosity and pore-size distribution in a non-sample destructive and non-sample invasive procedure, thus allowing coral skeletons to be further analyzed with other techniques and/or for other scopes. Moreover, the method is particularly useful in the presence of very wide pore-size distributions, as in the case of coral skeletons, where ranges from 10 nanometers to tens of micrometers are expected (Laine et al. 2008; Fantazzini et al. 2013).

The method consists in the acquisition of the transverse relaxation curve of the ¹H nuclei of water molecules saturating the cleaned skeletons of the corals. These curves are multi-exponential so that the inversion from experimental relaxation curves gives the *T*₂ distribution of relaxation times (see Fig. 3). If the diffusion is fast enough to maintain the magnetization uniform inside the pore, condition usually satisfied, these distributions correspond to pore-

size distributions. The area below each distribution is proportional to the total NMR signals and therefore is proportional to the volume of water saturating the pore-space volume (V_p). If the slope of the distribution shows a strong increase at a certain T_2 value, this can be chosen as the point (called “cut-off”) of separation between smaller (shorter T_2) and larger (longer T_2) pores. “NMR microporosity”, for short “microporosity” will indicate the fraction in percent of V_p where the smaller pores are weakly coupled by water diffusion to the large ones at the *local relaxation time* scale. Microporosity is then defined as the fraction of ^1H signal with T_2 smaller than the cut-off, divided by the total ^1H signal and is computed as the ratio of the area under the distribution for T_2 smaller than the cut-off, to the total area under the distribution. For clarity, in this paper the complement to 100% of the microporosity will be considered and called “macroporosity”. In a recent paper (Fantazzini et al. 2013) it has been shown that in coral skeletons saturated with water a sharp boundary between two classes of pores does exist. On the basis of the comparison with mercury intrusion porosimetry, microporosity should correspond to pore sizes in the range from ~ 10 nm to ~ 10 - 20 μm . Macroporosity should correspond to a major fraction of pores, with sizes in the range 20-100 μm .

Results and Discussion

Seawater carbonate chemistry at the collection sites. Table 1 shows the values measured for pH, temperature (T), and total alkalinity (TA). From these data, along with the salinity (37‰), the chemical sea water data for the four sites (Fig.1) were computed. Only pH and the carbonate chemistry parameters show significant differences among sites ($p < 0.001$). It is worth to note the decrease of the aragonite saturation from site 1 to site 4 (Table 1, Fig. 1), and to note the absence of *B. europaea* specimens are in the latter (Goffredo et al. submitted).

NMR Relaxation time T_2 distributions. Figure 3 shows the T_2 distributions for three specimens with comparable mass of *B. europaea*, one for each site. All the distributions show a main peak at long relaxation times and a long tail, of smaller amplitude, about three orders of magnitude wide. At $T_2 \approx 600$ ms there is the cut-off that divides microporosity from macroporosity. The microporosity is about three orders of magnitude wide, and corresponds to about three orders of magnitude of pore-sizes from less than 10 nm to 10 μm (Fantazzini et al. 2013). The sharp boundary between the two classes suggests that they are not well connected by water diffusion during a *local relaxation time*. Moreover, the long tail indicates that the small pores are poorly connected with the other small pores and with the larger ones

in the major class. The two classes of pores are easily distinguished in the distributions for all the specimens, so that macroporosity and cut-off were determined for each distribution (Table 2).

Skeleton structure parameters in the three sites. Table 2 shows the means and standard errors in the three sites at different pCO₂ for the mass, pore-volume, total volume, porosity, bulk-density, micro-density, cut-off and macroporosity. The micro-density does not show significant differences among the three sites, and the observed values are consistent with the known value (Caroselli et al. 2011). Only porosity ($p < 0.001$), bulk density and macroporosity ($p < 0.01$) show significant differences among sites.

Table 3 shows the correlation matrix among the variables of interest. The measured values of pH correlate with the distances from the vent at high significant level ($p < 0.001$), showing the correctness of the choice of this place as a good natural laboratory to mimic the ocean acidification conditions. The mass is not-surprisingly highly correlated with volume and pore-volume. The larger the mass, the larger the volume and pore-volume. As expected, mass, pore-volume and total volume are correlated, as each one of the parameters is mathematically bound to the others. Likewise, it is expected that mass does not correlate with porosity: as the mass increases, also pore-volume and total volume increase in such a way that porosity may be unaffected. It is worth noticing that mass does not correlate with micro-density. Surprisingly, mass does not correlate significantly with macroporosity, in contrast with a previous result (Fantazzini et al. 2013), where a significant increase of macroporosity (decrease of microporosity) was observed with increasing mass. The explanation could be the different behavior of macroporosity in the three sites, and/or, as Table 2 shows, the narrower range of masses used in this research. Porosity and macroporosity are positively correlated with each other ($p < 0.001$), and both negatively correlated with pH ($p < 0.01$; Fig. 4).

In order to better analyze these correlations, Principal Component analysis was performed on porosity and macroporosity. Only two orthogonal factors, PC1 and PC2, were found. PC1 explains 75% of the overall variance and PC2 the remaining part (25%). In order to understand the influence of pH on porosity and macroporosity, the multivariate analysis (Eq.1) was performed assuming as independent variables x_j , time by time the variables pH, mass and the variable obtained as the residuals of the regression between macroporosity and pH (to take into account the dependence of porosity on the variance of macroporosity not explained by pH), to predict the dependent variables, y_j , porosity, macroporosity, PC1 and PC2 (Table 4). Models (1), (2) and (3) show that the mass does not affect the porosity, while

the pH has effectively a strong effect on the porosity. The same is obtained for macroporosity (models 4, 5, 6), for which the most important parameter is pH. Model (7) shows that the part of macroporosity non related to pH, is related to porosity. Model (8) shows that PC1 is dominated by pH ($p < 0.01$), while PC2 (model 9) is not related to pH.

In synthesis, most of the variance of porosity and macroporosity (driven by PC1) is related to pH.

Figure 4 shows the porosity and macroporosity of the specimens against the pH. The smaller the pH, the higher the porosity and the macroporosity. Quantile regression analyses were performed by assuming pH as independent variable and porosity or macroporosity as dependent variables. The straight lines in Fig. 4 are the best fit linear regressions for the total samples (OLS blue line) and for the 25%, 50% and 75% quantiles.porosity (75th quantile). All the regressions (except for the 75% line for macroporosity) show a significance of $p < 0.05$ or $p < 0.01$ level. The higher the porosity, the stronger the effect of the pH. The same is obtained for macroporosity: the higher the macroporosity, the higher is the effect of pH. Porosity and macroporosity increase more with pH for specimens with higher porosity and macroporosity.

Conclusion

TD-NMR of the water saturating the cleaned coral skeletons is a quick, non-sample invasive, non-sample destructive method that does not use ionizing radiation, that has been applied for the first time in this research to study the changes of the pore-space architecture of scleractinian corals along a natural CO₂-driven pH gradient. Even if this method cannot spatially locate the heterogeneity of the pore space, the existence of a clear cut-off in all the distributions (a very high slope at a certain point of the distribution) means that the smallest pores are not well connected by diffusion at the NMR time scale (corresponding to the local value of T_2) to the largest ones. In previous studies (Caroselli et al. 2011; Fantazzini et al. 2013) it has been shown that porosity depends on temperature for the zooxanthellate *B. europaea*, but not for the azooxanthellate *L. pruvoti*. It has been hypothesized that the increase in porosity with temperature in the zooxanthellate species could depend on an inhibition of the photosynthesis at elevated temperatures (Al-Horani 2005; Jokiel 1990) causing an attenuation of calcification (Al-Horani 2005) leading to possible negative consequences also on growth, population dynamics, and space colonization (Goffredo et al. 2007, 2008, 2009; Caroselli et al. 2011). Increased CO₂ could have effects on the skeleton and its pore-space structure. The NMR results indicate that the decrease of pH has effects on

the coral skeleton. The major effect is the increase in porosity with increasing CO₂ accompanied by an increase in macroporosity, meaning an increase of the fraction of the largest pores in the pore-space. Moreover, the larger the porosity (and the larger the macroporosity), the stronger are the dependences on the pH and on the distance from the vent. Our data show that pH, related with high statistical significance to the Principal component PC1 ($p < 0.01$), that in turn explain 75% of the variance between porosity and macroporosity, is the most important parameter leading to the increased porosity and macroporosity, but pH is not sufficient to account for the variance in the data. That means that our model is a good model of OA, because the biological and environmental variability determines only the 25% of the total variance. In our natural model of OA, the increased values of porosity and macroporosity with pCO₂ observed in *B. europaea* predict that increasing acidity could significantly reduce the resistance of this zooxanthellate species to mechanical stresses, which might have serious consequences for its survivorship in the envisaged acidified seawater of the next decades (Madin et al. 2012).

Materials and Methods

The corals. *Balanophyllia europaea* (Fig.2) is a solitary zooxanthellate scleractinian coral which is endemic to the Mediterranean. Its distribution is limited to depths of 0-50 m because of its symbiosis with zooxanthellae, which require light (Zibrowius 1980). Specimens of *B. europaea* (44 corallites) were randomly collected at three sites along the pH gradient (Fig. 1a,b,c,d) between November 2010 and May 2013. No polyps of *B. europaea* were present at the highest CO₂ levels (site 4). Coral tissue was totally removed and corals cleaned as described in (Caroselli et al. 2011). The skeletons were weighed to determine the mass (m). The pore volume (V_P) and the sample volume (V_T) were determined by hydrostatic measurements, from which porosity (p) and micro-density (d_r , *sensu* Bucher et al. 1998) were computed. The specimens were then saturated with water for NMR measurements.

Study site. The area is close to Panarea (Italy), an island belonging to the Aeolian Archipelago in the southern Tyrrhenian Sea in the Mediterranean (Fig. 1a), part of an active volcanic system. Close to Panarea Island there is an area delimited by the islets of Dattilo, Bottaro, Lisca Nera and Lisca Bianca, characterized by a widespread presence of gas vents (Fig. 1b). In the main vent, a crater 20 m x 14 m wide and ~10 m deep generates a sustained column of bubbles from the seabed to the sea surface. In this crater the hydrothermally stable CO₂ emissions generates a pH gradient (Fig. 1c) which extends for ~34 m from the center of

the crater to its periphery. Depth along the CO₂ gradient goes from 11.6 m at the crater to 9.2 m at the control site ~34 m distant (Fig. 1d). Measured pH was converted to the total scale (pH_{TS}) using CO2SYS software. The distances (d) and the corresponding mean pH values are: site 1 (S1) control, $d = 34$ m, pH_{TS} = 8.07; site 2 (S2), $d = 13$ m, pH_{TS} = 7.87; site 3 (S3), $d = 9$ m, pH_{TS} = 7.74 and site 4 (S4), $d = 3$ m, pH_{TS} = 7.40 (Fig. 1c). Temperature (T), salinity, total alkalinity (TA) and pH (NBS) were measured on different occasions from July 2010 to May 2013, with a multi-parametric probe (600R, YSI Incorporated, USA) powered from a small boat and operated by SCUBA divers. Additional temperature data was recorded every three hours by sensors (Thermochron iButton, DS1921G, Maxim Integrated Products, USA) placed in each site. Bottom water samples for determination of TA were collected at each site using sterile 120 ml syringes (two replicates for each site). After each dive upon return to the boat, the syringe samples were immediately transferred in labelled 100 ml amber glass bottles and immediately fixed with saturated mercuric chloride (HgCl₂) to avoid biological alteration, and stored in darkness at 4°C prior to measurement. TA was measured by Gran titration, using a 702 SM Titrino (Metrohm AG). Certified reference materials (Batch 121) from the Andrew Dickson Laboratory at UC San Diego were used to ascertain the quality of results obtained. Mean pH (back-transformed hydrogen ion concentrations) was calculated for each site; pH, T, salinity and TA were used to calculate carbonate system parameters (Table 1) using CO2SYS software with dissociation constants from Mehrbach et al. (1973) refit by Dickson and Millero (1987) and [KSO₄] using Dickson (1990). Temperature data ($n = 2580$ per site) was recorded every three hours by data loggers placed in each site from May to September 2012 and from November 2012 to April 2013. pH ($n = 103$ -110 per site) and salinity ($= 37\text{‰}$, $n = 107$ -110 per site) were measured in July 2010, September 2010, November 2010, March 2011, June 2011, July-August 2011, November-December 2011, April-May 2012, June 2012 and May 2013. TA (total alkalinity, $n = 8$ per site) was measured in September 2010, November 2010, March 2011, June 2011, July-August 2011, November-December 2011, April-May 2012 and June 2012.

TD-NMR measurements. A home-built relaxometer based on a 0.2 T permanent magnet operating at 8 MHz was used to detect the signal of ¹H nuclei of water saturating the pore-space of the coral skeletons. The relaxometer is equipped with a coil ≈ 2 cm in diameter in order to analyze the entire coral, without the need to break it into small pieces, and a Spinmaster console (Stelar, Mede, Pavia, Italy) for automatic pulse sequences transmission and data acquisition. The transverse relaxation data were acquired by using the Carr-Purcell-

Meiboom-Gill (CPMG) sequence (Cowan, 1997) with 200 μ s echo time. Relaxation data were inverted to T_2 distributions by the algorithm UPEN (Uniform-Penalty inversion algorithm), implemented in UpenWin software (Borgia et al. 2001; Fantazzini and Brown 2005; Bortolotti et al, www.unibo.it/Portale/Ricerca/Servizi+Imprese/UpenWin.htm).

Statistical Analysis. Statistical analyses (ANOVA, Correlation matrix, Principal Components, Multivariate analysis) were performed using Statistical Package STATA 9.0 (StataCorp LP). To test the significance of the differences among sites parametric and non-parametric tests were performed. Multivariate analyses were made using Ordinary Least Squares (OLS) robust to outliers. The model is described by the function:

$$y_i = a + \sum_{j=1}^M b_j \cdot x_j + \varepsilon_i \quad (1)$$

the index i refers to the n -observations, y_i is the value of the dependent variable and ε_i the corresponding error. The dependent variables y_j are porosity and macroporosity. The constants a , b_j ($j=1,M$) are the best fit parameters, to be determined by OLS referring to the independent variables x_j . A quantile analysis (<https://sites.google.com/site/econometricsacademy/econometrics-models/quantile-regression>) was performed to study the previous relationships for omogeneous groups of the dependent variable in the different sites. This analysis allows one to get a more comprehensive picture of the effect of the independent variable on the dependent variable as it can show different effects of the independent variable in different ranges of the dependent variable.

Acknowledgements

This research has received funding from the European Research Council under the European Union's Seventh Framework Programme (FP7/2007-2013) / ERC grant agreement n° 249930 – CoralWarm: Corals and global warming: the Mediterranean versus the Red Sea. B. Basile, F. Sesso, and Eolo Sub diving center assisted in the field. F. Gizzi and G. Polimeni helped during preparation and participated to field surveys. The Scientific Diving School collaborated to the underwater activities. We thank Francesco sesso for the picture of living specimen and Robert James Sidford Brown for carefully reading the manuscript.

References

- Al-Horani FA (2005) Effects of changing seawater temperature on photosynthesis and calcification in the scleractinian coral *Galaxea fascicularis*, measured with O₂, Ca²⁺ and pH microsensors. *Sci Mar* 69:347-354.
- Álvarez et al. The CO₂ system in the Mediterranean Sea: a basin wide perspective. *Ocean Sci Discuss* 10:1447-1504.
- Bethoux JP, Gentili B, Morin P, Nicolas E, Pierre C, Ruiz-Pino D (1999) The Mediterranean Sea: a miniature ocean for climatic and environmental studies and a key for the climatic functioning of the North Atlantic. *Prog Oceanogr* 44:131–146.
- Bethoux JP, Boukhary MS, Ruiz-Pino D, Morin P, Copin Montegut C. Nutrient, Oxygen and Carbon Ratios, CO₂ Sequestration and Anthropogenic Forcing in the Mediterranean Sea. *Hdb Environment Chemical* 2005, 5, 67-86.
- Berkelmans R, De'ath G, Kinnimonth S, Skirving WJ (2004) A comparison of the 1998 and 2002 coral bleaching events on the Great Barrier Reef: spatial correlation, patterns, and predictions. *Coral Reefs* 23:74-83.
- Borgia GC, Brown RJS, Fantazzini P (2001) Examples of marginal resolution of NMR relaxation peaks using UPEN and diagnostics. *Magn. Reson. Imaging* 19:473–475.
- Bortolotti V, Brown RJS, Fantazzini P *UpenWin: a software to invert multi-exponential decay data*; www.unibo.it/Portale/Ricerca/Servizi+Imprese/UpenWin.htm.
- Bucher DJ, Harriott VJ, Roberts LG (1998) Skeletal micro-density, porosity and bulk density of acroporid corals. *J Exp Mar Biol Ecol* 228:117-136.
- Calvo E, Simó R, Coma R, Ribes M, Pascual J, Sabatés A, Gili JM, Pelejero C (2011) Effects of climate change on Mediterranean marine ecosystems: the case of the Catalan Sea. *Climate Research* 50:1-29.
- Caroselli E, Prada F, Pasquini L, Nonnis Marzano F, Zaccanti F, Falini G, Levy O, Dubinsky Z, Goffredo S (2011) Environmental implications of skeletal micro-density and porosity variation in two scleractinian corals. *Zoology* 114:255-264.
- CIESM Impacts of ocean acidification on biological, chemical and physical systems in the Mediterranean and Black Seas. In *CIESM Workshop Monographs*, vol. 36 (ed. F. Briand), pp. 124. Monaco, 2008.
- Cowan B (1997) *Nuclear Magnetic Resonance and Relaxation*; Cambridge University Press: Cambridge, U.K.

- Dickson AG (1990) Thermodynamics of the dissociation of boric acid in synthetic sea water from 273.15 to 298.15 K. *Deep-Sea Res A* 37:755-766.
- Dickson AG, Millero FJ (1987) A comparison of the equilibrium constants for the dissociation of carbonic acid in seawater media. *Deep-Sea Res A* 34:1733-1743.
- Fantazzini P, Brown RJS (2005) Units in distributions of relaxation times. *Concepts Magn. Reson.* 27A:122–123.
- Fantazzini P, Mengoli S, Evangelisti S, Pasquini L, Mariani M, Brizi L, Goffredo S, Caroselli E, Prada F, Falini G, Levy O, Dubinsky Z (2013) Time-Domain NMR study of Mediterranean scleractinian corals reveals skeletal-porosity sensitivity to environmental changes. *Environ Sci Technol* 47:12679-12686.
- Field CB, Barros V, Stocker TF, Dahe Q (2012) Managing the Risks of Extreme Events and Disasters to Advance Climate Change Adaptation: Special Report of the Intergovernmental Panel on Climate Change. Cambridge University Press, Cambridge and New York.
- Goffredo S, Caroselli E, Mattioli G, Pignotti E, Dubinsky Z, Zaccanti F (2009) Inferred level of calcification decreases along an increasing temperature gradient in a Mediterranean endemic coral. *Limnol Oceanogr* 54:930-937.
- Goffredo S, Caroselli E, Mattioli G, Pignotti E, Zaccanti F (2007) Variation in biometry and demography of solitary corals with environmental factors in the Mediterranean Sea. *Mar Biol* 152:351-361.
- Goffredo S, Prada F, Caroselli E, Capaccioni B, Zaccanti F, Pasquini L, Fantazzini P, Fermani S, Reggi M, Levy O, Katharina F, Dubinsky Z, Falini G – Species abundance and biomineralization under ocean acidification. Submitted
- Hoegh-Guldberg et al. (2007) Coral reef under rapid climate change and Ocean Acidification, *Science* 318:1737-1742.
- Jokiel PL, Coles SL (1990) Response of Hawaiian and other Indo-Pacific reef corals to elevated temperature. *Coral Reefs* 4:155-162.
- Laine J, Labady M, Albornoz A, Yunes S (2008) Porosities and pore sizes in coralline calcium carbonate. *Materials Characterization* 59:1522-1525.
- Lough JM, Barnes DJ (2000) Environmental controls on growth of the massive coral *Porites*. *J Exp Mar Biol Ecol* 245:225–243.
- Madin JS, Hughes TP, Connolly SR (2012) Calcification, storm damage and population resilience of tabular corals under climate change. *PLOS ONE* 7:e46637.

- Mehrbach C, Culbertson CH, Hawley JE, Pytkowicz RM (1973) Measurement of the apparent dissociation constants of carbonic acid in seawater at atmospheric pressure. *Limnol Oceanogr* 18:897-907.
- Orr et al. (2005) Anthropogenic ocean acidification over the twenty-first century and its impact on calcifying organisms. *Nature* 437:681-686.
- Pandolfi et al. (2011) Projection Coral reef Futures under Global Warming and Ocean Acidification. *Science* 333:418-422.
- Richardson AJ, Poloczanska ES (2008) Under-resourced, under threat. *Science* 320:1294-1295.
- Sabine CL, Feely RA, Gruber N, Key RM, Lee K, Bullister JL, Wanninkhof R, Wong CS, Wallace DWR, Tilbrook B, Millero FJ, Peng TH, Kozyr A, Ono T, Rios AF (2004) The oceanic sink for anthropogenic CO₂. *Science* 305:367-371.
- Schneider A, Wallace DWR, Körtzinger A (2007) Alkalinity of the Mediterranean Sea. *Geophys Res Lett* 34:1-5.
- Six KD, Kloster S, Ilyina T, Archer SD, Zhang K, Maier-Reimer E (2013) Global warming amplified by reduced sulphur fluxes as a result of ocean acidification. *Nat Clim Chang* 3:975-978.
- Solomon et al. (2007) *Climate Change 2007: The Physical Science Basis*. Cambridge University Press.
- Sophie G. Dove et al. (2013) Future reef decalcification under a business-as-usual CO₂ emission scenario. *PNAS* 110:15342-15347.
- Touratier F, Goyet C (2009) Decadal evolution of anthropogenic CO₂ in the northwestern Mediterranean Sea from the mid-1990s to the mid-2000s, *Deep Sea Res Part I Oceanogr Res Pap* 56:1708–1716.
- Touratier F, Goyet C (2011) Impact of the Eastern Mediterranean Transient on the distribution of anthropogenic CO₂ and first estimate of acidification for the Mediterranean Sea. *Deep Sea Res Part I Oceanogr Res Pap* 58:1-15.
- Wilkinson CR (2004) *Status of Coral Reefs of the World: 2004*. Australian Institute of Marine Science, Cape Ferguson, Qld., Volume 1, 301 pp
- Yilmaz et al. 2008. *Impact of Acidification on Biological, Chemical and Physical Systems in the Mediterranean and Black Seas*, Mediterranean Science Committee (CIESM), Monograph Series, Vol. 36, pp. 124.
- Zibrowius H (1980) Les scléactiniaires de la Me'diterranée et del'Atlantique nord-oriental. *Mem Inst Oceanogr* 11:1-284.

Ziveri P (2012) Research turns to acidification and warming in the Mediterranean Sea, IMBER (Integrated Marine Biogeochemistry and Ecosystem Research), Newsletter, Issue n.#20.

Figure captions

Fig. 1. Location of the sites in Panarea where corals were collected. (a) The Aeolian Archipelago; (b) map showing where the crater is located; (c) the range in pH_{TS} (\square , $n = 103$ -110 per site) and Ω_{arag} (\times , $n = 96$ -104 per site) along the pH gradient; (d) the bathymetric profile of the four sites with the the associated mean pH_{TS} and Ω_{arag} in brackets.

Fig. 2. A living polyp of *B. europaea*.

Fig. 3. T_2 relaxation time distributions of ^1H NMR signal from cleaned skeletons of three specimens of *B. europaea*, after water saturation of the connected pore-space. The samples have about the same mass, but come from the three different sites. The ordinate, labeled signal density, is an approximation to $(dS)/(d \ln T_1)$, where S is the extrapolated signal per Neper (factor of e) of relaxation time. Therefore the total NMR signal (S_{NMR}) is represented by the area below each T_2 distribution. It is proportional to the amount of water saturating the pore-space, and therefore to the volume of the connected pore-space itself. The distributions were obtained by Inverse Laplace Transform (algorithm UPEN) of the experimental relaxation curves displayed in the inset.

Fig. 4. Scatterplots of the porosity (a) and “macroporosity” versus the pH values, for all the samples. The straight lines are the best fit linear regression from OLS (continue), 25% quantile (dashed), 50% (dashed blu) and 75% quantile (lower dashed).

Table 1. Seawater carbonate chemistry measurements for each study site off the Island of Panarea

	pH range (total scale)	T (°C)	TA ($\mu\text{mol kg}^{-1}$)	⁽¹⁾ pCO ₂ (μatm)	⁽¹⁾ HCO ₃ ⁻ ($\mu\text{mol kg}^{-1}$)	⁽¹⁾ CO ₃ ²⁻ ($\mu\text{mol kg}^{-1}$)	⁽¹⁾ DIC ($\mu\text{mol kg}^{-1}$)	⁽¹⁾ Ω_{arag}
Site 1 S1: d=34 m	8.07 (8.04-8.10)	19.2 (19.0-19.3)	2482 (2435-2529)	423 (387-460)	1923 (1888-1958)	229 (215-243)	2165 (2144-2187)	3.4 (3.2-3.7)
Site 2 S2: d=13 m	7.87 (7.83-7.90)	19.5 (19.3-19.7)	2478 (2424-2533)	698 (638-759)	2109 (2079-2140)	169 (157-182)	2301 (2281-2321)	2.5 (2.4-2.7)
Site 3 S3: d=9 m	7.74 (7.68-7.81)	19.5 (19.3-19.7)	2465 (2416-2513)	922 (764-1080)	2107 (2078-2136)	146 (135-158)	2283 (2262-2304)	2.3 (2.1-2.4)
Site 4 S4: d=7m	7.40 (7.33-7.49)	19.3 (19.2-19.5)	2432 (2377-2486)	1974 (1604-2344)	2192 (2165-2219)	98 (87-109)	2353 (2327-2380)	1.4 (1.3-1.6)
χ^2	183.3***	0.37	4.00	12.00***	83.19***	135.8***	77.25***	135.0***

Site 1 is the control and sites 2- 4 are the elevated CO₂ sites. Temperature (T, n = 2580 per site), pH (n = 103-110 per site), total alkalinity (TA, n = 8 per site). Mean pH values were calculated after conversion of data to hydrogen ion concentrations. DIC is the dissolved inorganic carbon. The symbol d represents the distance from the vent. Values in brackets are 95% CIs. The values of pH, T, TA and the value of salinity (37‰, n=107-110 per site) were used to calculate the carbonate system parameters (⁽¹⁾, n=96-107 for each site).

*** p < 0.001 Kruskal-Wallis equality-of-populations rank test.

Table 2. Descriptive and test statistics split by site

	S1: d=34 m pCO ₂ =423 μatm			S2: d=13 m pCO ₂ =698 μatm			S3: d=9 m pCO ₂ =922 μatm			F	χ^2
	n	mean	se	n	mean	se	n	mean	se		
m (mg)	16	1023	237	16	1227	209	12	1229	250	0.27	1.32
pore-volume (mm³)	16	171	48	16	260	50	12	245	46	1.02	4.42
total volume (mm³)	16	546	132	16	708	124	12	689	133	0.49	1.81
porosity(%)	16	30.0	0.9	16	35.3	1.2	12	36.2	1.7	7.30***	13.77***
micro-density (mg/mm³)	16	2.70	0.02	16	2.73	0.02	12	2.76	0.02	1.86	4.87
cut-off (ms)	16	558	41	16	645	36	12	613	67	0.96	2.12
macroporosity (%)	16	73.2	1.7	16	79.3	1.1	12	78.3	2.0	4.46**	6.87**

Number of observations (n), means, standard errors and statistical significances of differences of the variables mass (m), pore-volume, total volume (V_T), porosity, bulk-density, micro-density, cut-off, macroporosity for *B. europaea*. The values of F-test and χ^2 -test suggest statistical significance of differences among the three sites only for porosity (p < 0.001), bulk density (p < 0.01) and macroporosity (p < 0.01).

*** p < 0.001, **p < 0.01 Kruskal-Wallis equality-of-populations rank test.

Table 3. Correlation matrix among the variables of Table 2

	d (m)	pH	m (mg)	pore-volume (mm ³)	volume (mm ³)	Porosity (%)	bulk-density (mg/mm ³)	micro-density (mg/mm ³)	cut-off (ms)	macro-porosity (%)
d (m)	1.00									
pH	0.97***	1.00								
m (mg)	-0.11	-0.11	1.00							
pore-volume (mm ³)	-0.21	-0.19	0.94***	1.00						
total volume (mm ³)	-0.15	-0.13	0.99***	0.97***	1.00					
porosity (%)	-0.51**	-0.5**	0.17	0.44***	0.27	1.00				
micro-density (mg/mm ³)	-0.26	-0.28	0.28	0.30*	0.28	0.34*	0.03	1.00		
cut-off (ms)	-0.19	-0.16	-0.22	-0.19	-0.21	0.06	-0.12	-0.15	1.00	
macro-porosity (%)	-0.41**	-0.36**	0.23	0.36*	0.28	0.5***	-0.54***	0.00	0.07	1.00

***p < 0.001, **p < 0.01, *p < 0.05

Table 4 Multivariate analysis. OLS robust to outliers (Robust t-statistics in parentheses)

VARIABLES	(1) Porosity (%)	(2) Porosity (%)	(3) Porosity (%)	(4) Macroporosity (%)	(5) Macroporosity (%)	(6) Macroporosity (%)	(7) Porosity (%)	(8) PC1	(9) PC2
pH	-20.04*** (-3.747)		-19.54** (-3.535)	-17.71* (-2.305)		-16.73* (-2.197)	-19.83*** (-3.992)	-4.50** (-3.481)	-0.69 (-0.857)
m (mg)		0.001 (1.266)	0.001 (0.801)		0.002 (1.795)	0.001 (1.680)	0.000 (0.374)		
macro-no-pH (%)							0.299* (2.427)		
Constant	192.05*** (4.513)	32.38*** (25.929)	187.2*** (4.236)	216.8*** (3.570)	74.83*** (46.872)	207.47** (3.444)	190.04*** (4.814)	35.59** (3.462)	5.48 (0.861)
Observations	44	44	44	44	44	44	44	44	44
R2-adj	0.227	0.00511	0.223	0.111	0.0281	0.126	0.319	0.227	- 0.00588
F-test	14.04***	1.604	7.345***	5.311**	3.221	3.779*	5.851***	12.12***	0.734

The coefficients in the columns are the parameters a (Constant) and b_j of Eq. (1). The parameter macro-no-pH, used in the model (7) represents the residuals of the regression between macroporosity and pH (to take into account the dependence of porosity on the variance of macroporosity not explained by pH). Robust t-statistics in parentheses.

***p < 0.001, **p < 0.01, *p < 0.05.

Figure 1

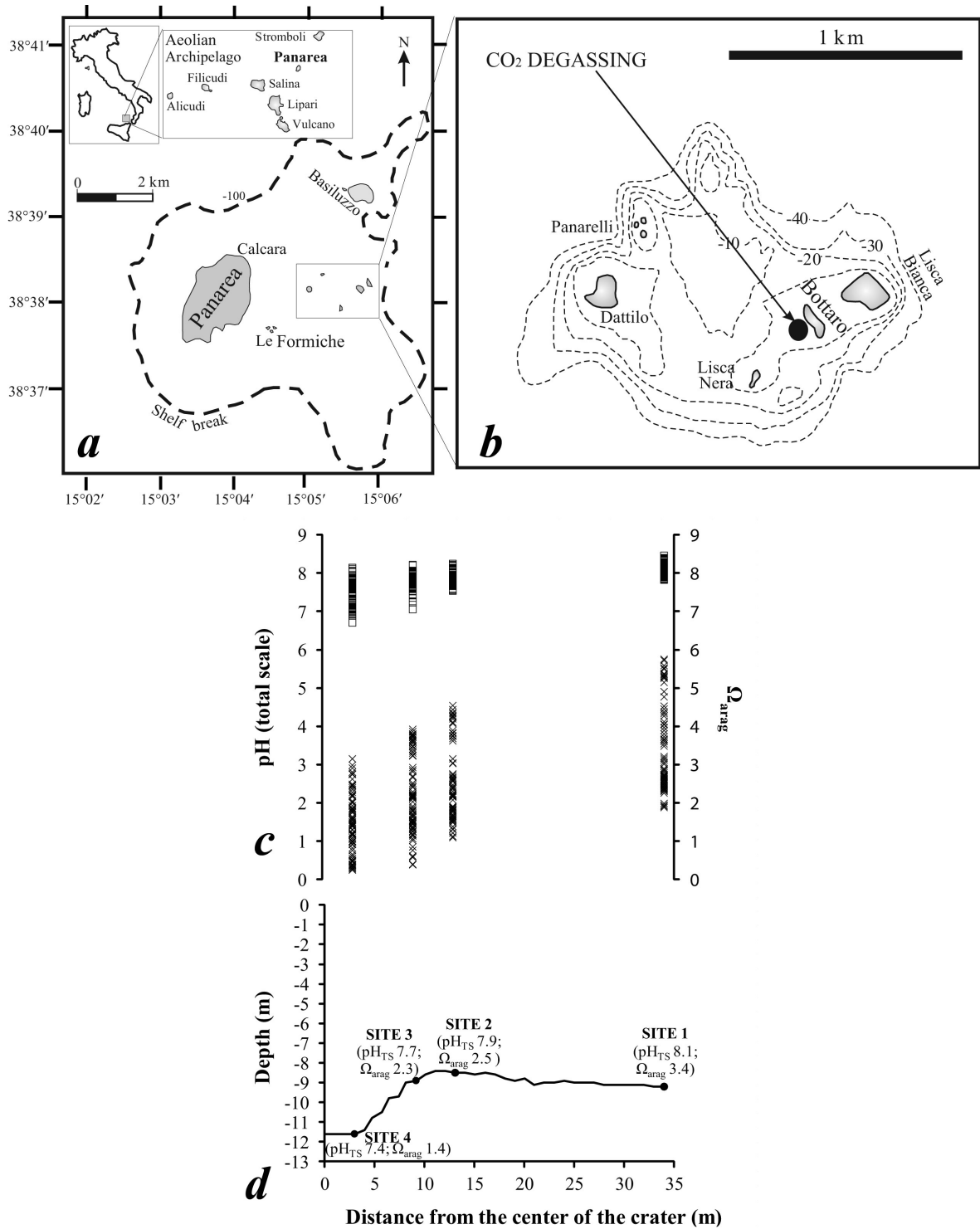


Figure 2



Figure 3

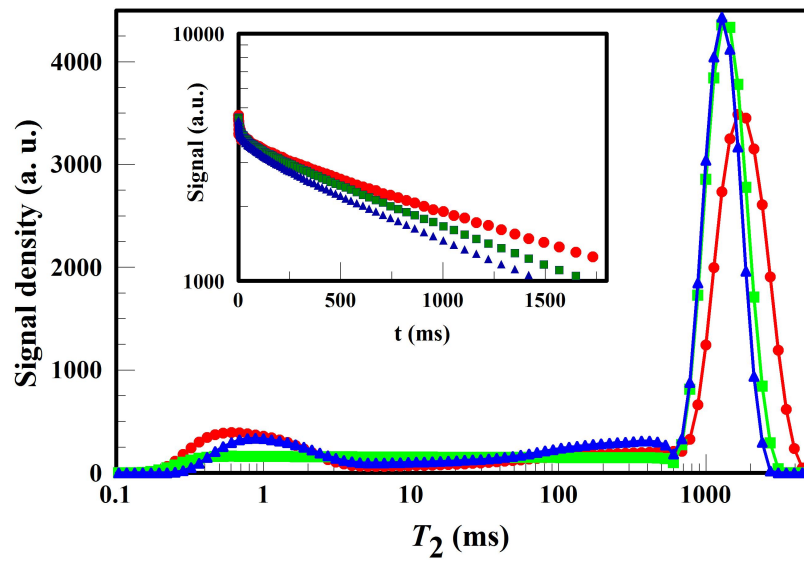
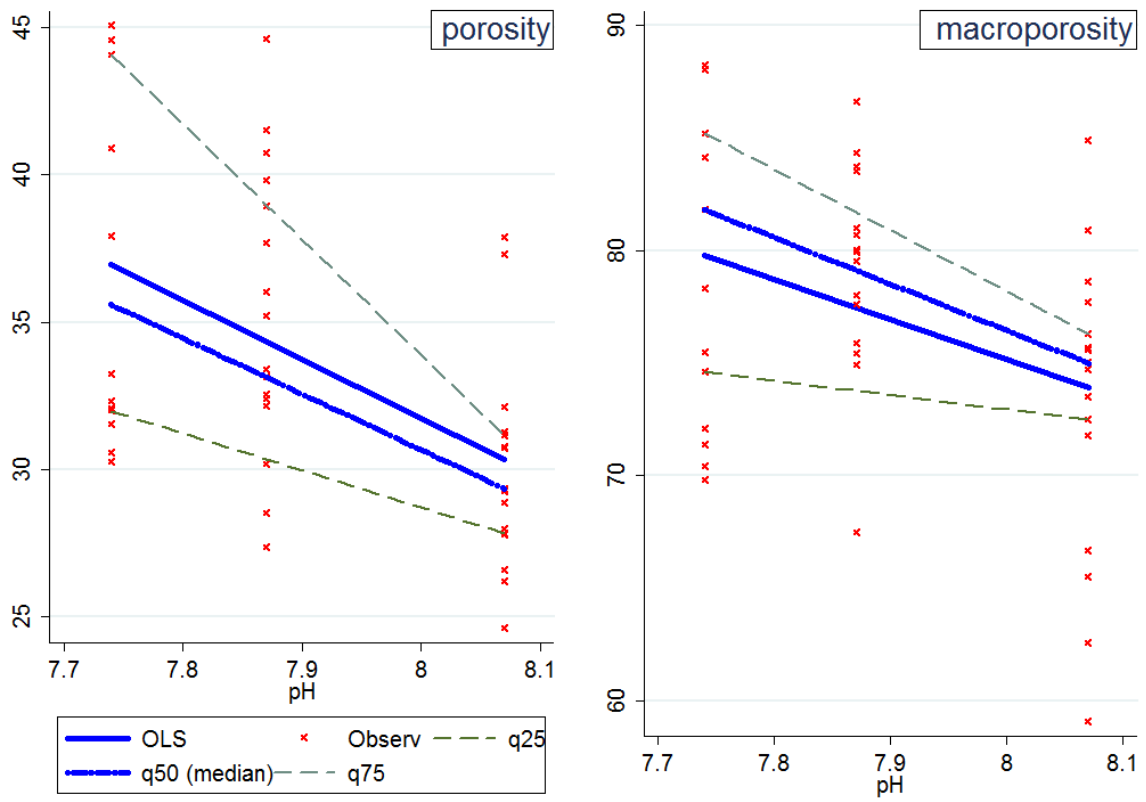


Figure 4



Chapter 7: Conclusions

Global environmental change, led by the current dramatic rise in sea surface temperature (SST) and carbon dioxide partial pressure ($p\text{CO}_2$), is expected to have a great impact on marine ecosystems. *Balanophyllia europaea*, which can count on both heterotrophy and symbiotic algae for its nourishment, seems to be negatively affected by increasing temperatures, while *Leptopsammia pruvoti*, which is fully heterotrophic, seems to be tolerant to higher temperatures. It seems likely that the symbiosis with zooxanthellae plays a role in determining the different sensitivities of these two species, as it is hypothesized that photosynthesis may be inhibited at high temperatures. Different modes of nutrition (mixotrophic/zooxanthellate versus heterotrophic/non-zooxanthellate) and/or biomineralization processes may also explain their potentially different responses to ocean acidification (OA). Growth of the zooxanthellate *B. europaea* transplanted along a natural CO_2 gradient was not affected by pH, perhaps because of increased photosynthesis of its symbionts at high CO_2 , whereas it decreased with decreasing pH in the two non-zooxanthellate species *L. pruvoti* and *Astroides calycularis*, showing an increased sensitivity to enriched CO_2 with increasing temperature. Temperature seemed to influence also the relationship between mortality rate and pH of these corals, with the highest mortalities measured in the warmest periods, in all three species.

Enhanced CO_2 had a negative impact on the abundance of several benthic organisms naturally occurring along the CO_2 gradient. The coverage of a coral (*B. europaea*), a mollusk (*Vermetus triqueter*), and two macroalgae (*Padina pavonica*, *Lobophora variegata*), one of which is a calcifier, significantly declined with increasing CO_2 . The only species that did not decline was the calcifying macroalgae *Acetabularia acetabulum*. The mineralization response to OA seems connected with the organism level

of control on biomineralization. Only the species with the weaker control on biomineralization were still observed under conditions of lower pH. In this natural model of OA, although growth of the transplanted *B. europaea* specimens was not influenced by lowered pH, perhaps because of increased photosynthesis of its symbionts at high CO₂, increased values of porosity and macroporosity with CO₂ were observed in the naturally occurring specimens. Increasing acidity could therefore significantly reduce the resistance of this zooxanthellate species to mechanical stresses. These findings, added to the negative effect of temperature on various biological parameters, generate concern on the sensitivity of this zooxanthellate species to the envisaged global climate change scenarios.

Research abroad and future perspectives

During the period of research and training that I conducted in Israel at the Mina and Everard Goodman Faculty of Life Sciences of the Bar-Ilan University (Ramat Gan), I worked under the supervision of Prof. Zvy Dubinsky and Dr Oren Levy on a project in collaboration with Prof. Aldo Shemesh at the Weizmann Institute of Science (Rehovot, Israel), which aims to determine the relation between coral isotopic composition and environmental parameters along the Italian coast. Measurements of $\delta^{13}\text{C}$ and $\delta^{18}\text{O}$ were performed on skeletons of Mediterranean scleractinian corals and on seawater samples collected along a latitudinal gradient from 44°20'N to 36°45'N, in seven different sites (Genova, Calafuria, Elba Island, Palinuro, Scilla, Panarea Island and Pantelleria Island). The species analyzed were: *Balanophyllia europaea* (solitary, zooxanthellate), *Leptopsammia pruvoti* (solitary, non-zooxanthellate), *Caryophyllia inornata* (solitary,

non-zooxanthellate), *Astroides calycularis* (colonial, non-zooxanthellate), and *Cladocora caespitosa* (colonial, zooxanthellate). The isotopic analysis of the corals and the surrounding waters was performed to understand the relation between the carbon isotopes of the corals and the isotopic composition of the dissolved inorganic carbon in seawater, to better comprehend the different mechanisms affecting the coral's organic carbon uptake. The two metabolic processes that can alter the isotopic composition of the carbon pool available for skeletogenesis in corals are photosynthesis and heterotrophy. Thus, the next step will be to verify the isotopic signature of plankton in the 7 study sites, to shed light on the observed skeletal isotopic composition of the 5 species. Data analysis is currently underway and effort will be made to publish the results in the coming months.

Acknowledgements

The research leading to these results was funded by the European Research Council under the European Union's Seventh Framework Programme (FP7/2007-2013) / ERC grant agreement n° 249930 – CoralWarm: Corals and global warming: the Mediterranean versus the Red Sea. I wish to thank the Marine Science Group and Scientific Diving School, that supplied scientific, technical, and logistical support. A special thanks goes to all my team, for the valuable insights gained through discussion and advice, and to everyone that was involved in the strenuous fieldwork. Thank you Vale, because if you hadn't been there in more than one occasion, I'm not so sure I would have made it through this incredible but tough journey. Thank you to my supervisor Dr Stefano Goffredo, for his guidance and support, for pushing me to always do better with his “Coraggio!” and to always ask myself “why” of things. I also acknowledge Prof. Zvy Dubinsky and Dr Oren Levy from Bar-Ilan University for watching over and supervising me during my one-year stay in Israel. Thank you also to all the lab members of the “Oren lab” and “Zvy lab” whose help was fundamental inside and outside the lab.

Last but definitely not least...

Thank you to my family and friends, for bearing with me during tough times and for encouraging me to see the light at the end of the tunnel when everything seemed dark. Thank you to my mother, for her patience, for accepting my frequent mood shifts and for being one of my biggest supporters. Thank you to my father, for his wisdom and knowledge, for always supporting me, no matter what, for being as happy or even more than me when I succeeded, and for encouraging me not to give up when I didn't. I dedicate this thesis to you.